Generation of a Generic Nanobody-based CAR-T Cell Platform

Doctoral thesis

to obtain a doctorate (PhD)

from the Faculty of Medicine

of the University of Bonn

Gonzalo Saavedra Pérez Salas

from Aguascalientes, Mexico

2025

Written with authorization of the Faculty of Medicine of the University of Bonn

First reviewer: Prof. Dr. med. Michael Hölzel

Second reviewer: Prof. Dr. Dr. Roland Ullrich

Day of oral examination: 03.06.2025

From the Institute of Experimental Oncology (IEO), Bonn

Table of Content

List of abbreviations

Special Characters	
%	Percent
#	Number
°C	Degree Celcius
µg	Microgram
µl	Microlitre
µM	Micromolar
mM	Milimolar
α	Alpha
β	Beta
γ	Gamma
ζ	Epsilon
Numbers	
3D	Three-dimensional
A	
ADCs	Antibody-drug conjugates
ALL	Acute lymphoblastic leukemia
C	
CARs	Chimeric antigen receptors
CAR-T	Chimeric antigen receptor T cells
CD	Cluster of differentiation
CD3	Cluster of differentiation 3
CD4	Cluster of differentiation 4
CD8	Cluster of differentiation 8
CD15	Cluster of differentiation 15
CD19	Cluster of differentiation 19
CD45	Cluster of differentiation 45
CDRs	Complementarity-determining regions

CRISPR	Clustered regularly interspaced short palindromic repeats
crRNA	CRISPR RNA
D	
DSBs	Double-strand breaks
E	
E:T	Effector-to-target
EGFR	Epidermal growth factor receptor
F	
FCS	Fetal calf serum
FIGO	International Federation of Gynecology and Obstetrics
FRα	Folate receptor alpha
G	
GFP	Green fluorescent protein
GPI	Glycosylphosphatidylinositol
GS	Glycine-serine
H	
HDR	Homology-directed repair
HER2	Human epidermal growth factor receptor 2
HGSOC	High-grade serous ovarian carcinoma
I	
ICIs	Immune checkpoint inhibitors
Ig	Immunoglobulin
ITAMs	Immunoreceptor tyrosine-based activation motifs
IFNg	Interferon gamma
IL	Interleukin
IL-2	Interleukin 2
IL-7	Interleukin 7
IL-15	Interleukin 15
IL-23	Interleukin 23

K	
KD	Dissociation constant
KI	Knock-in
KO	Knockout
M	
MPF	Megakaryocyte potentiating factor
MSCV	Murine stem cell virus
Msln	Mesothelin
N	
Nb-ALFA	Nanobody against ALFA-tag
Nb-Msln	Nanobody against Mesothelin
Nb-Nec2	Nanobody against Nectin-2
NHEJ	Non-homologous end joining
O	
OS	Overall survival
P	
PAMs	Protospacer-adjacent motifs
PARP	Poly (ADP-ribose) polymerase
PFS	Progression-free survival
R	
RTCA	Real-time cell analysis
S	
scFv	Single-chain variable fragment
sgRNA	Single-guide RNA
SPR	Surface plasmon resonance
T	
TCR	T cell receptor
TNFa	Tumor-necrosis factor alpha
tracrRNA	Trans-activating CRISPR RNA

Tregs	Regulatory T cells
V	
VEGF	Vascular endothelial growth factor
VHH	Variable heavy chain
W	
WT	Wild-type
Z	
ZFNs	Zinc finger nucleases

1 Introduction

1.1 Ovarian cancer

1.1.1 Epidemiology and etiology

Ovarian cancer is one of the most aggressive gynecological malignancies, ranking as the eighth most common cancer in women and causing nearly 5% of cancer-related deaths globally in 2020 (Sung et al., 2021; Webb & Jordan, 2024). Its incidence varies significantly across regions, with differences attributed to socioeconomic factors, reproductive trends, and genetic predispositions. Notably, contraceptive use and hormonal therapy have been linked to reduced incidence in some high-income countries (Webb et al., 2017; Webb & Jordan, 2024).

Over 90% of ovarian cancers originate from epithelial cells, predominantly in the fallopian tubes. High-grade serous ovarian cancer (HGSOC) is the most common subtype, accounting for up to 75% of cases (Figure 1.1). This aggressive form often presents bilaterally and is characterized by TP53 mutations, defects in homologous recombination repair, and genomic instability (Shih et al., 2021; Sung et al., 2021).

A significant hereditary burden is evident in up to 25% of cases, with BRCA1 and BRCA2 mutations being the most prominent contributors. These mutations are critical for genetic screening, particularly for patients with a family history of ovarian cancer (Konstantinopoulos et al., 2020). Other risk factors include infertility, endometriosis, polycystic ovarian syndrome, and ovulation-related changes, with prolonged periods of ovulation suppression (e.g., pregnancy or contraceptive use) shown to reduce risk (Gates et al., 2010; Tsilidis et al., 2011).

Late-stage diagnosis remains a major challenge, with 58% of cases identified at stages III or IV, where 5-year survival rates drop to 27% and 13%, respectively. Early detection, in contrast, results in survival rates exceeding 90%. Efforts to improve screening, such as transvaginal ultrasounds combined with CA125 biomarker tests, have shown limited efficacy in improving overall survival (Kurman et al., 2008; Menon et al., 2021). This lack of effective

preventive measures underscores why the current gold standard for ovarian cancer prevention among high-risk groups is bilateral salpingo-oophorectomy before tumor formation (Sung et al., 2021).

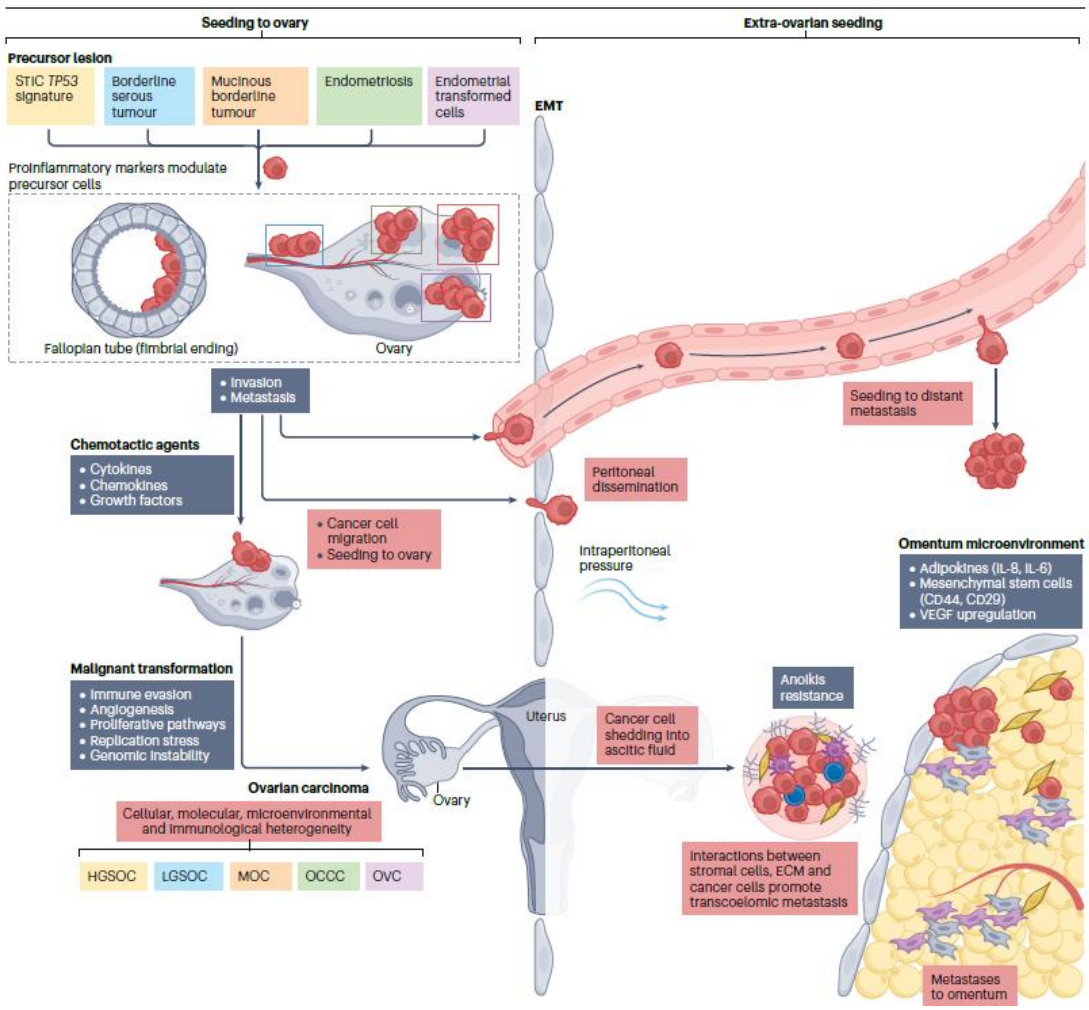

Figure 1.1: Formation of ovarian carcinoma
The heterogeneous complexity of ovarian cancer is depicted as a roadmap from its development as precursor lesion, its transformation into a mature malignant cell, and all the way to its spreading to the omentum and distant metastasis. During this process, the lesions differ into different subgroups that are important of the diagnosis and treatment. ECM, extracellular matrix; EMT, epithelial-mesenchymal transition; EOVC endometrial ovarian carcinoma, LGSOC, low-grade serous ovarian cancer; MOC, mucinous ovarian cancer; OCCC, ovarian clear cell cancer; STIC, serous tubal intra-epithelial cancer (Veneziani et al., 2023).

Clinical features of ovarian cancer often reflect advanced stages. Ascites, a hallmark symptom, arises from fluid accumulation in the peritoneal cavity due to tumor-secreted factors and impaired peritoneal drainage caused by metastasis. This contributes to a pro-inflammatory, immunosuppressive tumor microenvironment, complicating disease management (Kipps et al., 2013; Naora & Montell, 2005).

1.1.2 Treatment

The treatment of ovarian cancer is primarily dictated by disease stage, with most patients undergoing cytoreductive surgery followed by adjuvant chemotherapy. Staging adheres to the 2017 International Federation of Gynecology and Obstetrics (FIGO) classification and typically involves hysterectomy, bilateral salpingo-oophorectomy, and lymph node dissection (Berek et al., 2021). For cases with visible metastases, surgical debulking — including bowel or hepatic resections — is performed despite the significant risks and life-threatening complications associated with these procedures. While surgery remains a cornerstone for advanced ovarian cancer, recurrence is common, contributing to poor prognosis and high mortality rates (Onda et al., 2020; Winter et al., 2007).

Efforts to reduce recurrence and improve outcomes have introduced targeted therapies into first-line treatment. Vascular endothelial growth factor receptor (VEGF) inhibitors, which block angiogenesis, have modestly increased progression-free survival (PFS) without substantial improvement in overall survival (Marchetti et al., 2019; Veneziani et al., 2023). Homologous recombination defects in ovarian cancer have spurred the adoption of poly (ADP-ribose) polymerase (PARP) inhibitors, which are now standard care for platinum-sensitive patients. However, combined use of PARP inhibitors and platinum-based chemotherapy poses significant toxicity challenges (Banerjee et al., 2021).

Besides this, immunotherapy has revolutionized cancer treatment and holds significant potential in ovarian cancer, given its immunogenic nature. High levels of T cell infiltration observed in ovarian tumors underscore the presence of an anti-tumor immune response, suggesting opportunities for therapeutic intervention (Adams et al., 2009; Hamanishi et al., 2007). Immune checkpoint inhibitors (ICIs), such as anti-PD-1 and anti-CTLA-4 antibodies,

have shown efficacy in several malignancies but have been less successful in ovarian cancer due to factors like an immunosuppressive tumor microenvironment and low tumor mutation burden. Despite this, combining ICIs with other treatments such as VEGF inhibitors or PARP inhibitors is being investigated in clinical trials to enhance antitumor responses (Higuchi et al., 2015; Matulonis et al., 2019).

Other immunotherapy modalities are gaining traction in ovarian cancer treatment. Antibody-drug conjugates (ADCs) offer precision by delivering cytotoxic agents directly to cancer cells, minimizing off-target effects. Cancer vaccines aim to stimulate immune responses against tumor-specific antigens, while adoptive cell therapies, including chimeric antigen receptors (CAR) T cells, are emerging as promising approaches.

1.2 CAR-T cell therapy

1.2.1 Definition

Chimeric antigen receptors (CARs) are synthetic receptors that combine both antigen-binding and T cell activating functions into a single receptor expressed on T cells, thus bypassing traditional antigen presentation and directly target specific tumor antigens in a major histocompatibility complex (MHC)-independent manner. Upon recognition, CAR-T cells form a non-classical immune synapse that triggers a cytotoxic response, ideally leading to the elimination of tumor cells.

The structure of CARs consists of extracellular and intracellular components. The extracellular region contains a recognition domain responsible for antigen binding. Traditionally, this domain is engineered from the variable heavy and light chains of conventional antibodies, joined by a flexible linker to create a single-chain variable fragment (scFv) (Figure 1.2A).

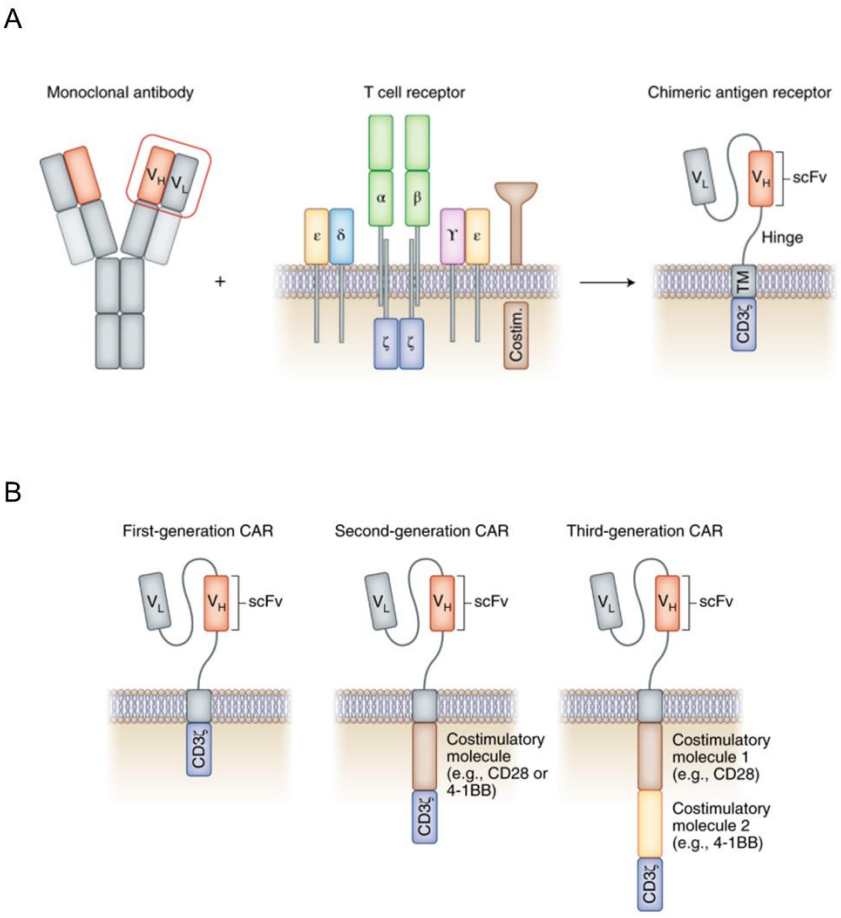

Figure 1.2: Structure and development of CAR-T cells
The specificity of antibodies fused to signaling components of the TCR comprise the fundaments of CAR structures. Throughout time, this concept has evolved to equip T cells with enough signals to improve its activation, proliferation, and persistence. Such efforts led to the key addition of co-stimulatory domains, resulting in second- and third-generation CARs. Currently, the FDA-approved CAR-T cell therapies are second generation CARs targeting hematological cancers. VL, variable light-chain; VH, variable heavy-chain (Majzner & Mackall, 2019).

This recognition domain is anchored to the cell membrane by a hinge and transmembrane domain, often derived from membrane proteins like Cluster of differentiation (CD) CD8 or CD28, to ensure flexibility and length that reduce steric hindrance and facilitate epitope access (Rafiq et al., 2020). The transmembrane domain connects to the intracellular region, which provides the signaling needed for full T cell activation. The most important part of this region is the signaling domain, commonly derived from the cytoplasmic tail of the CD3ζ (CD3 zeta) chain, which contains three immunoreceptor tyrosine-based activation motifs (ITAMs). Upon ITAM phosphorylation, the CAR molecule initiates a T cell receptor (TCR)-like signaling cascade that results in T cell activation (Guirado et al., 2002). This arrangement characterizes the first generation of CAR-T cells. To enhance CAR-T cell proliferation, cytotoxicity, and persistence, second-generation CARs introduced a co-stimulatory domain in the intracellular region. Currently, CAR designs have evolved to third- and fourth-generation CARs, which include two co-stimulatory molecules and an expression cassette for transgenic cytokine production, respectively (Figure 1.2B).

In a clinical setting, CAR-T cell therapy involves isolating T cells from the patient through leukapheresis. These cells are then activated and expanded to reach optimal numbers for gene transfer using a CAR vector. This process is predominantly achieved through viral-based gene delivery, commonly lentiviral transduction. Based on the efficiency of the transduction, CAR-T cells are further expanded and infused back into the patient following lymphodepletion (Stock et al., 2019).

The rapid growth of CAR-T cell research began in the last decade, following a case report by James N. Kochenderfer et al. that described the complete eradication of B-cells and regression of advanced follicular lymphoma in a patient who received a second-generation CAR-T cell regime targeting CD19. This remarkable response led to the first FDA-approved CAR-T cell therapy for pediatric and young adult acute lymphoblastic leukemia (ALL) (Kochenderfer et al., 2010). Today, over five CAR-T cell therapies are approved for various hematological malignancies, demonstrating the unprecedented efficacy of cell-based therapy in these diseases.

1.2.2 Challenges

Despite its impressive efficacy, CAR-T cell therapy remains limited in a range of malignancies, especially solid tumors. The factors underlying the poor outcomes in clinical trials for solid tumors are complex and likely multifactorial (D'Aloia et al., 2018). An important factor is the heterogeneity of solid tumors. Ideally, the target antigen should be uniformly expressed throughout the tumor to avoid relapse. In hematological malignancies, this issue is managed by targeting B-cell lineage antigens, with the adverse effects of B-cell depletion mitigated by intravenous immunoglobulin (Ig) replacement (Brentjens et al., 2011) For solid tumors, however, finding suitable tumor-specific antigens for CAR-T cell therapy is a much greater challenge.

Another obstacle with existing CAR-T therapies is antigen-independent tonic signaling, which causes CAR-T cell dysfunction and chronic activation in the absence of the target. This phenomenon has been linked to structural characteristics of the scFvs used as recognition domains. Studies show that the framework sequence between the complementarity-determining regions (CDRs) within the scFvs can influence CAR stability on the membrane (Fujiwara et al., 2020) Additionally, interactions among CDR loops in the heavy and light chains of scFvs have been found to impair CAR stability and function (Sarén et al., 2023). Altogether, CAR-T cell therapy may offer a valuable opportunity to improve the treatment landscape for various solid tumors, including ovarian cancer, but it requires new technologies to overcome these challenges.

A prominent mechanism of tumor resistance in CAR-T cell therapy is antigen loss. Immune pressure by effector cells often result in reduced antigen expression through various mechanisms such as: 1) downregulation, 2) lineage switching, or 3) emergence of splice variants (Figure 1.3) For instance, data from patients treated with anti-CD19 CAR-T cells for acute lymphoblastic leukemia (ALL) revealed that up to 24% of complete responders experienced relapse, with leukemic cells showing no detectable CD19 expression (Maude et al., 2014). Similarly, a case study of a patient with glioblastoma treated with anti-IL13Rα2 CAR-T cells reported recurrence accompanied by new tumor formations with decreased IL13Rα2 expression (Brown et al., 2016). These findings underscore the urgency to develop

advanced and reliable tools for tumor antigen screening to refine antigen selection and enhance the effectiveness of CAR-T cell therapies.

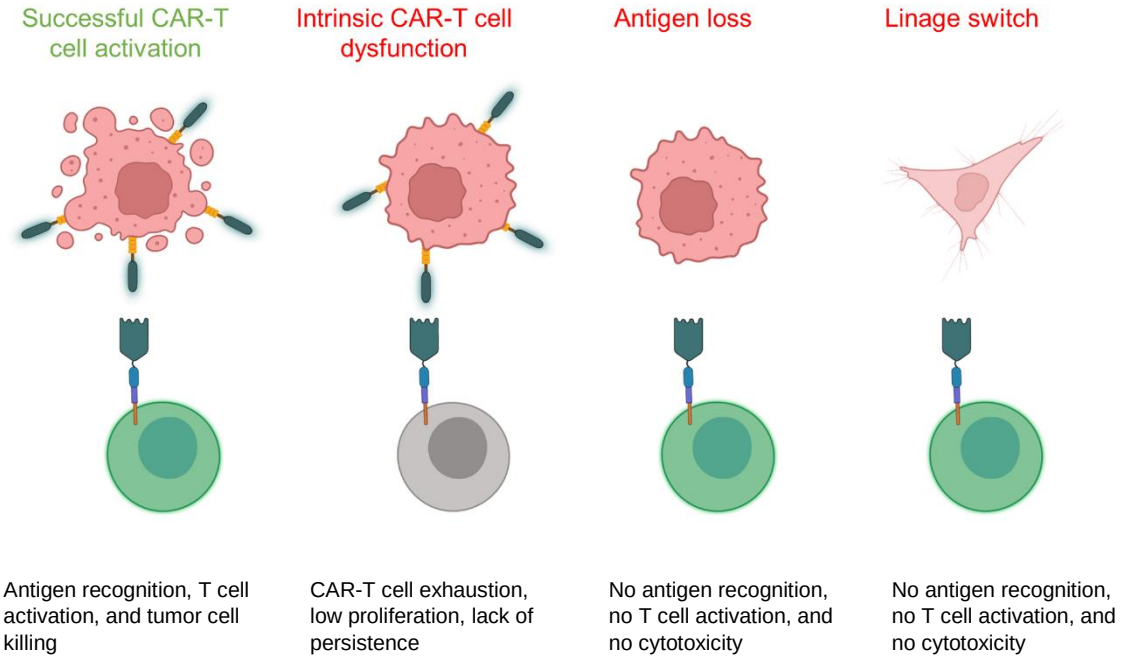

Figure 1.3: Mechanisms of CAR-T cell resistance
CAR-T cell fate illustrated by different factors. Intrinsic T cell factors like exhaustion or lack of persistence resulting in impaired CAR-T cell mediated killing. Tumor cell escape mediated mainly by tumor antigen modulation such as expressing alternative splice variants or complete antigen loss by downregulation or lineage switch. Adopted from (Majzner & Mackall, 2018). Figure created with BioRender.com.

1.2.3 Nanobody-based CAR-T cells

One promising approach to enhancing CAR-T cell therapy involves modifications of recognition domain. Specific properties such as stability, engineering flexibility, and affinity of the recognition moiety can significantly impact CAR-T cell efficacy. This has drawn attention to alternative binding molecules that might improve upon traditional scFvs. Heavy-chain antibodies, a subtype of immunoglobulins found in camelids, have shown potential as effective binding molecules in various applications, including CAR-T cell therapy. These antibodies contain only variable regions, which can be further reduced to their variable heavy chain (VHH) domain, known as nanobodies (Ingram et al., 2018; Xie et al., 2020).

Nanobodies are small (around 15 kDa), stable, and soluble proteins that exhibit high binding affinity for their targets. Additionally, their variable regions show substantial homology to human VH3 family regions, which results in lower immunogenicity compared to murine antibodies (Vincke et al., 2009). Consequently, researchers have developed nanobody-based CAR-T cells for several different tumors, showing promising results compared to traditional scFv-based CAR-T cells (D. Li et al., 2023; Xia et al., 2023). Currently, several clinical trials are investigating the use of nanobody-based CAR-T cells for treating both hematological malignancies and solid tumors. Nanobodies hold significant promise for advancing CAR-T cell therapy by improving antigen targeting and overcoming some limitations of traditional antibodies. Recently, a CAR-T cell bearing two single-domain antibodies was approved for treatment of relapsed or refractory multiple myeloma, highlighting the translational potential of nanobody-based CAR-T cells (Berdeja et al., 2021).

1.3 Ovarian cancer tumor antigen targets

1.3.1 Overview

As previously discussed, epithelial ovarian cancer represents a promising entity for CAR-T cell therapy. This approach is supported by evidence of T cell infiltration within tumors, which correlates with improved progression-free survival (PFS) and overall survival (OS) (Zhang et al., 2003). Conversely, a higher ratio of intratumoral regulatory T cells (Tregs) to effector cells (CD8+, CD4+) is associated with poorer prognosis, underscoring the importance of immune

activity within ovarian cancer (Knutson et al., 2015). However, limitations in CAR-T cell efficacy in ovarian cancer have become more apparent with emerging clinical data. Antigen selection is a critical factor requiring further investigation. Among the antigens targeted so far are Mesothelin (Msln), human epidermal growth factor 2 (HER2), folate receptor alpha (FRα), and epidermal growth factor receptor (EGFR), yet none have demonstrated clinical success as therapeutics (Mitra et al., 2023). This highlights the pressing need for experimental methods and screening tools to identify new tumor targets and optimize existing ones.

1.3.2 Mesothelin

Mesothelin is one of the most extensively targeted proteins in current immunotherapy research. It is overexpressed in various tumors, including ovarian, pancreatic, and lung adenocarcinomas, as well as mesotheliomas (O'Hara et al., 2016; Tang et al., 2013). It is a glycophosphatidylinositol (GPI)-anchored membrane protein. The full-length protein is synthesized as a 71-kDa precursor that undergoes cleavage by the endoprotease furin, resulting in a 40 kDa mature peptide. The cleaved end of the precursor molecule is a soluble protein called megakaryocyte potentiating factor (MPF).

The functionality of mesothelin is not fully understood. Reports of experimental knockout (KO) mice do not show a specific developmental phenotype, and mesothelin absence is not essential for growth in mice (Bera & Pastan, 2000). However, in cancer cells, mesothelin expression is linked to roles in cell adhesion, survival, tumor progression, and metastasis. For instance, higher mesothelin expression in epithelial ovarian cancer correlates with advanced disease and reduced OS (Cheng et al., 2009). This aggressive phenotype may be due to interactions between mesothelin and CA125 (also known as mucin-16; MUC16), a tumor antigen found on serous membranes like the peritoneum and pleura. Msln binding to CA125 promotes heterotypic cell adhesion, potentially facilitating ovarian cancer cell dissemination within the peritoneum (Rump et al., 2004).

Regarding CAR-T cell therapy, there are several ongoing clinical trials targeting mesothelin in different tumors, including ovarian cancer (Table 1.1). Unfortunately, the results thus far indicate limited efficacy and adverse effects, impeding its clinical application (Zhai et al.,

2023). Although generally safe, on-target off-tumor toxicity remains a hurdle in targeting mesothelin. This occurs when CAR-T cells attack mesothelin-expressing healthy cells, and/or when the on-tumor cytotoxicity becomes overwhelming, resulting in cytokine release syndrome (CRS Recently, Andrew R. Haas and colleagues reported two cases of severe pulmonary toxicity following Msln-specific CAR-T cell therapy, leading to one death from grade 5 pulmonary (Haas et al., 2023; X. F. Liu et al., 2024). These outcomes underscore the need for innovative approaches to enhance both the safety and efficacy of mesothelin-specific CAR-T therapies.

Trial ID	Target	Description	Phase	Main Location
NCT03692637	Mesothelin	Mesothelin-targeting CAR NKs for treating ovarian cancer.	Phase I/II	USA
NCT04503980	Mesothelin	Mesothelin-targeting CAR T cells alongside ICI treating ovarian and colorectal cancer.	Phase I/II	USA
NCT03907852	Mesothelin	CAR T cell therapy targets Mesothelin for patients with recurrent ovarian cancer and other solid tumors.	Phase II	USA, Germany
NCT03814447	Mesothelin	Mesothelin-directed fourth generation CAR-T cells to enhance anti-tumor activity in ovarian cancer.	Phase I	China
NCT06051695	Mesothelin	Logic-gated CAR-T cells in ovarian and other cancers.	Phase I/II	USA
NCT02159716	Mesothelin	Mesothelin-targeting CAR-T cell using different cyclophosphamide regimens for ovarian and other solid tumors.	Phase I	USA

Table 1.1: Clinical trials targeting mesothelin in ovarian cancer with CAR-T cells
List of selected ongoing clinical trials registered at the NIH (https://clinicaltrials.gov/). More than 40 clinical trials have been registered for mesothelin-specific CAR-T cell therapy, suggesting mesothelin as promising target for CAR-T cell therapy.

Additionally, different methods have been developed to leverage mesothelin in cancer for predictive and diagnostic applications. Previously, Andrew M. Prantner and colleagues developed and characterized an anti-Mesothelin nanobody (Nb-Msln) for use in various experimental applications (Prantner et al., 2015). The properties of this nanobody enable detection of mesothelin on ovarian cancer cells through multiple laboratory techniques, including flow cytometry, western blot, immunofluorescence, and microscopy. Nb-Msln exhibits a strong binding affinity (Kd = 46 ± 8 nM) toward N-terminus residues of the mature mesothelin, allowing robust and specific detection. Furthermore, Nb-Msln cross-reacts with both human and murine mesothelin, retaining binding capacity in syngeneic mouse models (Prantner et al., 2018). These characteristics suggest Nb-Msln as a promising tool for potential therapeutic exploration in preclinical and clinical settings.

Ongoing research highlights the versatility of anti-Msln nanobodies. For example, Abdennour Benloucif and colleagues recently described anti-Msln nanobodies suitable for imaging applications, which do not interfere with the epitope binding of other mesothelin-targeted drugs, allowing combination therapies or multi-targeting approaches (Benloucif et al., 2023). Additionally, anti-mesothelin nanobodies have been engineered as fusion proteins with recombinant immunotoxins, demonstrating efficacy in tumor cell lysis by directly targeting Mesothelin (Nguyen et al., 2023). These advances underscore the potential of anti-mesothelin nanobodies as versatile tools in cancer diagnostics and therapeutics.

1.3.3 Nectin-2

Another protein that has been studied for its properties and presence in cancer cells is Nectin-2 (also known as CD112). It belongs to a family of four membrane proteins (Nectin-1 to Nectin-4) that share similar structures, and are members of the immunoglobulin superfamily. These proteins mediate homophilic and heterophilic interactions within the Nectin family and with other related molecules (Sakisaka & Takai, 2004). Structurally, Nectin-2 is a type-I surface glycoprotein with three Ig-like extracellular domains, followed by a transmembrane region and an intracellular domain linked to an actin-binding protein called afadin. This structural motif connects Nectin-2 to the cytoskeleton and facilitates cell adhesion through interaction with adaptor molecules (Takai et al., 2008).

Interestingly, Nectin-4 has garnered attention as a promising tumor target for immunotherapies due to its high expression in various malignancies and its association with cancer progression and poor prognosis (Bouleftour et al. 2022). This success has spurred interest in investigating other members of the Nectin family as potential therapeutic targets in cancer.

In addition to its role in cell adhesion, Nectin-2 interacts with immune cells via receptors such as CD226 and TIGIT (T cell immunoreceptor with Ig and ITIM domains) (Rubinstein et al., 2013). These interactions indicate an immunomodulatory function; while binding to TIGIT inhibits natural killer (NK) cell cytotoxicity, interaction with CD226 enhances NK-mediated cytolysis (Bottino et al., 2003; Stanietsky et al., 2009).

Nectin-2 is prominently expressed in breast, pancreatic, and ovarian tumors, with minimal presence in healthy tissues (Bekes et al., 2019). Antibodies developed by Tsutomu Oshima and colleagues successfully inhibited growth and induced specific lysis in Nectin-2-positive ovarian cancer cells (Oshima et al., 2013). Similar efficacy was demonstrated *in vivo* using antibody-drug conjugates (ADC) in mouse xenograft models (Sim et al., 2022). Despite this promise, no clinical trials targeting Nectin-2 are currently registered, and CAR-T cell therapies against this antigen remain unexplored, highlighting its potential as a novel therapeutic target.

1.4 Genome editing

1.4.1 CRISPR-Cas9

Intentional genome modifications have been essential for understanding biological processes throughout time. Various techniques have enabled the manipulation of target DNA sequences for diverse applications. Since the late 20th century, with the introduction of zinc finger nucleases (ZFNs), advancements have continuously expanded into new and promising possibilities (Kim, 2016). The most significant recent development has been RNA-guided genome editing using CRISPR-Cas9.

The clustered regularly interspaced short palindromic repeats (CRISPR)–Cas9 system, unlike zinc finger nucleases (ZFNs), uniquely targets genetic sequences with the use of a

guide RNA molecule, bypassing the complex need to produce fusion proteins. Initially identified as an adaptive immune mechanism in prokaryotic cells, this system defends against foreign DNA by incorporating foreign sequences into CRISPR repeat clusters within the host's genome (Ishino et al., 1987). Interestingly, these repeats contain a conserved set of sequences within the acquired spacers known as protospacer-adjacent motifs (PAMs), which are crucial for the system’s recognition and targeting specificity (Deveau et al., 2008).

This method relies on the endonuclease Cas9, which introduces double-strand breaks (DSBs) at precise DNA locations designated by PAMs. This precision results from a duplex RNA structure composed of CRISPR RNA (crRNA) and trans-activating crRNA (tracrRNA), guiding Cas9 to the target homologous sequence (Deltcheva et al., 2011). An important advancement was the discovery that this complex could be simplified into a single chimeric RNA molecule called single guide RNA (sgRNA) (Jinek et al., 2012).

Initially, CRISPR-Cas9 technology was primarily applied using eukaryotic cells for gene knockouts, revolutionizing functional genomics by enabling precise gene disruption (Cho et al., 2013). Over time, its applications expanded to include knock-ins and other sophisticated genome modifications, broadening its utility across diverse fields (Hryhorowicz et al., 2023).

1.4.2 CRISPR-based gene tagging

One notable application of CRISPR-Cas9 is the knock-in (KI) of transcripts at specific gene loci. Ideally, KIs should be precise and efficient, avoiding unwanted modifications that could disrupt the native protein’s integrity. Various strategies have been developed to insert sequences after CRISPR-Cas9-induced DSBs by manipulating DNA repair pathways (Figure 1.4). In physiological conditions, DSBs are often repaired by non-homologous end joining (NHEJ), creating genetic diversity, as observed in V(D)J recombination (Schatz & Ji, 2011). Alternatively, homology-directed repair (HDR), primarily active during the S phase, enables high-fidelity repairs by copying homologous sequences from a template (San Filippo et al., 2008).

In genome editing, exogenous transcript integration predominantly relies on HDR. However, HDR is restricted to the S/G2 phase of the cell cycle, limiting its availability. HDR is also

slower and less robust than NHEJ, requiring long homology arms that may hinder intended insertions (Z. Mao et al., 2008). Recently, NHEJ has gained attention as a viable alternative for targeted genome editing, as it is active in all cell cycle phases and effective across a variety of cell lines and species (Auer et al., 2014; J. Li et al., 2016; Suzuki et al., 2016).

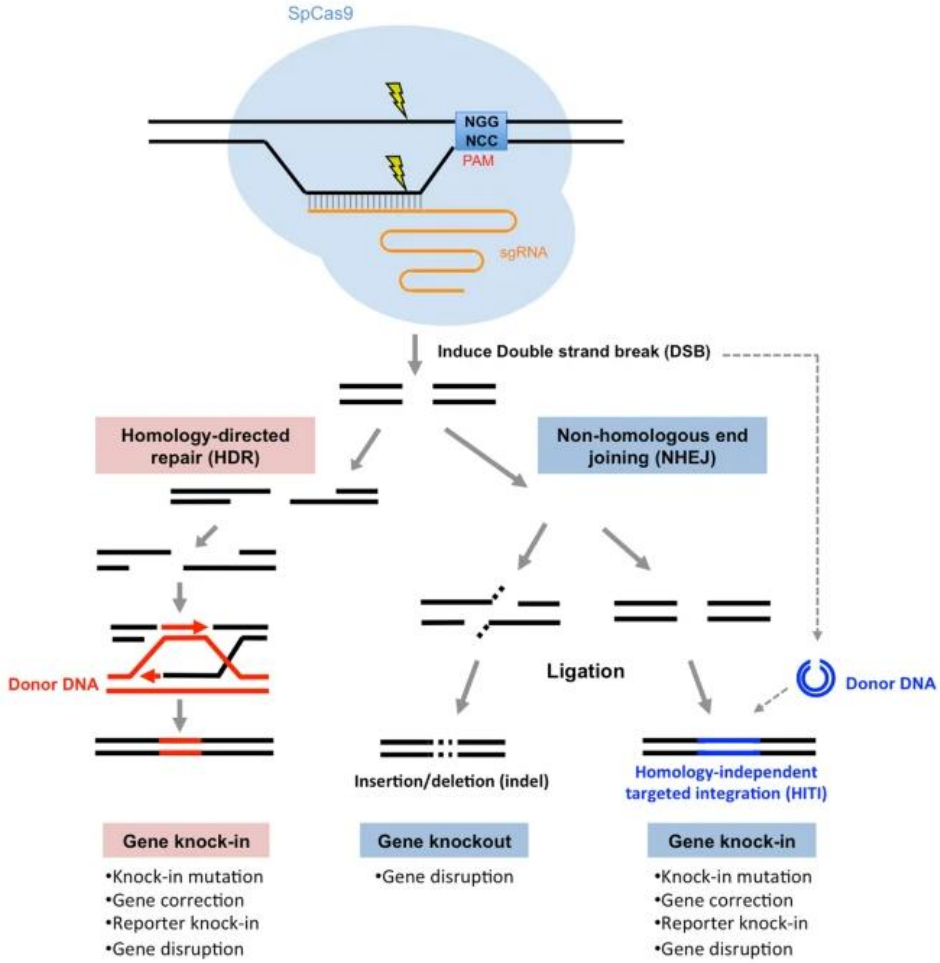

Figure 1.4: CRISPR-mediated repair mechanisms for genome editing
The DSB introduced by Cas9 at an exact location (three bases upstream of the PAM) can be repaired by two main mechanisms: (1) HDR based on a homologous sequence that lead to an error-free, high-fidelity repair, but less abundant and laborious, and (2) NHEJ which is more robust and directly ligates DNA ends, but is prone to introduce unwanted insertions or deletions (indels) (Suzuki & Izpisua Belmonte, 2018).

However, NHEJ can lead to random mutagenesis at the ligation site, resulting in genetic information loss (Deriano & Roth, 2013). Although challenging, these techniques allow the incorporation of foreign molecules, such as epitope tags, into specific genes, that enable specific targeting of endogenous proteins.

1.4.3 The ALFA-Tag

Epitope tagging is widely used for protein manipulation and analysis. This technique produces a fusion protein, where the tag is recognized by a binding molecule, often an antibody. Molecular biology achieves this through expression vectors that encode the epitope tag within the gene of interest, allowing transient or stable expression (Brizzard, 2008). Currently, epitope tags can be introduced into the genomic loci of the protein of interest without disturbing its endogenous regulation, using either HDR- or NHEJ-based approaches.

One example of this methodology is the CRISPR-assisted insertion tagging (CRISPaint) approach to precisely and efficiently tag an endogenous gene of interest (Schmid-Burgk et al., 2016). This strategy has been elegantly adopted by Maike Effern and colleagues to endogenously tag tumor antigens in a melanoma model. This enabled them to do specific adoptive T cell transfer against the modified cells, revealing important insights in tumor escape mechanisms (Effern et al., 2020). However, CRISPaint was primarily design to achieve C-terminusly fusion proteins, which is suboptimal for tagging type I transmembrane receptors or GPI-anchored proteins, the main class of tumor antigen targeted in CAR-T cell therapy.

There are numerous epitope tags, each with unique properties suitable for various experimental needs. For instance, the His-tag facilitates protein purification through metal chelation but performs poorly in immunostaining (Hochuli et al., 1988). Meanwhile, the HA-tag and myc-tag have strong antibody affinities but are derived from existing antigens, increasing their immunogenicity (Evan et al., 1985; Field et al., 1988).

Recent advancements in genomic tagging have resulted in the development of versatile tags that enable broad protein expression with minimal interference, while maintaining strong binding capacities. Recently, Hansjörg Götzke and colleagues developed the innovative

ALFA-tag, which, due to its high alpha-helical content, forms a stable α-helix that supports N- or C-terminus placement (Figure 1.5). The ALFA-tag is hydrophilic and completely synthetic, making it suitable for various assays (Götzke et al., 2019). The tag's binding partner is a high-affinity nanobody (Nb-ALFA), useful for detection, purification, and imaging. Nb-ALFA's impressive affinity towards the ALFA-tag makes it effective even for detecting low-expression target proteins.

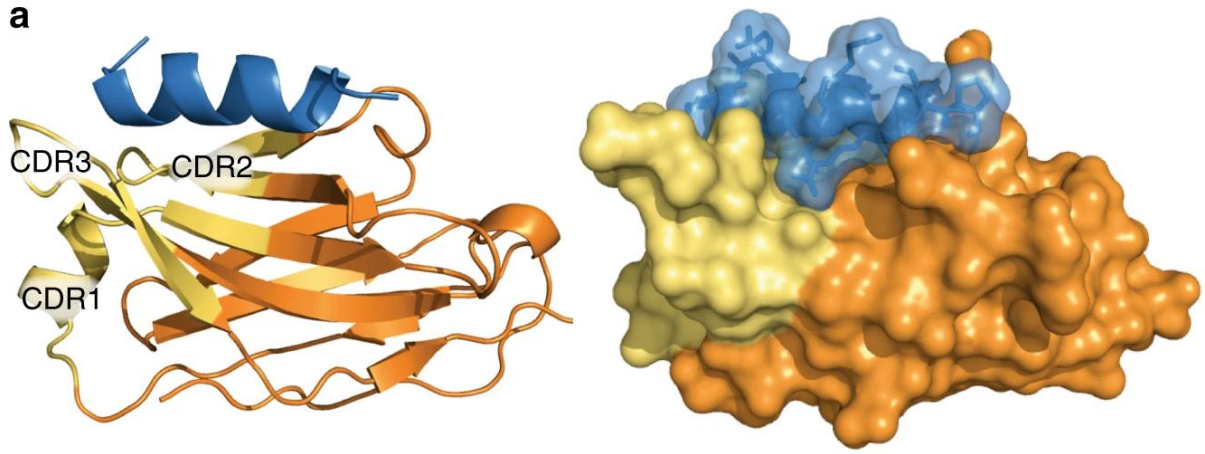

Figure 1.5: Structure of the ALFA-tag
Cartoon illustration (left) or surface representation (right) of the α-helical cylinder formed by the ALFA-tag (blue) in complex with its binding partner, the Nb-ALFA (orange). The CDRs of the Nb-ALFA are highlighted in yellow. Adopted from (Götzke et al., 2019).

1.5 Aims and objectives

In the past two decades, there have been significant advancements in cancer immunotherapies. Specifically, CAR-T cell therapy has transformed cell-based treatments for hematological malignancies. Consequently, various CAR-T cell strategies have been developed to target solid tumors, including ovarian cancer. Unfortunately, many of these efforts have not significantly improved patient prognosis, commonly due to tumor escape mechanisms like antigen loss.

There is an inherent need for new experimental platforms that facilitate the antigen selection process for CAR-T cell therapy. This would simplify the laborious need to repetitively produce antigen-specific CAR-T cells, which heavily rely on trial-and-error approaches.

Therefore, we aimed to develop an experimental platform for antigen screening by inserting an epitope tag that enables targeting using a unique nanobody-based CAR-T cell. This platform requires precise genomic modification of tumor antigens, allowing for insertions at various positions beyond the C-terminus, as the majority of CAR-T cell targets are inaccessible at such intracellular sites.

This would enable direct, side-by-side comparisons of different tumor antigens using the same CAR-T cell. Furthermore, we aimed to apply the results of this platform by producing and comparing CAR-T cells specific against the native antigens is needed. Additionally, we aimed at leverage the versatility of this platform in order to interrogate the importance of affinity in the functionality of CAR-T cell.

In summary, the experiments performed in this PhD dissertation are directed to reach the following aims:

1. Develop a CRISPR-Cas9-based endogenous tagging strategy that allows for the insertion of an epitope tag at any location within a tumor antigen gene.
2. Generate a nanobody-based CAR-T cell containing the epitope tag’s binding partner as the recognition domain and compare its functionality against tumor cells expressing endogenously tagged antigens.

3. Produce CAR-T cells targeting the specific native antigens used in the screening platform to validate its predictive potential.
4. Leverage the nanobody-based CAR-T cell platform to investigate the impact of the antigen-binding affinity on CAR-T cell functionality.

2 Materials and methods

2.1 Materials

2.1.1 Laboratory Equipment

Table 2.1: Overview of instruments

General laboratory equipment	Company
4D-Nucleofector® 96-well Unit	Lonza
Aurora spectral flow cytometer	Cytek®
Axio Vert A1 Microscope	Zeiss
Biacore™ 8K	Cytiva
Centrifuge (5417R/5810)	Eppendorf
CoolCell™ LX Cell Freezing Container	Corning®
Countess 3 Automatic Cell Counter	Thermo Fisher Scientific
FACS ARIA III	BD Biosciences
FACS Aria™ Fusion V	BD Biosciences
FACS LSR Fortessa	BD Biosciences
GelStick IMAGER Touch	INTAS Science Imaging Instruments
Heraeus® microbiological incubator	Thermo Fisher Scientific
ID7000™ Spectral Cell Analyzer (5 lasers)	Sony
ID7000™ Spectral Cell Analyzer (7 lasers)	Sony
MA900 Multi-Application Cell Sorter	Sony
Mini Trans-Blot® Cell	Bio-Rad
Mini-PROTEAN® Tetra Cell Systems	Bio-Rad
NanoDropTM 2000	Thermo Fisher Scientific
Odyssey® DLx Imaging system	LI-COR® Biosciences
PerfectBlue™ Horizontal Midi Gel System	VWR
Pipetboy pipetting aid	Integra Biosciences
PIPETMAN Classic™	Gilson™

Power Source	VWR, Avantor
PowerPacTM Basic Power Supply	Bio-Rad
T100™ Thermal Cycler	Bio-Rad
xCELLigence RTCA DP	Agilent

2.1.2 Consumables and plastics

Table 2.2: Overview of consumables and plastics

Consumables and plastics	**Company**
Blotting paper	VWR
Cell culture plate (6-, 12-, 24-, and 96-well, flat-bottomed)	Sarstedt
Cell culture plate (96-well, U-bottomed)	Greiner Bio-One
Cryo vials (CryoPure, 1.8 mL)	Sarstedt
DNA spin columns	Centic Biotec
FACS tubes	Sarstedt
Gloves (Peha-soft nitrile white)	Hartmann AG
Nitrocellulose membrane (pore size: 0.2 µm)	GE Healthcare
Parafilm® M	Amcor
Pasteur glass pipettes	VWR
PCR adhesive seals	Sarstedt
PCR plate, 96-well, standard	Thermo Fisher Scientific
PCR stripes and lids (8-well)	Axygen
Petri dishes	Sarstedt
Pipette tips, TipOne®	Star Lab
Reaction tubes (1-5, 2.0, 5 mL)	Eppendorf
Reaction tubes (15, 50 mL)	Sarstedt

RTCA E-Plate 16-well	Agilent
Series S Sensor Chip SA	Cytiva
Serological pipettes (5,10 and 25 mL)	Greiner Bio-One, Corning® Costar Stripettes
Syringe (1 mL, 5 mL)	B.Braun
Syringe pore filter, 0.45 µm	VWR
TC flask T-25, T-75, T-175	Sarstedt
Zymo Spin IIIC columns	Zymo Research

2.1.3 Chemicals and reagents

Table 2.3: Overview of chemicals and reagents

Chemicals and reagents	**Supplier**
2-Mercaptoethanol	Gibco – Life Technologies
Agar-agar	Carl Roth
Agarose	Carl Roth
All-in-One cDNA SuperMix	Biotool
Ampicillin	Carl Roth
Anti-PE MicroBeads	Miltenyi Biotec
GolgiPlug™ (Brefeldin A)	BD Biosciences
GolgiStop™ (Monensin)	BD Biosciences
Bovine serum albumin fraction V	Carl Roth
Broad Range Molecular Weight Markers	Santa Cruz Biotechnologies
Bromophenol blue	Carl Roth
DAPI	Thermo Fisher Scientific
Dimethyl sulfoxide (DMSO)	Carl Roth or Sigma-Aldrich
Dithiothreitol	Carl Roth
Dulbecco´s phosphate-bufferd	Gibco – Life Technologies

DNase-I	Roche or Sigma-Aldrich
dNTPs	Thermo Fisher Scientific
Ethanol	Carl Roth
FuGENE ® HD transfection reagent	Promega
Glycerol	Carl Roth
H2O Ampuwa	Fresenius
HEPES	Carl Roth
Ionomycin	Sigma-Aldrich
Interleukin-15 (IL-15), human	PeproTech
Interleukin-15 (IL-15), murine	PeproTech
Interleukin-2 (IL-2), human	PeproTech
Interleukin-2 (IL-2), murine	PeproTech
Interleukin-7 (IL-7), human	PeproTech
Interleukin-7 (IL-7), murine	PeproTech
Isopropyl alcohol	Carl Roth
LB-Medium (Lennox)	Carl Roth
Lenti-X™ Concentrator	Takara
LIVE/DEAD Fixable Aqua Staining kit	Thermo Fisher Scientific
LIVE/DEAD Fixable Blue Staining kit	Thermo Fisher Scientific
LIVE/DEAD Fixable NIR Staining kit	Thermo Fisher Scientific
Magnesium chloride	Carl Roth
Methanol	Carl Roth
p-formaldehyde, 37%	Carl Roth
Phorbol 12-myristate 13-acetate	Sigma-Aldrich
Potassium chloride	Carl Roth
Potassium phosphate	Carl Roth
Powdered milk	Carl Roth
Puromycin	Sigma-Aldrich
Red Blood Cell Lysing Buffer	Sigma-Aldrich

RetroNectin®	Takara
Retro-X™ Concentrator	Takara
RLT buffer	Qiagen
Roti®Histofix 4% Formaldehyde	Carl Roth
Rotiphorese®Gel 30 (37.5:1)	Carl Roth
RW1 buffer	Qiagen
Sodium azide	Carl Roth
Sodium chloride	Carl Roth
Sodium dodecyl sulphate	Carl Roth
Sodium hydroxide	Carl Roth
Tetramethylehtylenediamine	Carl Roth
Tris	Carl Roth
Triton X-100	Sigma-Aldrich
Trypan blue	Sigma-Aldrich
Tween-20	Carl Roth
Zymo RNA wash buffer	Zymo Research

2.1.4 Solutions and buffers

Table 2.4: Overview of solutions and buffers

Solutions and Buffers	**Formulation**
Annealing buffer	100 mM NaCl 50 mM HEPES 7.4 pH In H_2O
Blotting buffer (1x)	25 mM TRIS 192 mM Glycine 20% Methanol in H2O
BSA blocking buffer	50 g/l Albumin Fraction V

	in TBS-T
Direct lysis buffer	10 mM Tris-HCl 1 mM CaCl2 1 mM MgCl2 1 mM EDTA 1% Triton X 100
FACS buffer	DPBS 10% FCS 0.2 mM EDTA
HBS buffer (2x)	274 mM NaCl 10 mM KCl 1.4 mM Na2HPO4 15 mM D-Glucose in H2O, pH 7.05 (titration with NaOH)
Histofix	4% formaldehyde
Laemmli buffer (1x)	120 mM 1 M Tris-HCl pH 6.8 20% Glycerol 4% SDS 20 mM β-Mercaptoethanol 0.02% Bromophenol-blue
LB agar	20 g/l LB 15 g/l Agar in H2O
LB medium	20 g/l LB in H2O
Milk blocking buffer	50 g/l powdered milk in TBS-T
Plasmid miniprep buffer N3	4.2 M Guanidine Hydrochloride

	0.9 M Potassium acetate in H2O, pH 4.8
Plasmid miniprep buffer P1	50 mM Tris-HCl 10 mM EDTA 100 µg/mL RNAse A in H2O, pH 8.0
Plasmid miniprep buffer P2	200 mM NaOH 1% SDS in H2O
Plasmid miniprep buffer PE	10 mM Tris-HCl 80% Ethanol in H2O
Running buffer (10x)	25 mM TRIS 192 mM Glycine 0.1% SDS in H2O
SPR Running buffer	10 mM HEPES pH 7.4 200 mM NaCl 0.5 mM ADP 0.5 TCEP 2 mM $MgCl_2$ 1 g/L carboxymethyl dextran 0.05% Tween20 2% DMSO
TAE buffer (1x)	40 mM Tris pH 8.0 20 mM Acetic acid 1 mM EDTA in H2O
TBS buffer (10x)	30 g/l Tris base

	80 g/l NaCl in H2O, pH 7.6 (titration with HCl)
TBS-T buffer	10% TBS buffer (10x) 0.05% Tween-20 in H2O
Tris (1 M, pH 6.8)	121.1 g/l Tris base in H2O, pH 6.8 (titration with HCl)
Tris (1 M, pH 8.8)	121.1 g/l Tris base in H2O, pH 8.8 (titration with HCl)

2.1.5 Enzymes for molecular biology

Table 2.5: Overview of enzymes for molecular biology

Enzymes	**Company**
Proteinase K	Qiagen
PureLinkTM RNase A	Invitrogen
Phusion® High-Fidelity DNA Polymerase	New England Biolabs
Restriction enzymes: AccI	New England Biolabs
Restriction enzymes: BamHI	New England Biolabs
Restriction enzymes: BbsI-HF,	New England Biolabs
Restriction enzymes: BsaI-HFv2	New England Biolabs
Restriction enzymes: EcoRI	New England Biolabs
Restriction enzymes: FseI	New England Biolabs
Restriction enzymes: HindIII-HF	New England Biolabs
Restriction enzymes: MluI	New England Biolabs
Restriction enzymes: NotI	New England Biolabs
Restriction enzymes: SacII	New England Biolabs
Restriction enzymes: SpeI	New England Biolabs
RNAse A	Life Technologies

T4 DNA Ligase	New England Biolabs

2.1.6 Oligonucleotides

Table 2.6: Overview of oligonucleotides

Name	Oligonucleotides (5’ - 3’)	Application
cDNA_ALFA1.6_Fwd1	AAGAAGACTGACCGAACCTGC	Sanger Sequencing
cDNA_ALFA1.6_Rev1	CCTCCTCGAGACGGCTAGG	Sanger Sequencing
cDNA_ALFA1.6_Rev2	TTCTCAGCTCCTCCTCGAGAC	Sanger Sequencing
M13 Forward	TGTAAAACGACGGCCAGT	Sanger Sequencing
M13 Reverse	CAGGAAACAGCTATGAC	Sanger Sequencing
M13/pUC Forward	CCCAGTCACGACGTTGTAAAACG	Sanger Sequencing
M13/pUC Reverse	AGCGGATAACAATTTCACACAGG	Sanger Sequencing
Mouse_P2AFWR_Seq	CTACCAACTTCAGTCTGCT	Sanger Sequencing
Mouse_RQR8 FWR	GAATTCGCCACCATGGCCTCACCGTTGACCC	Sanger Sequencing
MSCV_Univ_FWR	CTTTAACCGAGACCTCATCA	Sanger Sequencing
NbMsln A1_MluI_PCR_Rev	ACGCGTAGATGAGGAGACGGTGACCTG	Sanger Sequencing
NbMsln A1_NotI_PCR_Fwd	GAAGCTGCGGCCGCTCAGGTCCAGTTGGTTGAG	Sanger Sequencing

pGEX 3'	CCGGGAGCTGCATGTGTCAGAGG	Sanger Sequencing
pRS-marker	CGGCATCAGAGCAGATTGTA	Sanger Sequencing
Seq_Mm_Nec2_i1_Fwd	GTGGTTGCTGGGATTTGAAC	Sanger Sequencing
Seq_Mm_Nec2_i1_Fwd 2	GCTGAGCCATCTCACCAG	Sanger Sequencing
Seq_Mm_Nec2_i2_Rev	GATTCCCAAGAGTTGTCTTCTG	Sanger Sequencing
Seq_Msln_e12_Rev	TGGATCAGGGACTCAGGATAG	Sanger Sequencing
Seq_Msln_e13_Rev	GGGCTGAAGTCACATAGATAGC	Sanger Sequencing
Seq_Msln_e8_Frw	AGGTTCTGAGGAGTGGAAGA	Sanger Sequencing
Seq_Msln_e9_Frw	AGTCCATCGTCCAGAGCATCCC	Sanger Sequencing
sgRNA_Msln_i9_1_TS	CACCTGACACTCAACTCACTACGC	Sanger Sequencing
sgRNA_Mus_Msln_i10_3_BS	AAACCTTATCCCTACTGTCCCATC	Endogenous Tagging
sgRNA_Mus_Msln_i10_3_TS	CACCGATGGGACAGTAGGGATAAG	Endogenous Tagging
sgRNA_Mus_Msln_i9_1_BS	AAACGCGTAGTGAGTTGAGTGTCAA	Endogenous Tagging
sgRNA_Mus_Msln_i9_1_TS	CACCTGACACTCAACTCACTACGC	Endogenous Tagging

sgRNA_Mus_Msln_i9_2_BS	AAACAGCAGCCTCAAAGCCAGGCT	Endogenous Tagging
sgRNA_Mus_Msln_i9_2_TS	CACCAGCCTGGCTTTGAGGCTGCT	Endogenous Tagging
sgRNA_Mus_Nectin2_i1.1_BS	AAACCCTACGTTATACAGGGTCTCACT	Endogenous Tagging
sgRNA_Mus_Nectin2_i1.1_TS	CACCAGTGAGACCCTGTATAACGT	Endogenous Tagging
sgRNA_Mus_Nectin2_i1.2_BS	AAACTCGACTGACCTACGTTATAC	Endogenous Tagging
sgRNA_Mus_Nectin2_i1.2_TS	CACCGTATAACGTAGGTCAGTCGA	Endogenous Tagging
sgRNA_Mus_Nectin2_i2.1_BS	AAACTAGGACACGGAGAAATAGCC	Endogenous Tagging
sgRNA_Mus_Nectin2_i2.1_TS	CACCGGCTATTTCTCCGTGTCCTA	Endogenous Tagging
sgRNA_Mus_Nectin2_i2.2_BS	AAACACACATTAAAGATGGTCAAC	Endogenous Tagging
sgRNA_Mus_Nectin2_i2.2_TS	CACCGTTGACCATCTTTAATGTGT	Endogenous Tagging

2.1.7 Vectors and plasmids

Table 2.7: Overview of vectors and plasmids

Vector and plasmids	**Origin/ Source**
Gag-pol	Gift from Eicke Latz
Mouse_pMSCV_ALFA_#10_P2A_FLAGtag	Generated during this study
Mouse_pMSCV_ALFA_#4_P2A_FLAGtag	Generated during this study
Mouse_pMSCV_ALFA_#8_P2A_FLAGtag	Generated during this study

Mouse_pMSCV_ALFA_#9_P2A_FLAGtag	Generated during this study
Mouse_pMSCV_ALFA_WT_P2A_FLAGtag	Generated during this study
pcDNA3.1_ALFA_Msln_1.1	Generated during this study
pcDNA3.1_ALFA_Msln_1.2	Generated during this study
pcDNA3.1_ALFA_Msln_1.3	Generated during this study
pcDNA3.1_ALFA_Msln_1.4	Generated during this study
pcDNA3.1_ALFA_Msln_1.5	Generated during this study
pcDNA3.1_ALFA_Msln_1.6	Generated during this study
pHEN6_VHH_MSLN_NbA1_LPETG_His	Gift from Nanobody Core Facility Bonn
pMSCV_NbALFA_CD28_CD3z_P2A_RQR8	Generated during this study
pMSCV_NbMsln(A1)_CD28_CD3z_P2A_RQR8	Generated during this study
pMSCV_NbNec2(H6)_CD28_CD3z_P2A_RQR8	Generated during this study
pRP233_GFP	Gift from Eicke Latz
pUCIDT-AMP-Donor_ER_Msln_ALFAtagged_i9.1_i10.2	Integrated DNA Technologies (IDT)
pUCIDT-AMP-Donor_ER_Msln_ALFAtagged_i9.1_i10.3	Integrated DNA Technologies (IDT)
pUCIDT-AMP-Donor_ER_Nec2_ALFAtagged_i1.1_i2.2	Integrated DNA Technologies (IDT)
pUCIDT-AMP-Donor_ER_Nec2_ALFAtagged_i1.2_i2.1	Integrated DNA Technologies (IDT)
px330-EGFP	Generated during this study
px330-EGFP_MslnALFA_BbsI i9.2_BsaI i10.2	Generated during this study
px330-EGFP_MslnALFA_BbsI i9.2_BsaI i10.3	Generated during this study

px330-EGFP_Nec2ALFA_BbsI i1.1_BsaI i2.1	Generated during this study
px330-EGFP_Nec2ALFA_BbsI i1.2_BsaI i2.2	Generated during this study
px333	Addgene plasmid #64073
px458	Addgene plasmid #62988
VSV-G	Gift from Eicke Latz

2.1.8 Commercially available kits

Table 2.8: Overview of commercially available kits

Name	Company
Canvax CleanEasy™ Mini Spin Columns	Canvax Biotech
Cytofix/Cytoperm™ Fixation/Permeabilization Kit	BD Biosciences
DNeasy® Blood & Tissue Kit	Qiagen
MEGAquick-spinTM Plus Total Fragment DNA Purification Kit	iNtRON Biotechnology
NucleoSpin® RNA kit	Macherey-Nagel
PureLinkTM HiPure Plasmid Midiprep Kit	Life Technologies
QIAquick Gel Extraction Kit	Qiagen
QuadroMACS™ Separator Kit	Miltenyi Biotec
SG Cell Line 4-D Nucleofector™ X Kit S	Lonza

2.1.9 Cell culture medium and supplements

Table 2.9: Overview of cell culture medium and supplements

Solution	Composition
Complete DMEM cell culture medium	DMEM 10% FBS 100 U/mL Penicillin 100 µg/mL Streptomycin 2 mM L-glutamine
Complete RPMI cell culture medium	RPMI1640 + GlutaMAX™ 10% FBS 100 U/mL Penicillin 100 µg/mL Streptomycin
Freezing Medium	Complete cell culture medium 10% DMSO
T cell activation medium	RPMI1640 + GlutaMAX™ 10% FBS 100 U/mL Penicillin 100 µg/mL Streptomycin 10 mM NEAA 1 mM HEPES 2 µM β-Mercaptoethanol 100 U/mL recombinant IL-2 2 µg/mL anti-mouse CD28

T cell maintenance medium	RPMI1640 + GlutaMAX™ 10% FBS 100 U/mL Penicillin 100 µg/mL Streptomycin 10 mM NEAA 1 mM HEPES 2 µM β-Mercaptoethanol 10 ng/mL recombinant IL-7 10 ng/mL recombinant IL-15

2.1.10 Cell lines and organisms

Table 2.10: Overview of cell lines and organisms

Cell lines / Organism	Origin / Source
Chemically competent Escherichia coli DH10β	Gifted by Veit Hornung, University Hospital Bonn
Human: HEK293T	Human immortalised embryonic kidney cell line, ATCC CRL-3216.
Human: Platinum-E (Plat-E) HEK293T	Human immortalised embryonic kidney cell line containing packaging retroviral genes. Kindley provided by Dr. Florian Schmidt
Mouse: C57BL/6J	Acquired from Charles River
Mouse: ID8 ovarian cancer	Mouse ovarian surface epithelial cell line frequently. Kindly provided by Winfried Barchet.
Mouse: ID8.p33 MslnALFA monoclone F5	*Msln* endogenously ALFA-tagged ID8.p53 sub-clone cell line.
Mouse: ID8.p53 ALFA-tag overexpression	Surface overexpression of the ALFA-tag on ID8.p53 cells

Mouse: ID8.p53 MslnALFA monoclone 1A3	*Cd112* endogenously ALFA-tagged ID8.p53 sub-clone cell line.
Mouse: ID8.p53 MslnALFA monoclone 1D2	*Cd112* endogenously ALFA-tagged ID8.p53 sub-clone cell line.
Mouse: ID8.p53 MslnALFA monoclone 1E7	*Cd112* endogenously ALFA-tagged ID8.p53 sub-clone cell line.
Mouse: ID8.p53 MslnALFA monoclone 1E8	*Cd112* endogenously ALFA-tagged ID8.p53 sub-clone cell line.
Mouse: ID8.p53 MslnALFA monoclone 2A3	*Cd112* endogenously ALFA-tagged ID8.p53 sub-clone cell line.
Mouse: ID8.p53 MslnALFA monoclone 2B8	*Cd112* endogenously ALFA-tagged ID8.p53 sub-clone cell line.
Mouse: ID8.p53 MslnALFA monoclone 2B9	*Cd112* endogenously ALFA-tagged ID8.p53 sub-clone cell line.
Mouse: ID8.p53 MslnALFA monoclone 2G10	*Cd112* endogenously ALFA-tagged ID8.p53 sub-clone cell line.
Mouse: ID8.p53 MslnALFA monoclone 2G11	*Cd112* endogenously ALFA-tagged ID8.p53 sub-clone cell line.
Mouse: ID8.p53 MslnALFA monoclone B6	*Msln* endogenously ALFA-tagged ID8.p53 sub-clone cell line.
Mouse: ID8.p53 MslnALFA monoclone B8	*Msln* endogenously ALFA-tagged ID8.p53 sub-clone cell line.
Mouse: ID8.p53 MslnALFA monoclone C10	*Msln* endogenously ALFA-tagged ID8.p53 sub-clone cell line.
Mouse: ID8.p53 MslnALFA monoclone C3	*Msln* endogenously ALFA-tagged ID8.p53 sub-clone cell line.
Mouse: ID8.p53 MslnALFA monoclone E11	*Msln* endogenously ALFA-tagged ID8.p53 sub-clone cell line.

Mouse: ID8.p53 MslnALFA monoclone E7	*Msln* endogenously ALFA-tagged ID8.p53 sub-clone cell line.
Mouse: ID8.p53 MslnALFA monoclone F6	*Msln* endogenously ALFA-tagged ID8.p53 sub-clone cell line.
Mouse: ID8.p53 MslnALFA monoclone F8	*Msln* endogenously ALFA-tagged ID8.p53 sub-clone cell line.
Mouse: ID8.p53 MslnALFA monoclone G10	*Msln* endogenously ALFA-tagged ID8.p53 sub-clone cell line.
Mouse: ID8.p53 MslnALFA monoclone G5	*Msln* endogenously ALFA-tagged ID8.p53 sub-clone cell line.
Mouse: ID8.p53 MslnALFA polyclonal	*Msln* endogenously ALFA-tagged ID8.p53 cells.
Mouse: ID8.p53 MslnALFA polyclonal	*Cd112* endogenously ALFA-tagged ID8.p53 cells.
Mouse: ID8.p53 ovarian cancer	ID8 mutated p53 clone. ovarian surface epithelial cell line that has a p53 mutation (Y217C). Generated by Wibke Rüdiger.

2.1.11 Antibodies

Table 2.11: Overview of antibodies and soluble peptides

Antibody / Clone	**Application**	**Company**
Ultra-LEAF Purified anti-mouse CD28 / 37.51	Activation	BioLegend
Ultra-LEAF Purified anti-mouse CD3 / 17A2	Activation	BioLegend
Anti-human CD34 (PE) / QBEND/10	Flow Cytometry	Invitrogen

Anti-mouse CD112 (nectin-2) / 829038	Flow Cytometry	BD Biosciences
Anti-mouse CD11b (PerCP Cy5.5) / M1/70	Flow Cytometry	BioLegend
Anti-mouse CD11c (BV570) / N418	Flow Cytometry	BioLegend
Anti-mouse CD19 (AF700) / 6D5	Flow Cytometry	BioLegend
Anti-mouse CD3 (APC) / 27A2	Flow Cytometry	BioLegend
Anti-mouse CD3 (BV650) / 17A2	Flow Cytometry	BioLegend
Anti-mouse CD4 (APC Cy7) / GK1.5	Flow Cytometry	BioLegend
Anti-mouse CD4 (BUV805) / GK1.5	Flow Cytometry	BioLegend
Anti-mouse CD4 (PerCP) / RM4-5	Flow Cytometry	BioLegend
Anti-mouse CD44 (BV510) / IM7	Flow Cytometry	BioLegend
Anti-mouse CD45.2 (BUV395) / 104	Flow Cytometry	BioLegend
Anti-mouse CD49b (Pacific Blue) / DX5	Flow Cytometry	BioLegend
Anti-mouse CD62L (BUV737) / MEL-14	Flow Cytometry	BioLegend
Anti-mouse CD8α (BV421) / 53-6.7	Flow Cytometry	BioLegend

Anti-mouse CD8α (BV805) / 53-6.7	Flow Cytometry	BioLegend
Anti-mouse Granzyme B (AF647) / GB11	Flow Cytometry	BioLegend
Anti-mouse IFN-g (APC) / MP6-XT22	Flow Cytometry	BioLegend
Anti-mouse IFN-g (BV711) / XMG1.2	Flow Cytometry	BioLegend
Anti-mouse Ly6C (BV605) / HK1.4	Flow Cytometry	BioLegend
Anti-mouse Ly6G (PE) / 1A8	Flow Cytometry	BD Biosciences
Anti-mouse TNF-a (APC) / MP6-XT22	Flow Cytometry	BioLegend
Anti-mouse TNF-a (PerCP Cy5.5) / MP6-XT22	Flow Cytometry	BioLegend
FITC-ALFA peptide	Flow Cytometry	Biomatik
Nanobody anti-ALFA-Tag (AF488)	Flow Cytometry	Nanobody Core Facility Bonn
Nanobody anti-ALFA-Tag (Biotin)	Flow Cytometry	Nanobody Core Facility Bonn
Nanobody anti-mesothelin A1 (Biotin)	Flow Cytometry	Nanobody Core Facility Bonn
Nanobody anti-mesothelin C6 (Biotin)	Flow Cytometry	Nanobody Core Facility Bonn
Nanobody anti-nectin2 H6 (Biotin)	Flow Cytometry	Nanobody Core Facility Bonn
IRDye® Donkey anti-Rabbit (800CW)	Western Blot	LICORbio™

IRDye® Goat anti-Mouse (700CW)	Western Blot	LICORbio™
IRDye® Streptavidin (800CW)	Western Blot	LICORbio™
Mouse anti-human β-Actin / C4	Western Blot	Santa Cruz Biotechnologies
Nanobody anti-ALFA-Tag (Biotin)	Western Blot	Nanobody Core Facility Bonn
Rabbit anti-human β-Actin / 13E5	Western Blot	Cell Signaling Technology
Recombinant anti-ALFA mouse-FC / 1G5	Western Blot	NanoTag

2.1.12 Software and algorithms

Table 2.12: Overview of software and algorithms

Software and algorithms	Company / Source
AlphaFold Server 3	Google DeepMind
Alt-R™ CRISPR Custom Guide RNAs	IDT
Benchling (Biology Software)	Benchling
BioRender	www.biorender.com
FACS Diva	BD
FlowJo v10.7.1	Tree Star, Inc.
GPP sgRNA Designer	BROAD Institute
Graphpad prism v10	GraphPad
Image Studio™	LI-COR®
Microsoft Office	Microsoft
PyMOL Molecular Graphics System	Schrödinger, LCC
RTCA Software Pro	Agilent

SnapGene Viewer	GSL Biotech LLC
SpectroFlo®	Cytek
Zen Software	Carl Zeiss

2.2 Methods

2.2.1 Molecular cloning techniques for endogenous tagging

2.2.1.1 Restriction enzyme digest

All plasmid modifications in this study were performed using restriction enzyme-based cloning. Plasmid DNA (10 µg) was digested by incubating with 10 U of corresponding restriction enzyme at 37 °C for 4-8 hours. For PCR amplification products, the reaction setup remaind the same, but the incubation time was reduced 2-4 hours. Reactions were stabilized using buffers recommended by the manufacturer to reach high enzymatic activity.

2.2.1.2 Gel electrophoresis

Processed DNA fragments (>100 bp) were analyzed by gel electrophoresis. For each sample, 6x gel loading buffer was mixed with the DNA products. Size-dependent separation was performed in 0.7%, 1%, or 2% agarose gels, depending on the fragment size, with DYBR green dye added for DNA staining. Electrophoresis was conducted at 140 V for 30 minutes. Visualization of DNA-stained gels was achieved using SafeBlue fluorescence system and recorded with the GelStick IMAGER instrument. GeneRuler 1 kb or 100 bp DNA ladders were used as molecular size references.

2.2.1.3 Oligonucleotide annealing

Oligonucleotides were diluted in H_2O to a final concentration of 100 µM. For annealing matching sgRNA oligonucleotides, 1 µl each of the top- and bottom-strand oligonucleotide was mixed in a total volume of 50 µl annealing buffer (100 mM NaCl, 50 mM HEPES in H_2O; pH 7.4). The annealing reaction was performed in a thermocycler using the following conditions:

90 °C	5x Phusion HF Buffer
70 °C	dNTPs (10 mM)
69 °C	1 min (decrease by 1 °C / min until RT
12 °C	-

2.2.1.4 Ligation

Ligation was achieved by mixing matching inserts and linearized plasmids according to the formula recommended by the manufacturer:

Required mass insert (g) = desired insert/vector molar ratio x mass of vector (g) x ratio of insert to vector lengths

Linearized plasmid DNA (50 ng) and the calculated mass of the insert were incubated with 2 µl of 10x T4 DNA ligase buffer and 1 µl of T4 DNA ligase in a total reaction volume of 10 µl. The reaction was carried out overnight at 16 °C.

2.2.1.5 Two-Step Restriction and Ligation for sgRNA Oligonucleotides

For ligating annealed sgRNA oligonucleotides into the px333-EGFP plasmid, a two-step restriction and ligation process was performed:

- Step 1:

100 ng of BbsI-digested px333-EGFP plasmid was mixed with 1 µl of the corresponding annealed oligonucleotides, 1 µl of T4 DNA ligase, and the appropriate buffer in a 10 µl reaction.

The reaction was incubated overnight at 16 °C.

- Step 2:

The ligated plasmid from Step 1 was digested with BsaI under standard reaction conditions.

The resulting digested plasmid was then incubated with the corresponding annealed oligonucleotides, 1 µl of T4 DNA ligase, and the appropriate buffer in a 10 µl reaction, following the same protocol as Step 1.

2.2.1.6 Transformation

Chemically competent *Escherichia coli* DH10β 50 µl aliquots were thawed on ice and mixed with 5 µl of the ligation reaction. The mixture was incubated for 5 minutes on ice, followed by a 45 second heat shock at 42 °C. The mixture was immediately placed on ice and incubated for 5 minutes before streaked onto LB agar plates containing 100 µl/mL ampicillin. To allow for bacteria growth, the plates were incubated overnight at 37 °C.

2.2.1.7 Plasmid preparation

For small-scale plasmid preparations (miniprep), 2 ml of LB broth containing 100 µg/ml ampicillin was inoculated with a single E. coli colony.

For medium-scale preparations (midiprep), 100 ml of LB broth containing 100 µg/ml ampicillin was inoculated similarly.

Cultures were incubated overnight at 37 °C with shaking at 180 rpm.

Miniprep plasmid preparation:

Bacteria were pelleted by centrifugation at 6,000 × g for 10 minutes. The pellet was resuspended in 180 µl of Resuspension Buffer P1 (containing RNAse A). After resuspension, 180 µl of Lysis Buffer P2 was added, and the tube was inverted six times to mix. Neutralization Buffer N3 (250 µl) was then added, and the solution was mixed by inversion six times. The mixture was centrifuged at maximum speed for 10 minutes, and the supernatant was transferred to CleanEasy^{TM} mini spin columns for DNA isolation.

The spin column was centrifuged at 10,000 rpm, and the plasmid DNA bound to the membrane was washed twice with 750 µl of Wash Buffer PE.After a dry spin at maximum speed, the plasmid DNA was eluted with 40 µl of ultrapure H_2O

Midiprep plasmid preparation:

This process was carried out using the PureLink® HiPure Plasmid Midiprep Kit according to the manufacturer's instructions. DNA was reconstituted in 100-200 µl ultrapure H_2O. The DNA concentration was measured using a NanoDrop 200 spectrophotometer.

2.2.1.8 Tissue culture

All cell lines were maintained at 37 °C, 5% CO_2 in a humidified incubator. ID8-derived cell lines and the MC-38 cell line were cultured in complete RPMI growth medium and passaged three times per week upon reaching 80-90% confluence. HEK293T cells were cultured in complete DMEM growth medium and passaged twice per week under the same confluence conditions.

For cell harvesting and passaging, 0.05% trypsin-EDTA was used as the dissociation solution. The enzymatic reaction was inactivated with complete growth medium, and the cells were washed with DPBS solution before reseeding.

All cell lines used in this study were routinely tested for Mycoplasma by PCR. The cells were kept for a maximum 2 months in culture, after which they were replaced with fresh stocks. Cryopreserved stocks were generated and stored at -80 °C for short-term use and at -150 °C for long term storage.

2.2.2 Generation of CRISPR-Cas9 endogenously tagged cells

2.2.2.1 sgRNA/Cas9 selector plasmid

To introduce an epitope tag into the genomic location of tumor antigens, sgRNAs were designed using two tools: the sgRNA Designer from the BROAD Institute and the custom Alt-RTM CRISPR-Cas9 Guide RNA tool. Selected sgRNA candidates were engineered with 5′ overhangs compatible with either the BbsI or BsaI restriction sites. Oligonucleotides were annealed and ligated into the sgRNA/Cas9 selector plasmid using T4 DNA ligase.

The plasmid used was px330-U6-Chimeric_BB-CBh-hSPCas9, which was modified to include an additional U6 promoter for dual sgRNA production (designated as px333). To further enhance this plasmid, an EGFP selection cassette was incorporated by excising the cassette from the px458 plasmid with FseI and NotI restriction enzymes. The linearized EGFP cassette was inserted into px333 at the same restriction sites using T4 DNA ligase.

2.2.2.2 Donor plasmid

The donor plasmid was designed to include a homology sequence spanning the sgRNA target sites, with the epitope tag integrated at the desired genomic location. The sequence was flanked by sgRNA target sites, including the PAM sequence, to facilitate DSB-based release by the Cas9 system. To prevent additional cutting post-insertion, the flanking sequences were reversed relative to the original target sequence. Donor plasmids were synthesized by Integrated DNA Technologies (IDT) as pUCIDT-AMP plasmids.

Transfection of endogenous tagging plasmids

To generate endogenously tagged ID8.p53 cell lines, both selector and donor plasmids were transfected. Approximately 3.5 × 10^5 cells were harvested and resuspended in nucleofector SG solution complemented with corresponding supplement solution (4.5:1 ratio). Plasmids were mixed at equimolar ratios (1500 ng selector and 500 ng donor plasmid) and added to each condition.

The substrate mixture was transferred into nucleocuvette strips, and transfection was performed using the CA-137 program on a 4D-Nucleofector® 96-well unit. After transfection, cells were cultured in fresh medium and incubated under standard conditions.

2.2.3 Genomic validation of CRISPR-Cas9 endogenously tagged cells

2.2.3.1 RNA Isolation

Following EGFP positive selection, cells were harvested to assess correct insertion of the epitope tag via reverse transcription PCR (RT-PCR) using specific primers for the inserted DNA fragments. To do so, RNA isolation was performed by lysing 1 × 10^6 cells with 350 µl of RLT lysis buffer, followed by incubation at -80 °C for 15 minutes. RNA purification was completed using the Zymo RNA Clean protocol. Lysates were thawed, mixed with 70% ethanol, and applied to a Zymo-Spin™ II column. The following steps were performed:

1. Spin at 10,000 × g for 60 seconds.
2. Wash with 500 µl RW1 buffer and spin at 10,000 × g for 60 seconds.

3. Wash with 500 µl Zymo Wash Buffer and spin at 10,000 × g for 60 seconds.
4. Perform a final dry spin at 20,000 × g for 2 minutes.
5. Elute RNA by adding 20–40 µl ultrapure H_2O directly to the column, incubating for 5 minutes at room temperature, and spinning at 10,000 × g for 1 minute.

RNA concentrations were measured using a NanoDrop 2000 spectrophotometer and stored at -80 °C for later use.

2.2.3.2 cDNA synthesis

Total RNA (300–1000 ng) was reverse-transcribed into cDNA in a 10 µl reaction using the All-in-One cDNA Synthesis SuperMix, following the manufacturer's instructions. The following protocol was employed to ensure high-quality cDNA:

1. 10 minutes at 25 °C
2. 30 minutes at 42 °C
3. 5 minutes at 85 °C

The resulting cDNA was stored at -20 °C until further analysis.

RT-PCT

Amplification of the knockin segment to detect correct insertion was performed using the DNA high-fidelity Phusion® Polymerase. An insertion-specific primer was combined with a primer targeting wildtype cDNA. The reaction was achieved by combining the following components:

4 µl	5x Phusion HF Buffer
0.4 µl	dNTPs (10 mM)
1 µl	Forward primer (10 µM)
1 µl	Reverse primer (10µM)
2 µl	Template DNA
0.2 µl	Q5® High-Fidelity DNA Polymerase
11.4 µl	ultrapure H2O

The thermocycling conditions for the amplification reactions were adopted from the manufacturer´s protocol, and are as follow:

	Step	Temperature	Time
	Initial denaturation	98 °C	30 s
30x	Denaturation	98 °C	10 s
	Annealing	50-70 °C *primer dependent	30 s
	Extension	72 °C	30 s/kb
	Final extension	72 °C	2 min
	Hold	4 °C	-

*Annealing temperature was calculated 2-3 °C below the melting temperature of the primers.

Depending on the experimental needs, different DNA quantities (>250 ng) were used. All amplifications were carried out based on the manufacturer's recommendations. Visualization of DNA-stained gels was achieved using SafeBlue fluorescence system and recorded with the GelStick IMAGER instrument. GeneRuler 1 kb or 100 bp DNA ladders were used as molecular size references.

2.2.4 Immunological techniques

2.2.4.1 Immunoblotting

Lysates were prepared by adding 150 µl of 1x Laemmli buffer to $1x10^6$ cells, followed by incubation at 95 °C for 5 minutes. The lysate samples were separated using 10% SDS-PAGE at 100 V for 10 minutes, followed by 140 V for 90 minutes. Proteins were transferred onto a nitrocellulose membrane (0.45 µm pore size) via wet blotting at 450 mA for 1.5 hours. The membrane was blocked with 5% BSA in TBS for 1 hour at room temperature (RT).

Primary antibodies were diluted in 5% BSA buffer (1:1000) and incubated with the membrane overnight at 4 °C. After thorough washing with TBS buffer, secondary antibodies diluted in 5% BSA buffer (1:14,000) were added and incubated for 1 hour at RT in the dark.

Prior to visualization, the membrane was washed with TBS-T buffer to remove unbound antibodies. Protein detection was performed using the Odyssey SA Imaging System (LI-COR Biosciences).

2.2.4.2 Flow cytometry

Cells were harvested and resuspended in 500 µl of culture medium, and $2x10^5$ cells per condition were seeded onto round-bottom 96-well plates. Cells were pelleted by centrifugation at 1,000 g for 2 minutes and washed once with 200 µl of FACS buffer. To minimize nonspecific background, cells were incubated with Mouse BD Fc block for 15 minutes at 4 °C. An unstained control was included for every experiment.

For living cells detection, a viability staining was prepared separately and added to the cells before primary staining. A viability control was prepared by incubating cells at 65 °C for 10 minutes to induce cell death. Primary cell surface staining was performed using specific antibodies diluted in DPBS. The cells were incubated with the antibody mixture for 30 minutes at 4 °C in the dark. For biotinylated primary antibodies, a secondary staining step was performed using fluorophore-conjugated streptavidin, incubated for 15 minutes at 4 °C in the dark. Washing steps with 200 µl of FACS buffer was always performed between antibody stainings.

To detect intracellular proteins, cells were fixed and permeabilized using the BD Cytofix/Cytoperm™ Fixation/Permeabilization Kit, following the manufacturer's instructions. After permeabilization, intracellular staining was performed by incubating cells with the antibody mix for 30 minutes at 4 °C in the dark. To reduce background signal, cells were washed twice with 1x Perm/Wash buffer, with each wash step lasting 15 minutes. Analysis was performed with the FlowJo software (Tree Star, Inc.).

2.2.4.3 Flow cytometry-based cell sorting

Flow cytometry-based cell sorting was performed for the selection and purification of modified cells. Cells were harvested and resuspended in 2 mL of complete RPMI medium in 15 mL tubes. All subsequent staining and washing steps were conducted under sterile conditions within a tissue culture hood.

To detect living cells, a viability stain was prepared separately and added to the cells prior to primary antibody staining. A viability control was prepared by incubating cells at 65 °C for 10 minutes to induce cell death. Surface staining was performed using specific antibodies diluted

in DPBS. The cells were incubated with the antibody mixture for 30 minutes at 4 °C in the dark. After staining, cells were washed with FACS buffer and resuspended at a final density of 1 x 10^6 cells per 500 µl.

Cell sorting was carried out by members of the Flow Cytometry Core Facilities at the University Hospital Bonn. Following sorting, enriched cell populations were washed and resuspended in complete RPMI medium. The sorted cells were then cultured under standard conditions in a humidified incubator at 37 °C, 5% CO_2.

2.2.5 Experimental models

2.2.5.1 Mice

C57BL/6 mice were purchased from Charles River, Jackson. Animals were housed under specific pathogen-free conditions in ventilated cages. All experiments were performed using 6- to 15-week-old mice and were approved by local government authorities (LANUV, NRW, Germany). Experiments were conducted in compliance with both national and institutional guidelines for laboratory animal care and use.

2.2.5.2 T cell isolation and activation

Spleens were harvested from sacrificed C57BL/6 mice to isolate splenocytes. Cell suspensions were prepared by meshing spleens through a 40 µm cell strainer, followed by washing with complete RPMI medium. Cells were pelleted by centrifugation at 500 × g for 5 minutes at 4 °C and resuspended in 1 mL red blood cell lysis buffer for 2 minutes. The lysis reaction was neutralized with 24 mL of complete RPMI medium, followed by centrifugation and resuspension in fresh complete RPMI medium.

To activate T cells, 6-well plates were pre-coated with 5 µg/mL anti-CD3 in 1.5 mL DPBS 24 hours prior to isolation. The isolated splenocytes were resuspended in T cell activation medium (complete RPMI supplemented with 100 U/mL IL-2 and 2 µg/mL anti-CD28) at a density of 3 × 10^6 cells/mL. The cells were then seeded into anti-CD3-coated plates and incubated for 24 hours.

2.2.5.3 Production of retroviral particles

HEK293T cells were plated at a density of 1 × 10^6 cells per well in a 6-well plate containing complete DMEM medium and allowed to adhere for 6–8 hours. Retroviral particles were produced via calcium phosphate transfection. The transfection mixture was prepared as follows:

1. 1x HBS buffer (200 µl): Mixed with 1.5 µg gag-pol, 1.5 µg VSV-G, and 3 µg transfer plasmid.
2. 2.5 M $CaCl_2$ (10 µl): Added to the solution, which was incubated for 20 minutes at room temperature.

The transfection solution was added dropwise onto the adherent HEK293T cells. After 48 hours, the supernatant containing retroviral particles was harvested, filtered through a 0.45 µm filter, and used immediately for transduction. pRpGFP retroviral particles were produced as a transduction control for every experiment.

2.2.5.4 Generation of retroviral particle producer cells

A retroviral particle producer cell line was established for CAR-T cell production. E-Plat HEK293T cells were plated at a density of 1 × 10^6 cells per well in complete DMEM medium. The following day, the medium was replaced with 2 mL of retroviral supernatant (MSCV-based particles).

Transduction efficiency was evaluated by surface expression of the RQR8 transfer plasmid marker using flow cytometry. To enhance retroviral production, RQR8-positive producer cells were magnetically sorted. Cells were stained with PE-conjugated anti-CD34 antibodies, followed by positive selection using an Anti-PE MicroBeads Kit (Miltenyi Biotec), according to the manufacturer’s instructions.

2.2.5.5 Generation of CAR-T cells

For genetic modification of T cells, retroviral transduction was performed using spinfection. Non-TC-treated 24-well plates were coated with RetroNectin (10 µg/mL in DPBS) and incubated for 24 hours at 37 °C, 5% CO_2. Plates were washed with DPBS and blocked with 1 mL of 2% BSA solution for 30 minutes at room temperature. After blocking, wells were

washed again, and 0.5 mL of retroviral particle-containing supernatant was added. Plates were sealed with parafilm and centrifuged at 2,000 × g for 2 hours at 32 °C.

Activated T cells were harvested, counted, and assessed for viability using trypan blue and an automated cell counter. 1 × 10^6 activated T cells per well were added to the retroviral-coated plates, followed by a second centrifugation step at 800 × g for 90 minutes (acceleration = 1, deceleration = 1) to enhance cell-virus contact. After centrifugation, cells were incubated for 24 hours at 37 °C, 5% CO_2. The following day, cells were washed to remove residual virus and cultured in fresh T cell maintenance RPMI medium (10 ng/mL IL-7, 10 ng/mL IL-15). Transduction efficiency was verified 48-72 hours post-transduction by detection of the surface expression of the RQR8 marker using flow cytometry.

2.2.5.6 CAR-T cell activation assay

To evaluate the specific activation of CAR-T cells, co-culture assays with tumor cell lines were performed. Tumor cells were seeded in a 96-well plate 24 hours before CAR-T cell treatment to ensure proper antigen expression. CAR-T cells were harvested and resuspended at a 1x10^6 cells per mL density and incubated with GolgiStop™ and GolgiPlug™ (1:1000 dilution). Positive controls were stimulated with PMA (50 ng/mL) and Ionomycin (1 µg/mL). CAR-T cells were added at 1:1 effector-to-target (ET) ratio to the corresponding tumor cells and incubated for 4-72 hours at 37 °C, 5% CO_2. Following incubation, the co-cultures were harvested by manual pipetting and prepared for surface and intracellular staining procedures.

2.2.5.7 CAR-T cell expression and dynamics

To assess the CAR molecule expression on CAR-T cells following stimulation with tumor cells expressing ALFA-tag affinity variants, co-culture assays were performed. Tumor cells were seeded at higher densities 24 hours prior to CAR-T cell treatment. CAR-T cells were added at a 1:1 ET ratio, and samples were harvested at 3, 6, 12, and 24 hours post-treatment in order to analyze CAR expression with flow cytometry.

To evaluate the recovery of CAR molecules after stimulation with affinity variants, CAR-T cells from co-cutures were magnetically sorted using the Anti-PE MicroBeads Kit (Miltenyi

Biotec), following the manufacturer's instructions. Sorted cells were washed and cultured in fresh T cell maintenance RPMI medium. CAR expression was analyzed after 3, 6, 12, and 24 hours post-sorting using flow cytometry.

2.2.5.8 RTCA xCELLigence assay

To evaluate the killing dynamics of CAR-T cells against tumor cell lines, the RTCA xCELLigence assay was performed. Background impedance of all wells was standardized with 50 µl of complete RPMI culture medium. Tumor cells were harvested and seeded at a density of $0.5x10^5$ cells in 50 µl per well on an E-plate 16 PET. After a 24 hour incubation, CAR-T cells were added to the wells in 100 uL of complete RPMI culture medium at the indicated ET ratios. Impedance measurements were recorded every 15 minutes, and the resulting cell index was normalized to the time of CAR-T cell addition.

2.2.5.9 SPR spectroscopy

Surface plasmon resonance (SPR) spectroscopy was performed to calculate the binding affinity between the anti-ALFA nanobody (Nb-ALFA) and ALFA-tag variants. These experiments were performed by Michael Marleaux using a Biacore™ 8K instrument at the Institute of Structural Biology, Bonn. The instrument was equipped with a streptavidin-coated sensor chip (Series S sensor chip SA), and the system was set to 25°C and flushed with SPR running buffer before inserted into instrument and normalized according to the manufacturers recommendations.

Sensor Conditioning: Three consecutive injections of 1 M NaCl in 50 mM NaOH were applied at a flow rate of 10 µL/min for 1 minute. Washing was performed using 50% isopropanol in 1 M NaCl and 50 mM NaOH.

Binding Measurements: Binding was measured in single-cycle kinetics mode. Increasing concentrations of ALFA-tag variants (0.390, 1.562, 6.25, 25, 100, 400, 1600, 6400, and 25600 pM analyte concentrations) were injected at 30 µL/min with an association phase of 480 seconds and a dissociation phase of 1800 seconds. Data were collected at a rate of 10 Hz. The dissociation constant (KD) was determined by the ratio of the association and dissociation constants.

The association constant (k_a) and dissociation constant (k_x) were calculated using a 1:1 binding model. The affinity (K_D) was determined as:

Equilibrium dissociation constant (K_D) = Dissociation constant (kd) / Association constant (ka)

2.2.5.10 Statistical analysis

All statistical analyses and graph generation were performed using GraphPad Prism v10. Results were presented as mean ± standard deviation (SD). Statistical significances were determined using the unpaired Student´s t-test or two-way ANOVA with correction for multiple comparisons by either the Tukey method. Statistical significances are indicated in the diagrams using the * symbols. p-values less than 0.05 were considered to be statistically significant: *p<0.05, **p<0.01, ***p<0.001, ****p<0.0001.

3 Results

3.1 Generation of a CRISPR-Cas9-based endogenous tagging approach

Ovarian cancer is one of the most aggressive forms of gynecological malignancies. Despite advances in treatment, there are still limited therapeutic options that significantly alter the disease's progression. Several novel strategies, such as targeted immunotherapies including chimeric antigen receptor T (CAR-T) cells, have been explored to treat ovarian cancer. Although these approaches show promise, many fail to advance through clinical trials due to various challenges such as acquired tumor resistance through antigen loss. Therefore, there is a critical need to develop precise tumor antigen screening tools in order to improve antigen selection and enhance the efficacy of CAR-T cell therapies.

In this study, a CRISPR-Cas9-based strategy was developed to the precise insertion of an epitope tag into various genomic locations within tumor antigen genes. Unlike most genome editing tools, this approach must allow unrestricted placement of the epitope tag at any genomic site of the protein of interest, ensuring accessibility for CAR-T cell targeting. Additionally, the tag itself must minimize the risk of disrupting the structural integrity of the tumor antigen, regardless of its insertion site. To meet these requirements, an endogenous tagging strategy was designed to target any exon within a gene, replacing it with a homologous exon fused to the ALFA-tag.

To validate this approach, Mesothelin, a well-characterized tumor antigen was selected. Mesothelin is anchored to the cell membrane via a glycosylphosphatidylinositol (GPI) linkage at its C-terminus region. The precursor peptide undergoes a posttranslational modification at a furin-cleavage site (FCS), resulting in an N-terminus domain located at position D298 of the mature membrane-bound Mesothelin protein (Figure 3.1A-B). Consequently, ALFA-tag insertions were strategically designed at this region. As an initial structural analysis, the ALFA-tag was added at various positions downstream of the FCS. To test stability, these ALFA-tagged mesothelin variants included alanine linkers of multiple lengths (Figure 3.1C).

The ALFA-tagged mesothelin variants were cloned into an expression plasmid under a human cytomegalovirus (CMV) promoter and transfected into HEK293T cells. Cells were

harvested 48 hours post-transfection and analyzed using immunoblotting and flow cytometry to detect ALFA-tag expression (Figure 3.2A). Every construct showed expression of the ALFA-tag compared to the untransfected control. Interestingly, the A2 and A4 variants exhibited lower levels of the mature peptide and higher levels of the pro-peptide, suggesting impaired cleavage (Figure 3.2B). Similarly, flow cytometry analysis revealed reduced surface expression of the ALFA-tag for these two variants (Figure 3.2C).

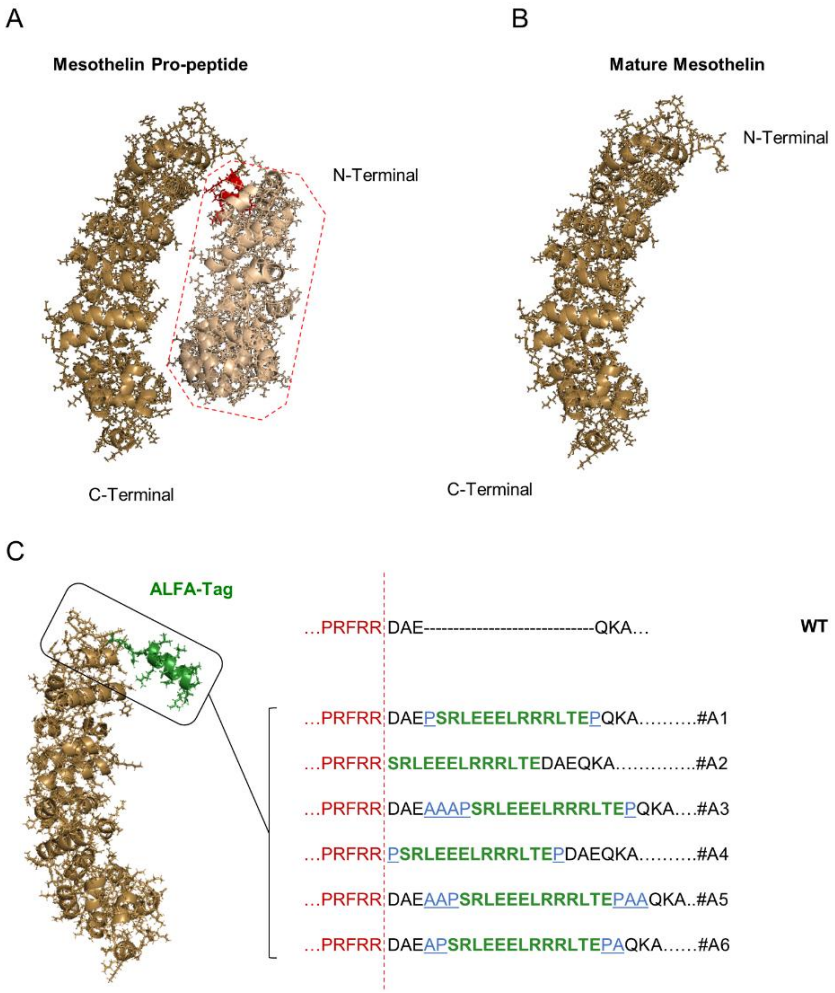

Figure 3.1: Structural analysis of murine mesothelin
(A) AlphaFold prediction of the full-length murine mesothelin amino acid sequence. The pro-peptide is susceptible to cleavage by a FCS sequence (red ribbons), which results in the release of the Megakaryocyte Potentiating Factor (dotted rectangle). (B) Membrane-bound mature mesothelin. (C) *In silico* design of different ALFA-tag (green) positions and linkers (blue) at the N-terminus region of the mature mesothelin.

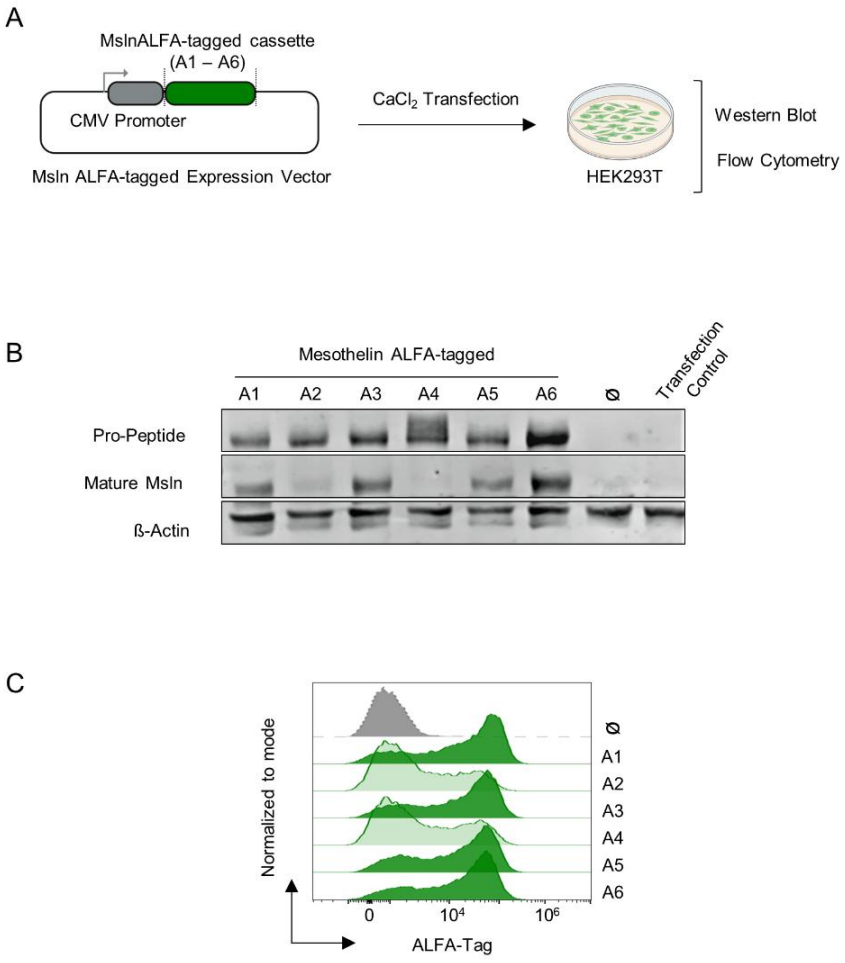

Figure 3.2: Transient expression of ALFA-tagged mesothelin
(A) Graphical depiction of six ALFA-tag (green) variants located downstream of the FCS (red) within the N-terminus region the mature mesothelin, expressed on HEK293T cells for structural analysis. Figure created with BioRender.com. (B) Immunoblot analysis of the expression of ALFA-tagged Mesothelin on transfected HEK293T cells. Untransfected control: ∅; Transfected control: empty vector. (C) Representative flow cytometry histograms showing the expression levels of the ALFA-tag in the Mesothelin protein compared to untransfected controls (grey).

The ALFA-tag position in A2 and A4 is immediately upstream of the FCS, while the other four variants include a 3-amino-acid spacer between the FCS and the ALFA-tag. Based on these findings, the A6 variant, was selected for endogenous tagging.

3.2 Endogenous tagging of mesothelin

To insert the ALFA-tag into the specific selected location of the *Msln* gene, a CRISPR-Cas9-based endogenous tagging approach was designed using two different plasmids: A sgRNA/Cas9 selector plasmid, and an ALFA-tag donor plasmid. The sgRNA/Cas9 selector plasmid includes a dual U6 promoter for two different sgRNAs that were designed to target the intronic sequences flanking exon 10 of *Msln*. This exon corresponds to the selected ALFA-tag location previously described (Figure 3.3A). Additionally, the selector plasmid includes a green fluorescent protein (GFP) cassette to monitor transfection.

The donor plasmid contains the replacement exon sequence fused to the ALFA-tag, flanked by homologous sgRNA target sequences that enable Cas9 to release the template from the plasmid (Figure 3.3B). Importantly, the sgRNA sequences in the donor plasmid were designed in the reverse orientation in order to avoid Cas9 activity after insertion.

Forty-eight hours after co-transfection of ID8.p53 cells with selector and donor plasmids, GFP-positive cells were isolated by flow cytometry-based. Given the relatively low success rate after initial transfection, ALFA-tag positive cells were sorted for enrichment (Figure 3.4A-B).

The ID8.p53 cell line is derived from ovarian surface epithelial cells and was modified to recapitulate the TP53 aberrations commonly observed in HGSOC. This was achieved by introducing a Y217C point mutation using the CRISPR-Cas9-based prime editing technique, performed by Wibke Rüdiger and Dr. Helena Boll.

In order to verify successful genomic ALFA-tag integration, a polymerase chain reaction (PCR) using specific primers for the ALFA-tag sequence (forward) and the *Msln* gene (reverse) was designed. A PCR using *Msln*-specific primers was used as control, showing

corresponding amplification bands for both ID8.p53 wild-type (WT) and modified cells (ID8.p53 Msln-ALFA). Importantly, only ID8.p53 Msln-ALFA cells showed an amplification product when using the ALFA-specific primer combination, suggesting correct genomic insertion of the ALFA-tag without any evident disruption at transcriptional level. (Figure 3.5A)

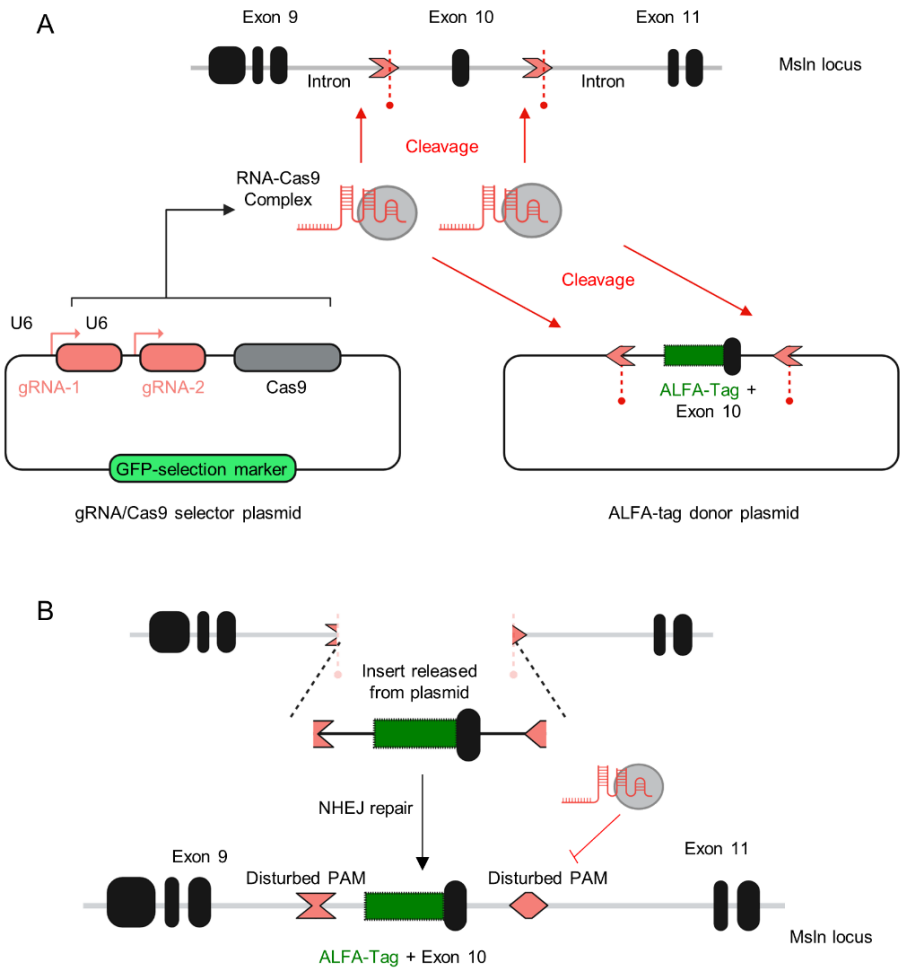

Figure 3.3: CRISPR-Cas9-based exon replacement strategy to introduce the ALFA-tag into the mesothelin gene

(A) Schematic representation of the exon replacement approach using two plasmids: a gRNA/Cas9 selector and an ALFA-tag donor. Arrows indicate the corresponding sgRNA target sequence (pink) for Cas9 induced-DSBs both in the Msln locus and in the donor plasmid. (B) Schematic of the desired genomic integration of the donor exon plus de ALFA-tag (green) mediated by NHEJ. Remaining indels are only present in the intronic sequence (grey). Figure created with BioRender.com.

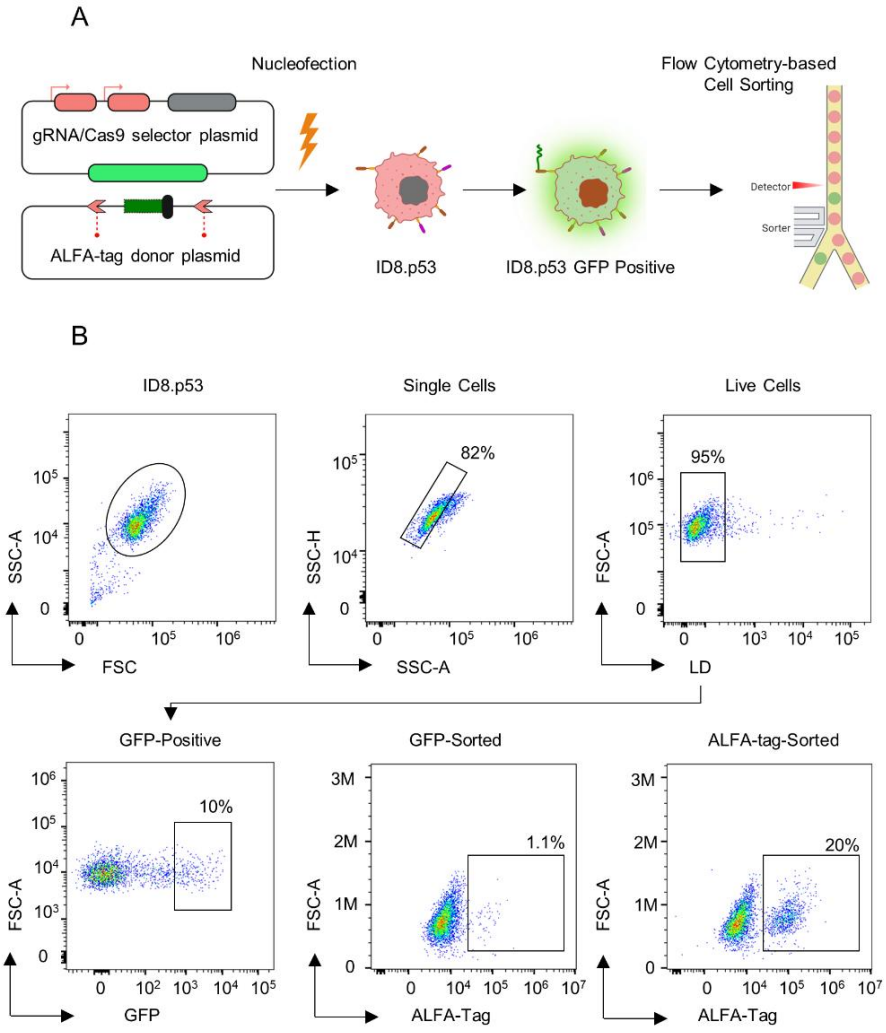

Figure 3.4: Generation and purification of CRISPR/Cas9-modified ID8.p53 Msln-ALFA cells

(A) Schematic of co-transfection of ID8.p53 cells with the gRNA/Cas9 selector plasmid specific for the *Msln* loci and the ALFA-tag donor plasmid, which includes a GFP selection cassette for flow cytometry-based cell sorting. Figure created with BioRender.com. (B) Representative flow cytometry plots showing the gating strategy for GFP-positive cells. Subsequent measurement of the ALFA-tag expression before and after cell sorting enrichment.

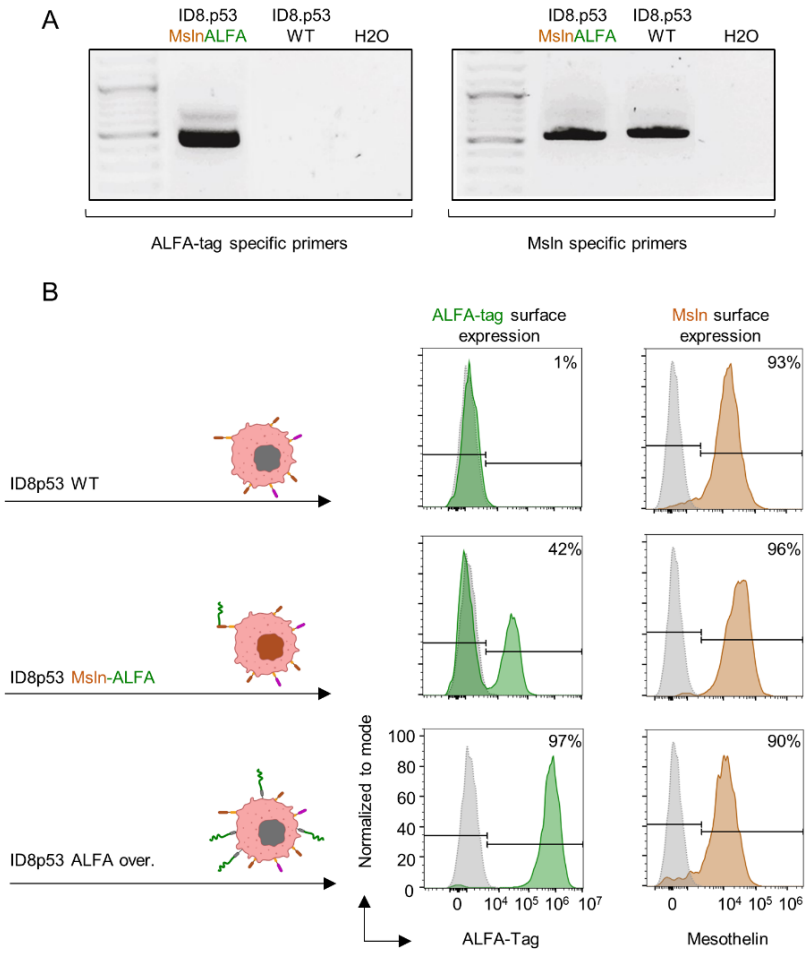

Figure 3.5: Characterization of endogenously tagged mesothelin in ID8.p53 cell line
(A) Detection of the ALFA-tag by PCR analysis of cDNA from modified ID8.p53 cells. The amplified regions correspond to ALFA-tag specific primers (left). Wild-type Msln specific primers served as controls (right). (B) Representative flow cytometry histograms showing ALFA-tag (green) and Mesothelin (brown) surface expression on indicated cell lines. Unstained ID8.p53 control cells are shown in grey. Figure created with BioRender.com.

Successful tagging of the endogenous *Msln* should produce an N-terminus fusion with the ALFA-tag, which enables detection with the anti-ALFA specific nanobody (Nb-ALFA). To validate the ID8.p53 Msln-ALFA cell lines, flow cytometry analysis was performed using individual fluorophore-conjugated nanobodies targeting the ALFA-tag and mesothelin. Importantly, ALFA-tag expression was detected in ID8.p53 Msln-ALFA cells, whereas no expression was observed in ID8.p53 WT cells (Figure 3.5B).

As positive control, ID8.p53 cells were transduced with an overexpression vector encoding the ALFA-tag fused to a CD8 stalk (designed by Benjamin McEnroe). All tested cell lines exhibited comparable levels of mesothelin surface expression, confirming that endogenous tagging with the ALFA-tag did not interfered with the endogenous regulation of mesothelin.

3.3 Endogenous tagging of nectin-2

Another tumor antigen under investigation as a potential immunotherapy target for ovarian cancer is nectin-2 (*Cd112*). Endogenous tagging of nectin-2 was performed using the same CRISPR-Cas9-based approach as described above. Structurally, nectin-2 is a type I transmembrane protein, comprising a signal peptide, an extracellular domain with three Ig-like domains, a transmembrane region, and a C-terminus intracellular domain (Figure 3.6A). The transmembrane domain anchors the protein to the cell membrane, positioning its extracellular region for interactions with other cell surface receptors.

The ALFA-tag insertion was designed into the N-terminus region, immediately downstream of the signal peptide (Figure 3.6A), encoded by the 2nd exon of the *Cd112* gene. In order to do so, two distinct sgRNAs were designed to flank exon 2 by targeting intronic sequences and were cloned into the selector plasmid. The donor plasmid included homologous sgRNA target sequences in reverse orientation to facilitate template release and prevent further Cas9 activity post-integration (Figure 3.6B).

Both plasmids were simultaneously transfected into ID8.p53 cells, and GFP-positive cells were enriched through flow cytometry 48 hours post-transfection. Subsequently, ALFA-tag-positive cells were sorted and further characterized (Figure 3.7A).

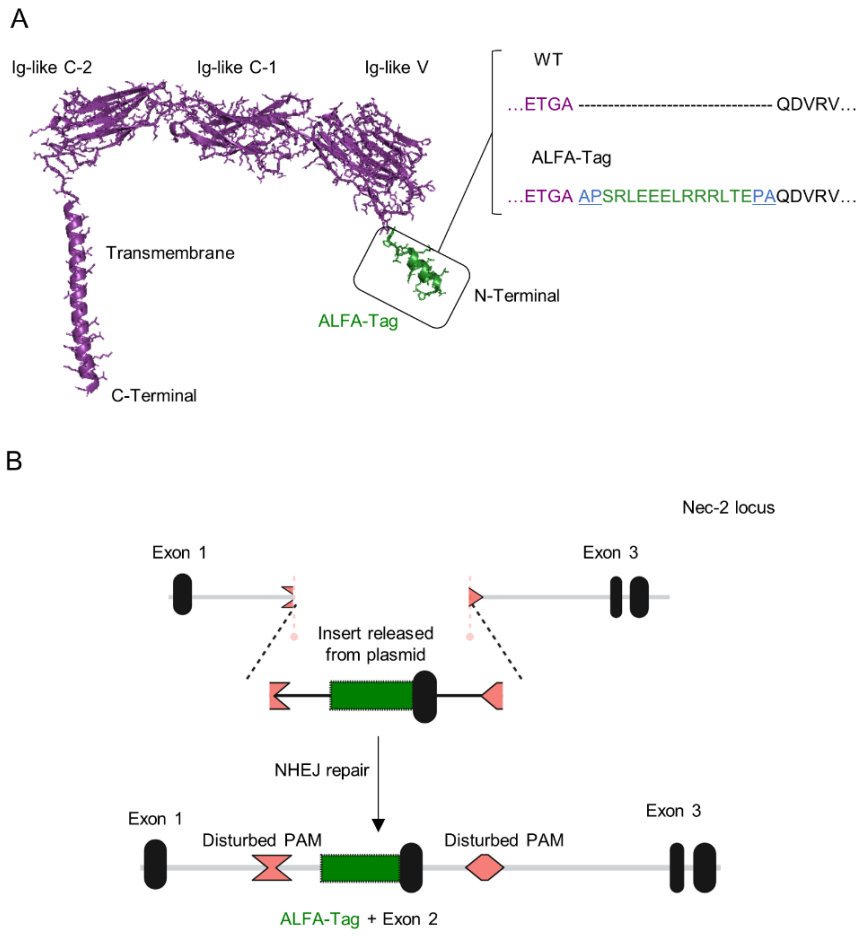

Figure 3.6: CRISPR-Cas9-based exon replacement strategy to introduce the ALFA-tag into the nectin-2 gene

(A) AlphaFold prediction of the complete murine nectin-2 amino acid sequence, with the three main Ig-like domains indicated. Desired position of the ALFA-tag (green) immediately following the signal peptide in the N-terminus region of the mature protein. (B) Schematic of the desired genomic integration of the donor exon plus de ALFA-tag (green) mediated by NHEJ. Remaining indels are only present in the intronic sequence (grey). Figure created with BioRender.com.

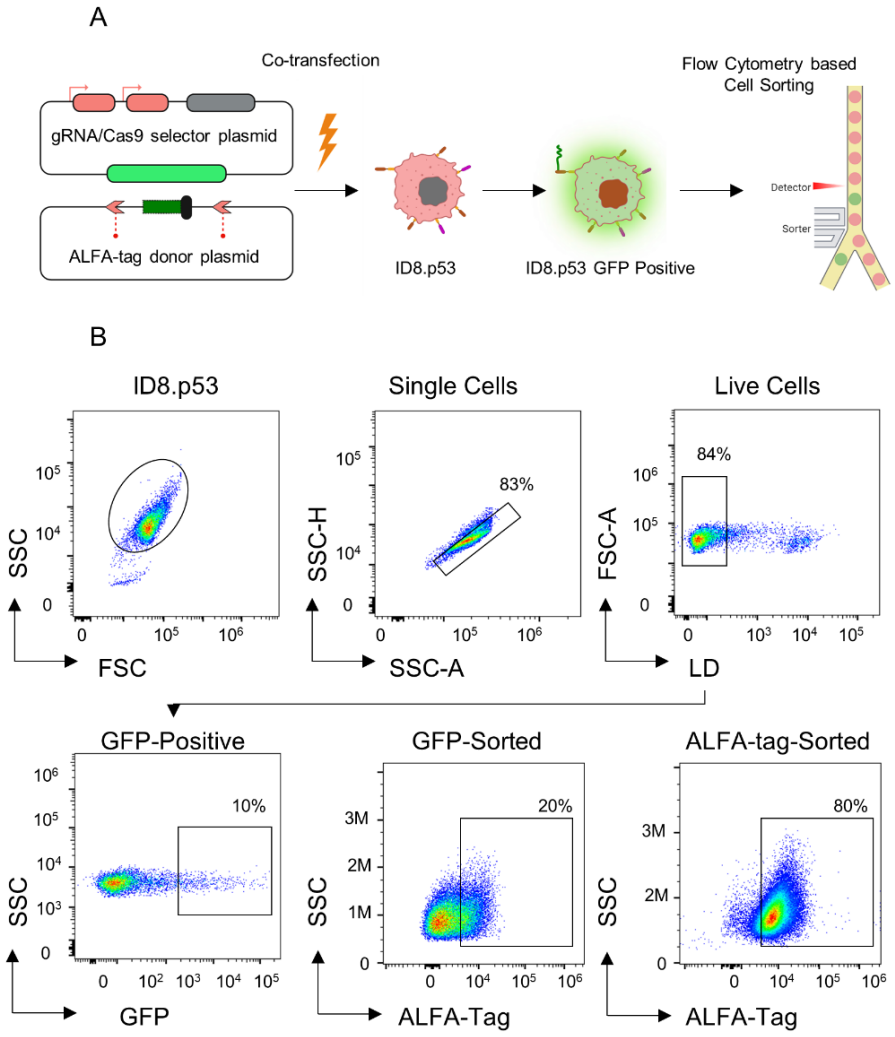

Figure 3.7: Generation and purification of CRISPR/Cas9-modified ID8.p53 Nec2-ALFA cells

(A) Schematic of co-transfection of ID8.p53 cells with the gRNA/Cas9 selector plasmid specific for the Nec-2 loci and the ALFA-tag donor plasmid, which includes a GFP selection cassette for flow cytometry-based cell sorting. Figure created with BioRender.com. (B) Representative flow cytometry plots showing the gating strategy for GFP-positive cells. Subsequent measurement of the ALFA-tag expression before and after flow cytometry-based cell sorting enrichment. Experiments carried out together with Carolin Birr.

Initial validation of the endogenous tagging was performed via PCR, with amplification observed only in ID8.p53 Nec2-ALFA cells and not in WT controls (Figure 3.8A). Flow cytometry confirmed the presence of membrane-bound ALFA-tagged Nectin-2 in ID8.p53 Nec2-ALFA cells and positive controls, but not in WT cells (Figure 3.8B).

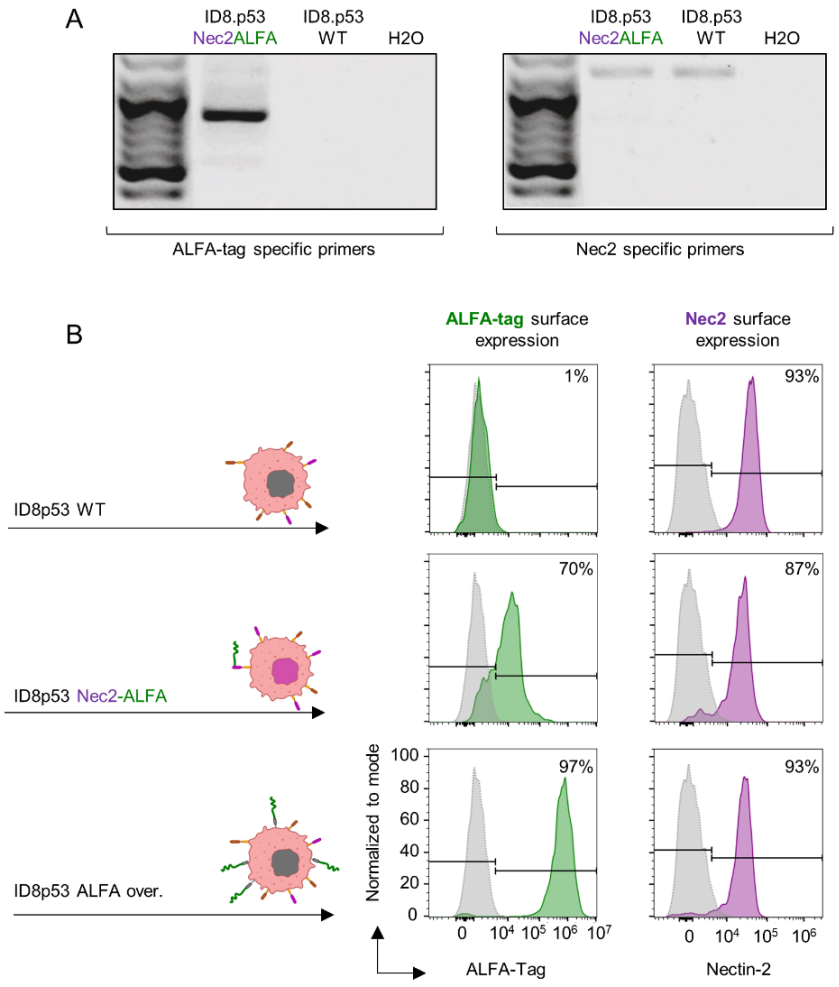

Figure 3.8: Characterization of endogenously tagged Nectin-2 in the ID8.p53 cell line
(A) Detection of the ALFA-tag by PCR analysis of cDNA from modified ID8.p53 cells. The amplified regions correspond to ALFA-tag specific primers (left). Wild-type Nec2 specific primers served as controls (right). (B) Representative flow cytometry histograms showing ALFA-tag (green) and Nectin-2 (purple) surface expression on indicated cell lines. Unstained ID8.p53 control cells are shown in grey. Experiments were carried out together with Carolina Birr. Figure created with BioRender.com.

To optimize purity and ensure consistency, monoclonal cultures of endogenously ALFA-tagged mesothelin and nectin-2 cells were established. Single ALFA-tag-positive cells were seeded into 96-well plates using flow cytometry-based sorting. Constant monitoring by microscopy was employed to confirm the exclusion of doublets and ensure the successful establishment of monoclonal lines (Figure 3.9A).

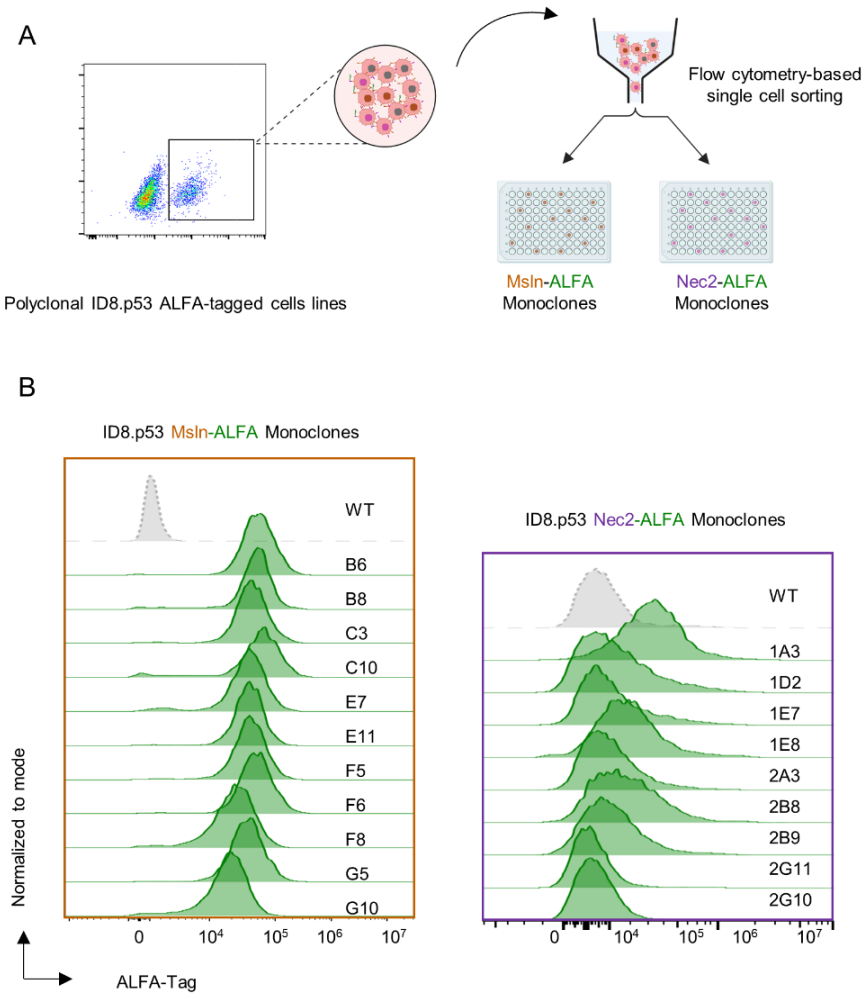

Figure 3.9: Generation of ID8.p53 ALFA-tagged monoclones
(A) Graphical depiction of flow cytometry-based single cell sorting of ID8.p53 Msln-ALFA and ID8.p53 Nec2-ALFA polyclonal cultures. Figure created with BioRender.com. (B) Representative flow cytometry histograms showing ALFA-tag expression on various monoclonal cultures of ID8.p53 Msln-ALFA (left) and ID8.p53 Nec-2ALFA (right) compared to wild-type (WT) control (grey).

Expanded cultures were analyzed for genomic integration using PCR with ALFA-tag-specific primers, which confirmed correct incorporation of the tag ALFA-tag (data not shown). Additionally, surface expression of the ALFA-tag was validated by flow cytometry, demonstrating successful tagging without altering the native protein expression. The resulting cell lines exhibited robust and reproducible ALFA-tag expression, as seen in the flow cytometry profiles (Figure 3.9B). Based on these evaluations, two monoclonal lines were selected for further experiments: ID8.p53 Msln-ALFA.B8 and ID8.p53 Nec2-ALFA.1A3. This step was critical to generate genetically uniform cell lines, which are essential for reproducibility in downstream experiments and for minimizing variability caused by heterogeneous populations

3.4 Establishment of the ALFA-CAR: a second-generation, nanobody-based, ALFA-tag specific CAR-T cell

As mentioned before, one of the most challenging aspects of CAR-T cell therapy in solid tumors is antigen selection. This process is primarily achieved by studying the expression levels of antigens present on cancer cells while minimizing potential off-target effects by ensuring limited expression on healthy tissues. An alternative strategy involves aiming at ubiquitous targets, such as linage proteins, while managing the associated toxicity in heathy cells. This approach has been successfully implemented in clinically approved anti-CD19 CAR-T cell therapies, which have demonstrated acceptable safety profiles.

Once a suitable target antigen is identified, a specific recognition domain must be designed. Commonly, the recognition domains of these constructs are based on traditional antibodies. Unfortunately, this process can be both costly and time-consuming. Furthermore, critical factors influencing CAR-T cell functionality, such as affinity and epitope localization, are difficult to control with conventional approaches.

In response to these challenges, an experimental CAR construct was designed to test and compare multiple tumor antigens in a preclinical fashion. For this, a "universal" CAR was designed to allow for the evaluation of multiple tumor antigens using the same CAR-T cell platform under highly controlled conditions (Figure 3.10A). This approach facilitates the side-

by-side, direct comparison of tumor antigens within the same tumor model, using CAR-T cells that are identical in all functional aspects. Additionally, this modular experimental platform provides the flexibility to optimize affinity and epitope targeting, providing valuable preclinical insights into different aspects of CAR-T cell functionality.

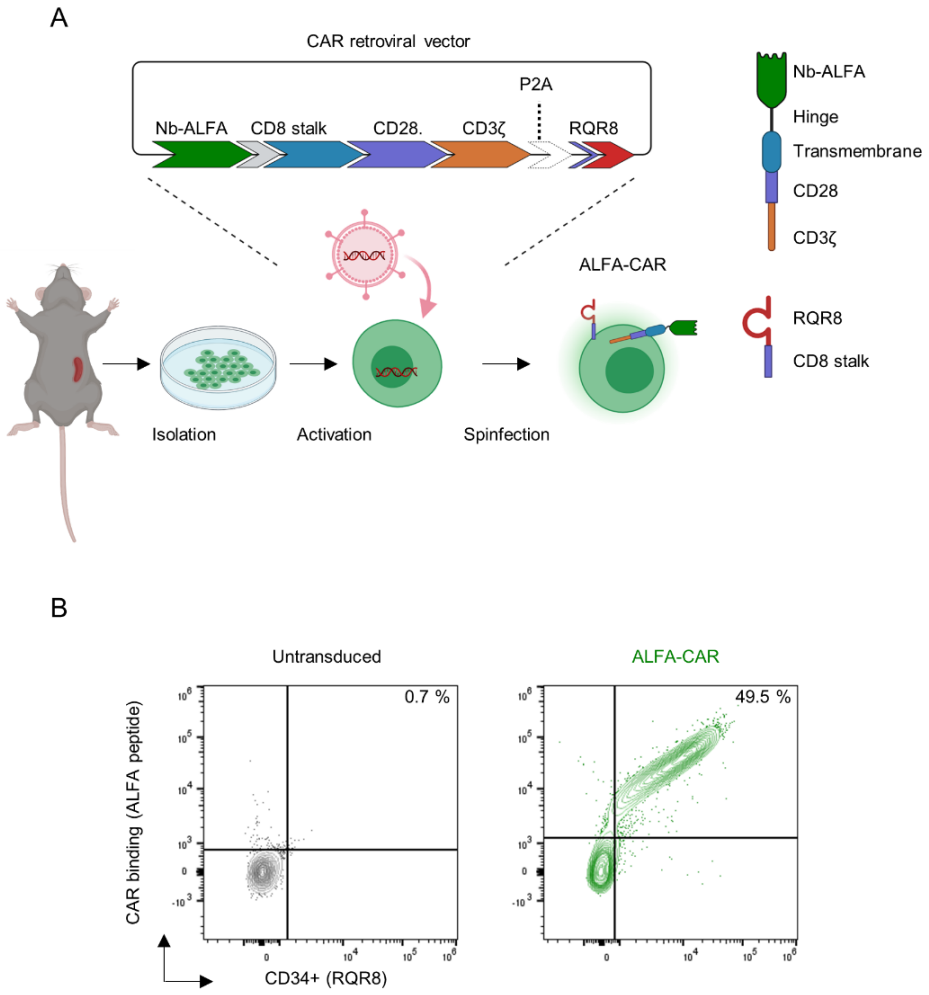

Figure 3.10: Transduction of murine T cells with the ALFA-CAR construct
(A) Illustration of the second-generation CAR retroviral vector, which includes the Nb-ALFA, CD8 stalk, CD28, CD3ζ, and RQR8 marker. Figure created with BioRender.com. (B) Representative flow cytometry plots showing transduction efficiency in murine splenocytes five days after transduction compared to untransduced controls.

To implement this strategy, a nanobody targeting the ALFA-tag (Nb-ALFA) was incorporated as the recognition domain in a second-generation CAR construct, called the "ALFA-CAR." This construct includes a 45-amino-acid hinge region and a transmembrane domain derived from the CD8α stalk. Its intracellular signaling domain was designed with a CD28 co-stimulatory motif followed by the CD3ζ signaling region, in order to induce activation and persistence of CAR-T cells.

A P2A-linked RQR8 surface marker was also included into the construct. This highly compact protein (Philip et al., 2014) is a fusion peptide containing the epitopes of both CD34 and CD20, and therefore can be detected by an anti-CD34 antibody, serving as a CAR transduction efficiency marker.

To facilitate T cell transduction, the construct was inserted into a Murine Stem Cell Virus-derived (MSCV) vector. Following transduction, the surface expression of the RQR8 marker on T cells was measured by an anti-CD34 antibody. Additionally, direct detection of the CAR molecule on the cell surface was achieved using a fluorophore-conjugated soluble ALFA peptide, demonstrating a transduction efficiency of up to 50% (Figure 3.10B).

3.5 Activation and killing capacity of ALFA-CARs targeting endogenously-tagged ID8.p53 cell lines

To assess whether the ALFA-CAR is capable of eliciting a pro-inflammatory response against ALFA-tagged-modified ID8.p53 cell lines, *in vitro* co-culture assays were performed. ALFA-CARs were generated from splenocytes of wild-type C57BL/6 mice, and transduction efficiency was confirmed three days post-infection. Subsequently, a 4-hour co-culture was performed against the indicated target cell lines. Intracellular expression of IFN-γ and TNF-α in ALFA-CAR T cells was measured by flow cytometry (Figure 3.11A). PMA/Ionomycin treated T cells were used as a positive control.

The specificity of the ALFA-CAR activation was investigated by comparing its response across cell lines with different tumor antigens tagged with the ALFA epitope. While ID8.p53 WT cells failed to induce cytokine production, ALFA-CAR-positive T cells showed a significant intracellular IFN-γ and TNF-α expression when co-cultured with ALFA-tag overexpressing

ID8.p53. ALFA-CAR T cell activation was also observed in ID8.p53 Msln-ALFA and ID8.p53 Nec2-ALFA cell lines, confirming that the ALFA-tagged antigens were effectively recognized (Figure 3.11B).

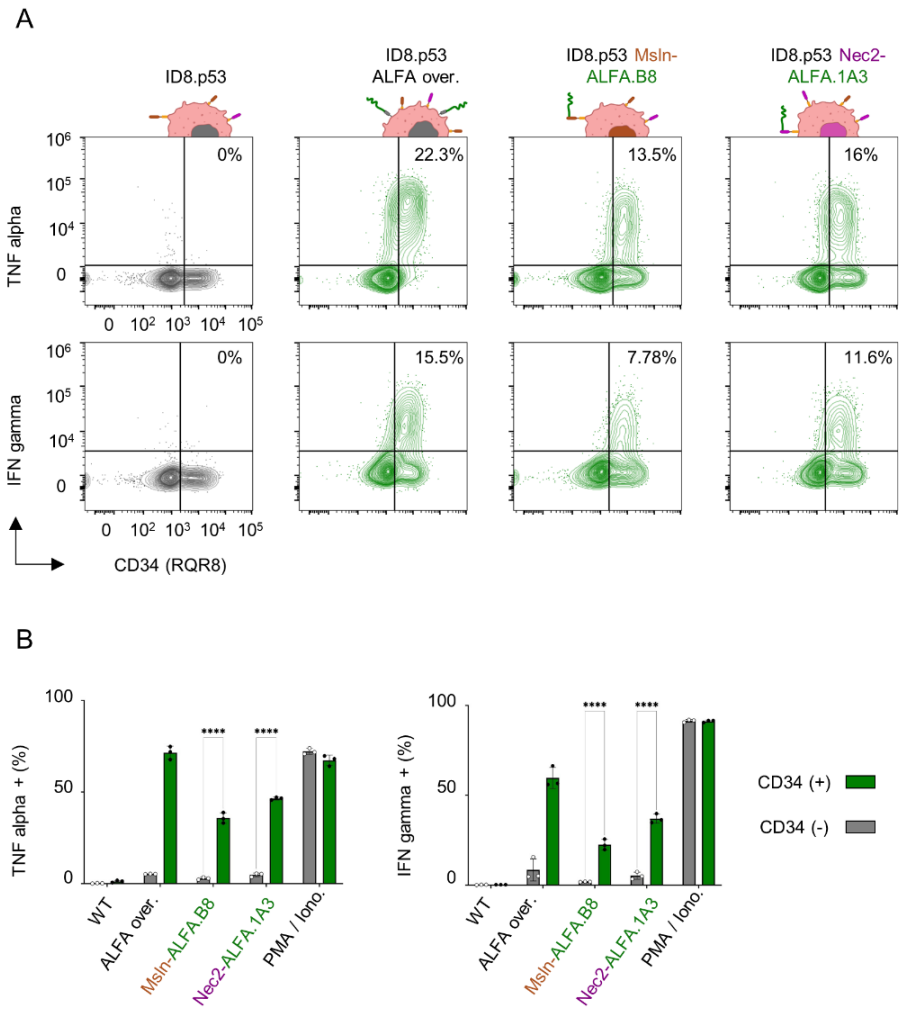

Figure 3.11: Activation capacity of ALFA-CARs upon stimulation with ALFA-tagged cells

(A) Representative flow cytometry plots showing TNF alpha and IFN gamma expression in CD34+ ALFA-CARs after 4 hours of co-culture with indicated ID8.p53 cell lines. WT cells were used as negative controls (grey). Figure created with BioRender.com. (B) Corresponding quantification of TNF alpha and IFN gamma expression in CD34+ ALFA-CARs (n=3; mean ± s.d.). Statistics: ***p < 0.001, Tukey's multiple comparison test.

Furthermore, these results validate the accessibility of the ALFA-tag epitope when fused to different tumor antigens. The lack of response of untransduced T cells suggests specificity of the ALFA-CARs against the ALFA-tag. Together, these findings demonstrate that ALFA-CARs can mediate antigen-specific activation and pro-inflammatory responses, showing their potential as a screening tool for ALFA-tagged tumor-associated antigens.

The cytolytic capacity of ALFA-CARs was assessed using a xCELLigence RTCA assay. For this, ALFA-tagged cell lines were seeded onto impedance biosensor-embedded plates and cultured for 20 hours before ALFA-CAR treatment. Growth kinetics, measured as the normalized cell index over time, showed steady proliferation of untreated ID8.p53 cell lines (Figure 3.12A).

ALFA-CAR treatment had no effect on WT cells. However, a significant reduction in cell index was observed for ALFA-tag-positive cell lines, indicating effective cytolysis and confirming its specificity (Figure 3.12B). Notably, ALFA-CARs reduced ID8.p53 Nec2-ALFA cell index by 36 hours, matching the killing kinetics of ALFA-tag overexpressing cells. In contrast, targeting ID8.p53 Msln-ALFA resulted in slower and less pronounced cytolysis, suggesting antigen-specific differences in CAR-T cell killing within this model.

The cumulative cytotoxic effect of the ALFA-CAR against each cell line was assessed by calculating the area under the curve (AUC). The AUC analysis revealed that the ALFA-CAR exhibited a significantly higher cytotoxic effect against ALFA-tagged nectin-2 compared to ALFA-tagged mesothelin (Figure 3.12C). Notably, the cytotoxic effect of the ALFA-CAR against Nec2-ALFA was comparable to that observed for the positive control.

3.6 Validation of the ALFA-CAR platform: Generation of nanobody-based CAR-T cells against mesothelin and nectin-2

Next, CAR-T cells targeting the native mesothelin and nectin-2 proteins were developed. To mitigate structural bias and improve antigen specificity, nanobodies were chosen as the recognition domain of the CARs.

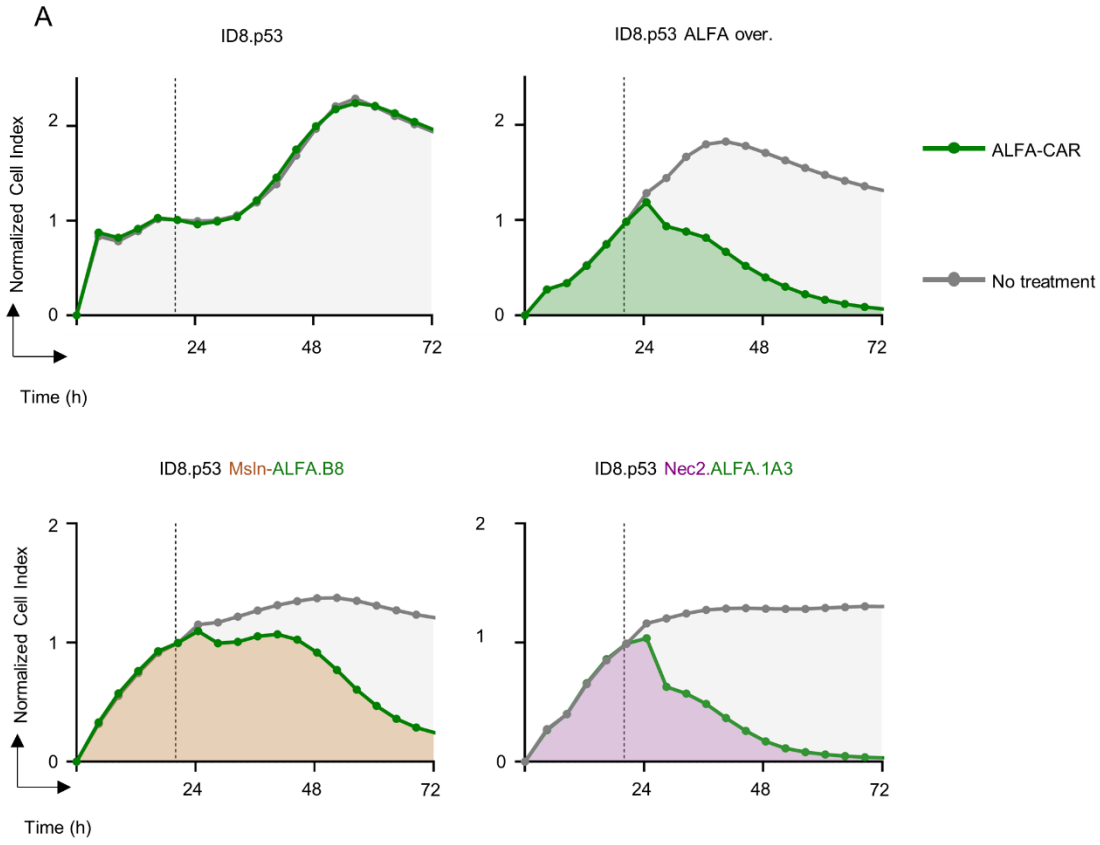
A
ID8.p53
ID8.p53 ALFA over.
ID8.p53 MsIn-ALFA.B8
ID8.p53 Nec2.ALFA.1A3
Normalized Cell Index
Time (h)
ALFA-CAR
No treatment
B
Mean AUC (units x hrs)
ns
****
WT
ALFA over.
MsIn-ALFA.B8
Nec2.ALFA.1A3
C
ns
*
***
ALFA-CAR
No treatment

Mesothelin targeting was facilitated by a previously characterized anti-Mesothelin nanobody (Nb-Msln) developed by Andrew M. Prantner and colleagues (Prantner et al., 2015). This nanobody exhibits a high binding affinity (K_D = 46 ± 8 nM) and reliably detects mesothelin on ovarian cancer cells. Nb-Msln is cross-reactive with both human and murine mesothelin, and its binding epitope overlaps with residues near the N-terminus region of the mature protein (Prantner et al., 2018).

For Nectin-2, nanobody candidates were generated and provided by the Nanobody Core Facility of the University Clinic Bonn. Their initial characterization was conducted by Carolin Birr, a member of the Glodde Laboratory. Among the candidates, two nanobodies demonstrated cross-reactivity, and one was selected (Nb-Nec2) for subsequent experiments. Importantly, binding affinity and epitope localization of this nanobody is yet to be experimentally determined.

The CAR constructs were engineered by replacing the Nb-ALFA recognition domain from the second-generation ALFA-CAR with the sequences of Nb-Msln and Nb-Nec2 through conventional molecular cloning techniques (Figure 3.13A). The remaining components of the CAR design, including the hinge length, transmembrane, co-stimulatory, and signaling domains, were kept intact to ensure functional comparability between constructs.

Figure 3.12: Killing dynamics of ALFA-CARs against ALFA-tagged cells
(A) ALFA-CAR (green) killing efficacy against indicated ID8.p53 cell lines measured by xCELLigence real-time cell analysis (RTCA) shown as the mean normalized cell index (n=6; mean). Untreated cells (grey) were used as negative controls. The dotted line indicates the time of treatment. (B) Graphs showing the specificity of the ALFA-CAR shown as the area under the curve (AUC) of ALFA-CAR treated cell lines measured by xCELLigence RTCA: Untreated (grey), ID8.p53 ALFA overexpression (green), ID8.p53 Msln-ALFA.B8 (brown), and ID8.p53 Nec2-ALFA.1A3 (purple). Data shown as the mean AUC (n=6; mean ± s.d.). Statistics: ns=not significant, ****p < 0.0001, Unpaired t test. (C) Graphs showing the different killing dynamics of the ALFA-CAR shown as the AUC of ALFA-CAR treated cell lines: ID8.p53 ALFA overexpression (green), ID8.p53 Msln-ALFA.B8 (brown), and ID8.p53 Nec2-ALFA.1A3 (purple). Data shown as the mean AUC (n=6; mean ± s.d.). Statistics: ns=not significant, *p < 0.05, ***p < 0.001, Tukey's multiple comparisons test.

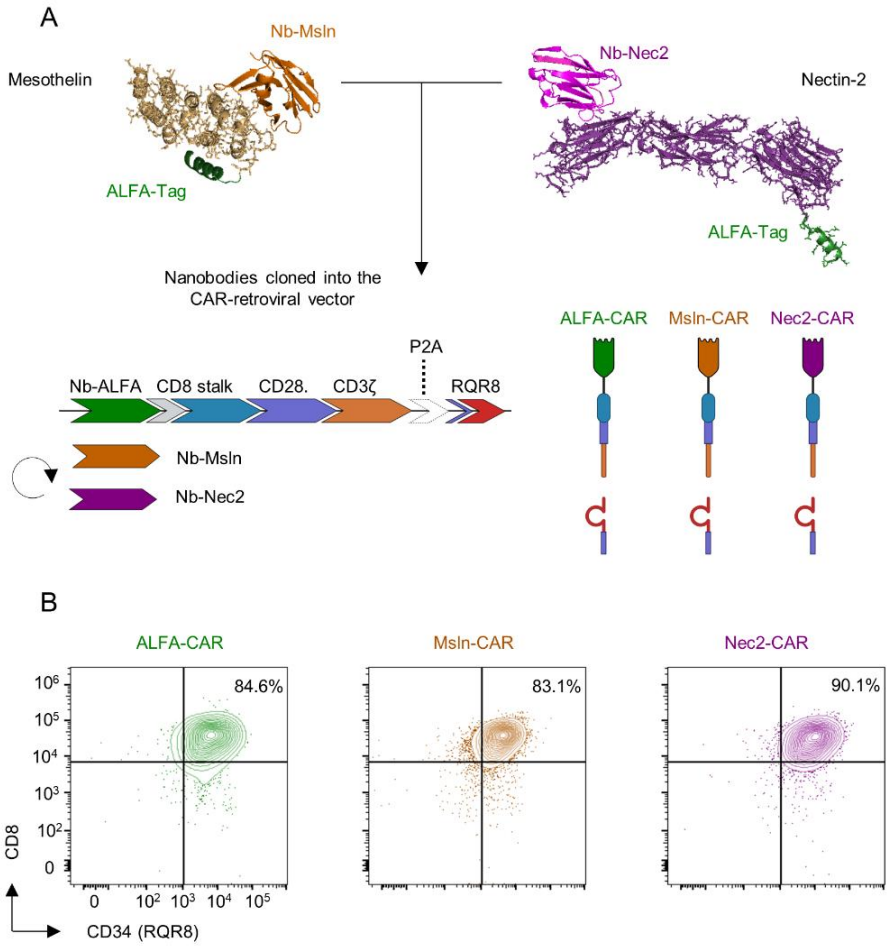

Figure 3.13: Generation of mesothelin-specific and mectin2-specific CAR-T Cells
(A) AlphaFold prediction of the binding site of (left) Nb-MsIn on the mature ALFA-tagged Mesothelin peptide and of (right) Nb-Nec2 on Nectin-2. The nanobodies were cloned in the recognition domain of the CAR-retroviral construct. Figure created with BioRender.com. (B) Representative flow cytometry plots showing the CAR-expression levels of ALFA-CAR (green), MsIn-CAR (yellow), and Nec2-CAR (purple) cells after CD8+CD34+ flow cytometry-based cell sorting.

To ensure robust functional analysis, CD8 and-RQR8-positive CAR-T cells were purified five days post-transduction via flow cytometry-based cell sorting. The following day, RQR8 expression was verified, confirming a purified population of CD8-positive CAR-T cells for subsequent experiments (Figure 3.13B).

3.7 Specificity of anti-mesothelin and anti-nectin2 CARs

To assess the response of the CAR-T cells targeting native tumor antigens, a co-culture assay was performed. Tumor cells were seeded 24 hours prior to treatment with the indicated CAR-T cells. Four-hours post co-culture, intracellular expression of pro-inflammatory cytokines was analyzed by flow cytometry.

T cell activation was assessed by measuring the expression of IFN-γ and TNF-α. All CARs resulted in robust activation in response to ID8.p53 ALFA overexpressing cells, which includes endogenous levels of mesothelin and nectin-2. As expected, the ALFA-CAR showed no activation when co-cultured with ALFA-tag negative cells. Similarly, no activation was observed for either CAR when exposed to MC38, a cell line negative for both nectin-2 and mesothelin. PMA/Ionomycin treated T cells were used as a positive control (Figure 3.14).

3.8 Activation and cytotoxicity comparison between anti-mesothelin CARs and anti-nectin2 CARs

To compare the activation capacity between the Msln-CAR and Nec2-CAR, a co-culture assay was performed. ID8.p53 ALFA overexpressing cells were seeded 24 hours prior to treatment with the indicated CAR-T cells. Seventy-two hours post co-culture surface expression of activation markers was analyzed by flow cytometry.

T cell activation was assessed by measuring the surface expression of CD69 and CD25, indicative of early and late activation stages, respectively. CD69 is rapidly upregulated upon T cell engagement and serves as an immediate indicator of CAR-T cell activation, while CD25 reflects sustained activation and potential proliferation. CAR-T cells demonstrated robust activation profiles, with no differences between CARs targeting native tumor antigens (Figure 3.15A).

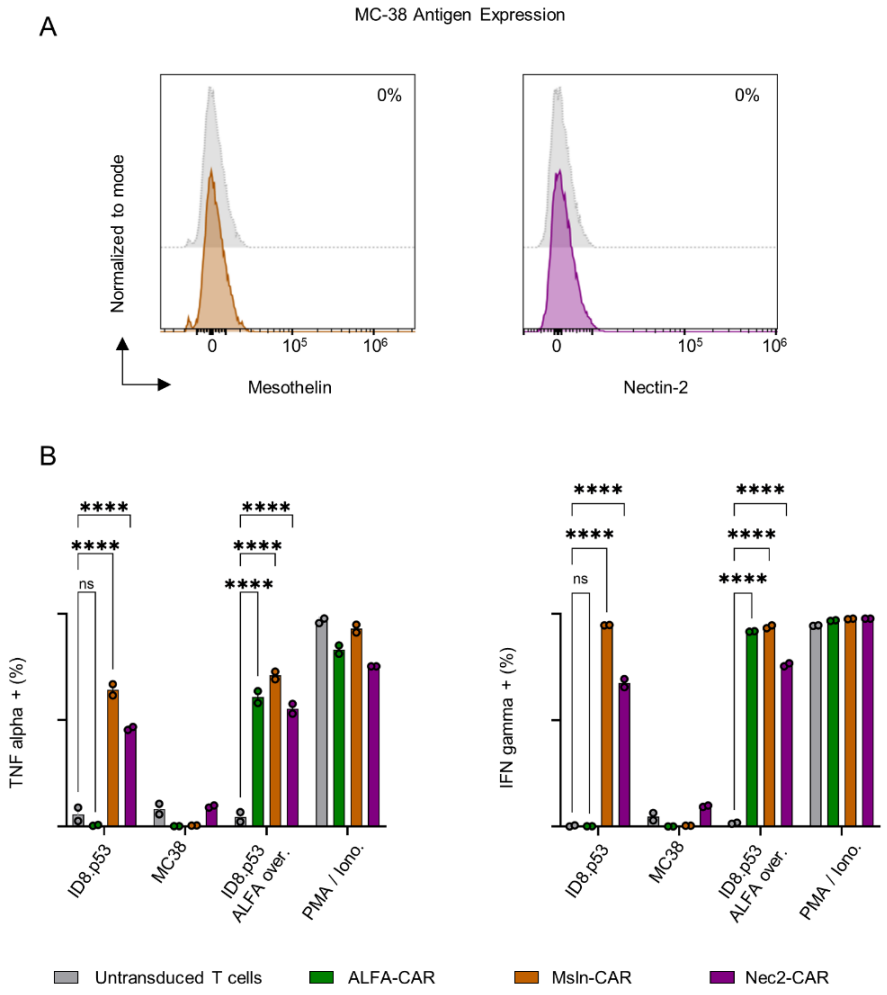

Figure 3.14: Pro-inflammatory profile of ALFA-CAR, MsIn-CAR, and Nec2-CAR
(A) Representative flow cytometry histograms showing the expression levels of mesothelin (brown) and nectin-2 (purple) on MC-38 cells. (B) Quantification of TNF alpha and IFN gamma expression in CD34+ ALFA-CARs after 4 hours of co-culture with indicated cell lines. Untransduced T cells were used as negative controls (grey). (n=2; mean ± s.d.). Statistics: ***p < 0.001, Tukey's multiple comparison test.

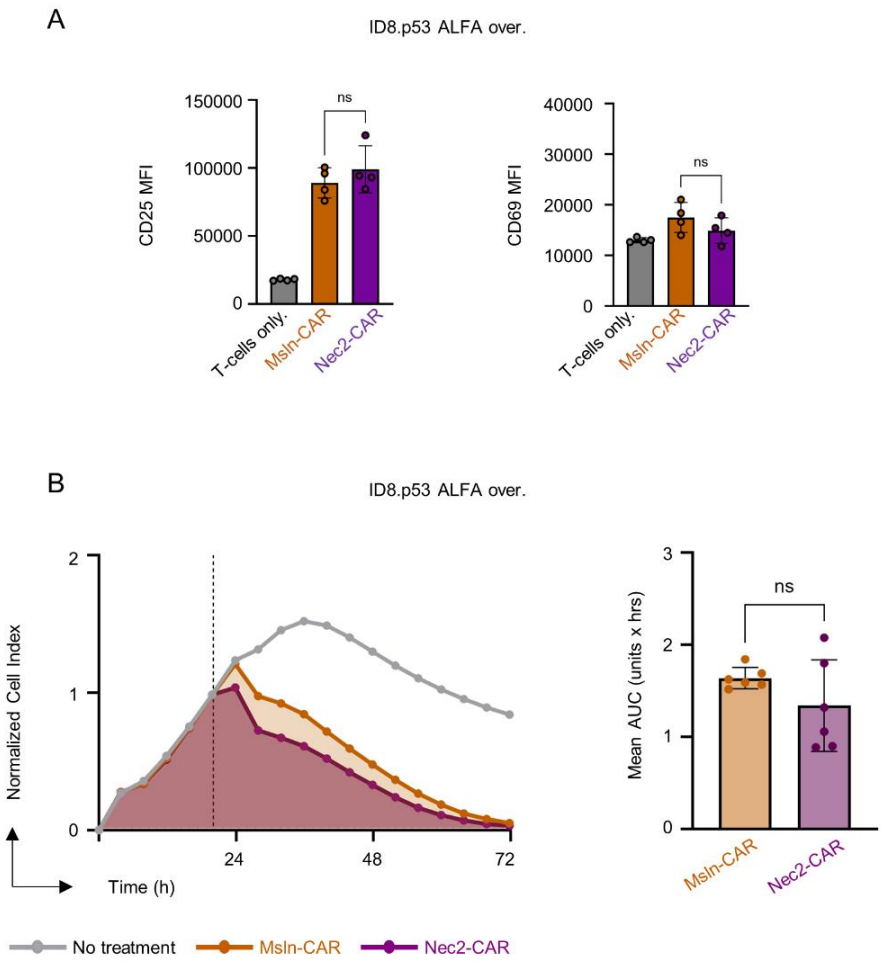

Figure 3.15: Activation and killing of MsIn-CARs and Nec2-CARs
(A) Quantification of CD25 and CD69 expression on CAR-T cells after 72 hours co-culture with ID8.p53 ALFA overexpressing cells at ET 1:1 ratios. Expression determined by flow cytometry shown as mean fluorescence intensity (MFI) (n=4; mean ± s.d.) Statistics: ns=not significant, Tukey's multiple comparison test. (B) Killing dynamics of MsIn-CAR (brown) and Nec2-CAR against ID8.p53 ALFA overexpressing cells measured by xCELLigence RTCA. Untreated cells (grey) were used as negative controls. The dotted line indicates the time of treatment. Graphs (n=6; mean ± s.d.) showing the area under the curve (AUC) of MsIn-CAR (brown), and Nec2-CAR (purple). Statistics: ns=not significant, Unpaired T-test.

To evaluate the direct tumor-killing capacity of Msln-CARs and Nec2-CARs, an xCELLigence RTCA assay was performed. ID8.p53 ALFA-overexpressing cells were seeded onto impedance biosensor-embedded plates and allowed to adhere for 20 hours prior to CAR-T cell treatment, ensuring optimal target expression. The RTCA system provided continuous monitoring of tumor cell viability over a 72-hour co-culture, capturing the kinetics of CAR-T cell-mediated cytotoxicity (Figure 3.15B).

Nec2-CARs and Msln-CARs demonstrated similar killing dynamics when targeting the endogenous expression of their respective antigens. A slight trend was observed in which Nec2-CARs exhibited faster and more pronounced cytotoxic activity compared to Msln-CARs; however, this difference was no longer detectable by the end of the co-culture.

To further quantify the difference in targeting nectin-2 versus mesothelin, the AUC was calculated to assess the overall cytotoxic effect. The AUC analysis also showed the trend, indicating slightly faster for Nec2-CARs compared to Msln-CARs when targeting ovarian cancer cells with endogenous levels of both antigens, but the observed differences did not reach statistical significance.

3.9 Generation of ALFA-tag variants for affinity modulation

Affinity has emerged as a critical factor in optimizing the efficacy of CAR-T cell therapy. The binding affinity of the CAR's antigen recognition domain can influence T cell activation, persistence, and tumor-killing capacity. However, whether higher or lower affinity is preferable remains unclear. Studies have demonstrated that high-affinity interactions may lead to T cell exhaustion or damage to normal tissues expressing low levels of the target antigen, while lower-affinity CARs may lack sufficient potency to eradicate tumors (Hudecek et al., 2015; Xiaojun Liu et al., 2015). As previously discussed, the Nb-ALFA interacts with the ALFA-tag with very high affinity. The reported dissociation constant (K_D) of this interaction is in the picomolar range. This feature, although advantageous for some applications, can be detrimental for CAR-T cell functionality.

The ALFA-tag was designed to form a stable alpha-helical cylinder, with its structure maintained by key intermolecular interactions. This helical conformation allows for efficient

and specific binding to the Nb-ALFA, mediated by both polar and hydrophobic interactions. Polar interactions with the CDR2 loop of the Nb-ALFA occur at the N-terminus (E5) of the ALFA-tag. Additional hydrogen bonds are formed at the C-terminus (R11, E14) regions of the ALFA-tag, establishing strong binding sites (Götzke et al., 2019). A hydrophobic cluster comprising residues L4, L8, and L12 of the ALFA-tag plays a significant role in stabilizing these interactions.

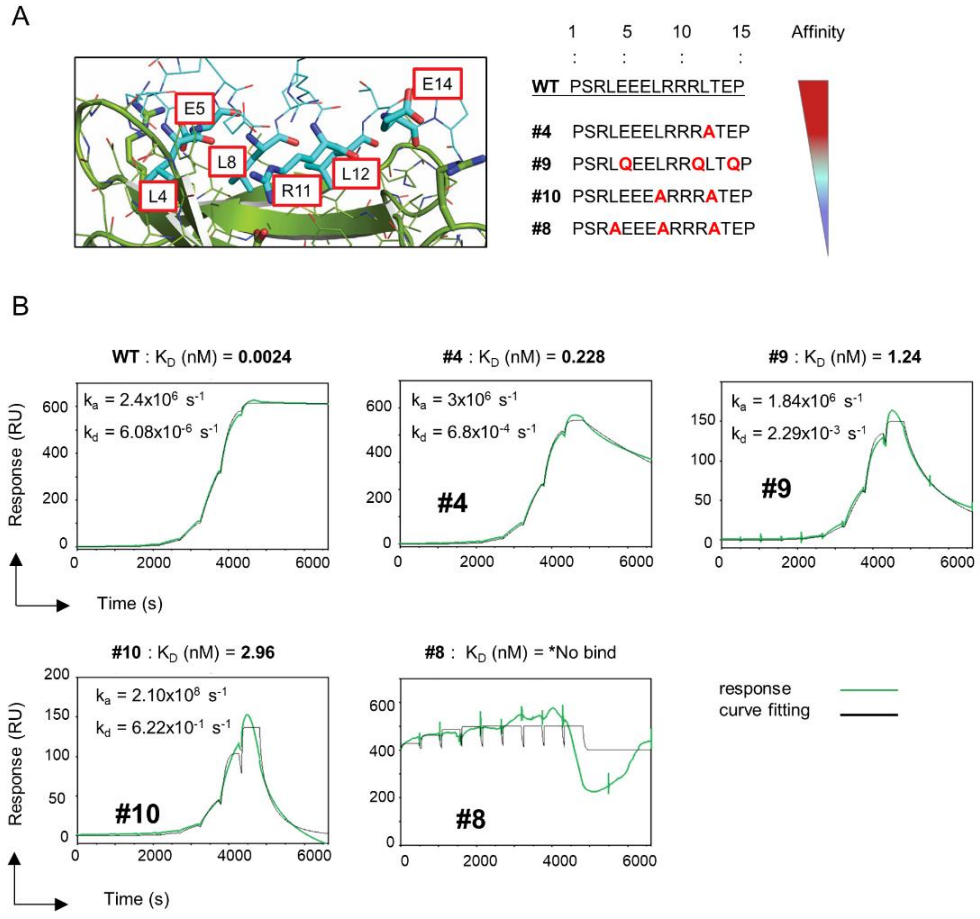

Figure 3.16: Validation of ALFA-tag affinity variants
(A) Predicted structure of the Nb-ALFA and ALFA-tag complex generated by AlphaFold, showing Nb-ALFA (green) and ALFA-tag (blue) with interacting ALFA-tag amino acid residues highlighted in red. Alignment of the ALFA-tag sequence with variants, including amino acid substitutions. (B) Sensograms of the specific binding of Nb-ALFA with different ALFA-tag variants immobilized on a sensor chip and measured by SPR. Experiments performed by Dr. Michael Marleaux and Nicole Florin.

As high-affinity interactions may promote T cell exhaustion and healthy tissue damage, targeted amino acid substitutions were introduced at these interaction sites of the ALFAtag to reduce the binding affinity of Nb-ALFA while maintaining the structural integrity (Figure 3.16A). These variants were designed in collaboration with Prof. Dr. Matthias Geyer, director of the Institute of Structural Biology (ISB), Bonn.

Substitutions of specific leucines (L) with alanines (A) aiming to reduce the hydrophobic interacting surface resulted in affinity reduction (L12A; #4, L8L12-AA; #10) compared to ALFA-tag WT, measured by surface plasmon resonance (SPR). In fact, substitution of all leucines with alananiens (3L-to-3A; #8) showed complete binding disruption (Figure 3.16B). Similarly, hydrogen bonds formed by glutamic acid and arginine were weakened by substitutions with glutamine (ERE-to-3Q; #9), resulting in reduced affinity. Expression of ALFA-tag variants and SPR measurements were performed by Dr. Michael Marleaux and Nicole Florin, both members of the ISB.

3.10 Expression of ALFA-tag affinity variants on ID8.p53 cells

To investigate the impact of varying ALFA-tag affinities, variants were cloned into a retroviral MSCV vector. To ensure surface expression, the sequences for the affinity variants were preceded by a CD8α signal peptide. A CD8α stalk fused with a glycine-serine (GS) linker served as the membrane anchor, setting up proper display of the tag on the cell surface. Additionally, a FLAG-tag sequence was included downstream of the ALFA-tag, separated by a P2A auto-cleavage site, enabling independent detection of transduced cells (Figure 3.17A).

Using these constructs, ID8.p53 ovarian cancer cells were transduced. Seven days post-transduction, ALFA-tag expression was analyzed by flow cytometry using the Nb-ALFA for detection. To account for potential disruption of Nb-ALFA binding caused by affinity-reducing mutations, an anti-FLAG antibody was also used as a transduction control.

As expected, cells transduced with the wild-type (WT) ALFA-tag construct exhibited high expression of both the ALFA-tag and FLAG-tag (Figure 3.17B). Consistent with the surface plasmon resonance (SPR) data, cells expressing affinity variant #8 were undetectable by Nb-ALFA staining but retained strong FLAG-tag expression, confirming successful transduction.

Affinity variant #4 showed reduced Nb-ALFA detection but comparable transduction efficiency to WT. Interestingly, cells expressing affinity variants #9 and #10 were also undetectable by Nb-ALFA, suggesting significant decline of binding capacity while maintaining FLAG-tag expression.

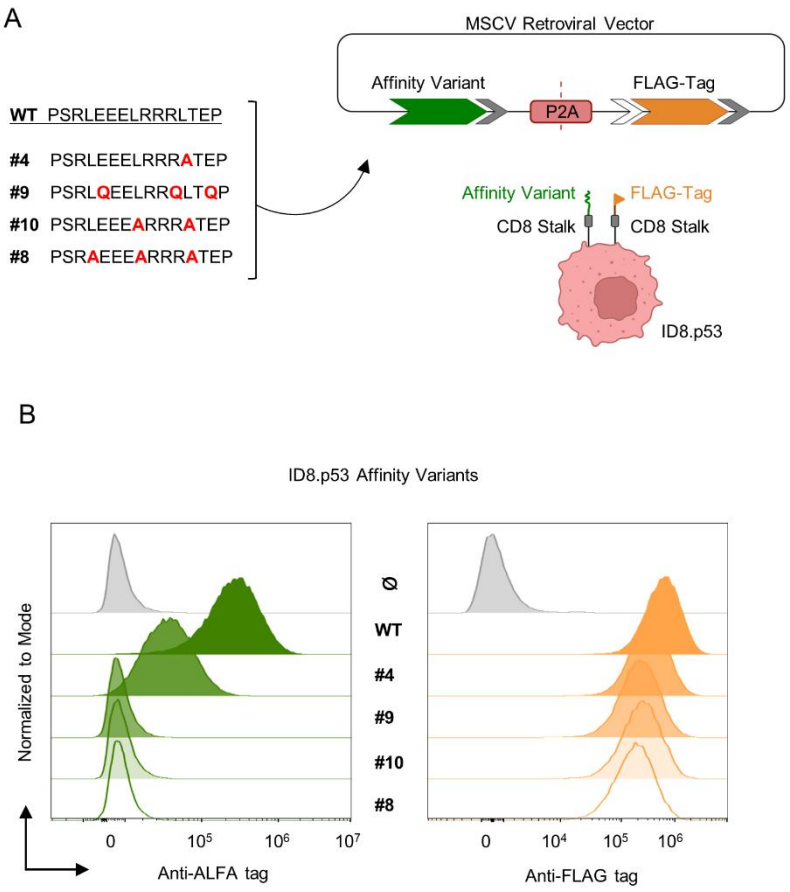

Figure 3.17: Expression of the ALFA-tag on ID8.p53 affinity variants
(A) Different ALFA-tag affinity variants cloned into a retroviral expression vector for transduction into ID8.p53 cells. Figure created with BioRender.com. (B) Representative flow cytometry histograms showing the expression of the ALFA-tag (green) stained with the Nb-ALFA and FLAG-tag (orange) stained with anti-FLAG tag in ID8.p53 affinity variants. ID8.p53 WT cells served as negative controls (grey).

3.11 Impact of antigen affinity on ALFA-CAR cytotoxicity

To evaluate the impact of antigen affinity on the cytotoxic function of ALFA-CARs, a xCELLigence RTCA assay was performed using ID8.p53 tumor cells expressing the ALFA-tag affinity variants. Tumor cells were seeded onto impedance biosensor-embedded plates and incubated for 20 hours prior to treatment. Tumor cell viability was monitored continuously for 72 hours during co-culture with ALFA-CARs at an equal 1:1 ET ratio.

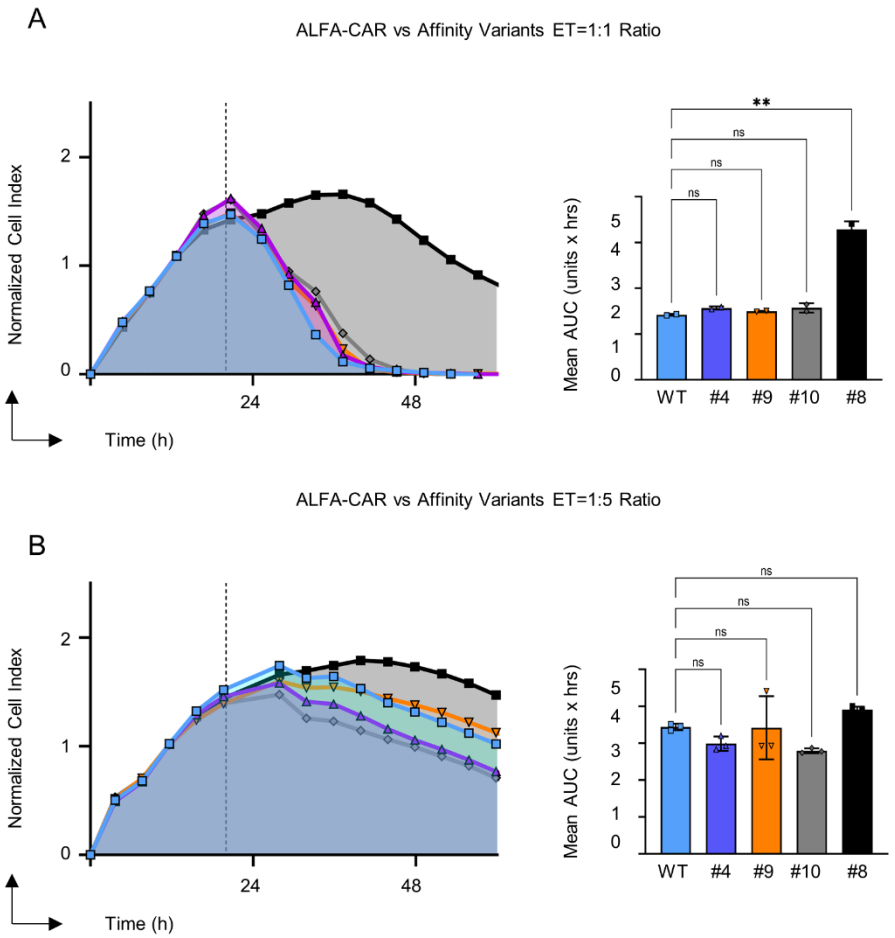

Figure 3.18: Killing efficiency of the ALFA-CAR against affinity variants
(A) ALFA-CAR killing efficacy against different ID8.p53 affinity variants measured by xCELLigence real-time cell analysis (RTCA) shown as the mean normalized cell index (n=3; mean), and corresponding graphs showing the area under the curve (AUC) of ALFA-CAR treated cell lines measured by xCELLigence at 1:1 ET ratio, and (B) 1:5 ET ratio. The dotted line indicates the time of treatment. Statistics: **p <0.01, ns=not significant, Tukey's multiple comparison test.

Sharp and rapid cytotoxicity was observed against cells expressing the ALFA-tag WT, consistent with high-affinity binding (Figure 3.18A). Surprisingly, no significant differences in cytotoxicity were noted between the WT ALFA-tag and variants #4, #9, and #10, suggesting that these variants retained sufficient affinity to effective CAR-T cell killing. In contrast, cells expressing affinity variant #8 were completely resistant to ALFA-CAR-mediated killing, confirming a total binding disruption of the Nb-ALFA.

Given that the influence of affinity in CAR-T cell functionality is directly related to antigen expression levels, cytotoxicity was further analyzed at 1:5 ET ratio. No significant differences in killing efficiency were observed throughout 48 hours between all affinity variants at this ratio (Figure 3.18B).

3.12 ALFA-CAR expression dynamics influenced by affinity variants

The mechanisms by which affinity modulate CAR-T cell cytotoxicity and persistence remain unclear. To explore the direct impact of affinity on CAR-T cells at a molecular level, co-culture assays were performed using the ALFA-CAR platform against the ALFA-tag affinity variants expressed on ID8.p53 cells. To do so, target cells were seeded 24 hours before ALFA-CAR treatment. Cells were then analyzed at 3, 6, 12, and 24 hours (Figure 3.19A). Direct surface expression of CAR molecules was possible by using an ALFA-peptide conjugated to a fluorophore, enabling flow cytometry measurement.

Initial ALFA-CAR loss was detected at the 3-hour time point across all affinity variants (Figure 3.19B). Baseline levels of ALFA-CAR expression were determined using the unmodified ID8.p53 cell line as a negative control. Interestingly, “lower-affinity” variants (#9, #10) exhibited less pronounced ALFA-CAR molecule loss compared to “higher-affinity” variants (WT, #4). After initial loss, CAR detection levels remained unchanged at 6, 12, and 24 hours.

To further investigate the capacity of ALFA-CAR rescue, a recovery assay was performed. After the 24-hour co-culture, ALFA-CAR cells were magnetically sorted based on RQR8 expression. As expected, ALFA-CAR expression remained low at baseline in cells stimulated with all affinity variants compared to cells stimulated with ID8.p53 negative control (Figure 3.19C). Strikingly, ALFA-CARs stimulated with “lower-affinity” variants showed steady

recovery of CAR surface expression. In contrast, ALFA-CAR loss induced by “higher-affinity” variants persisted at baseline levels up to 24 hours after stimulation.

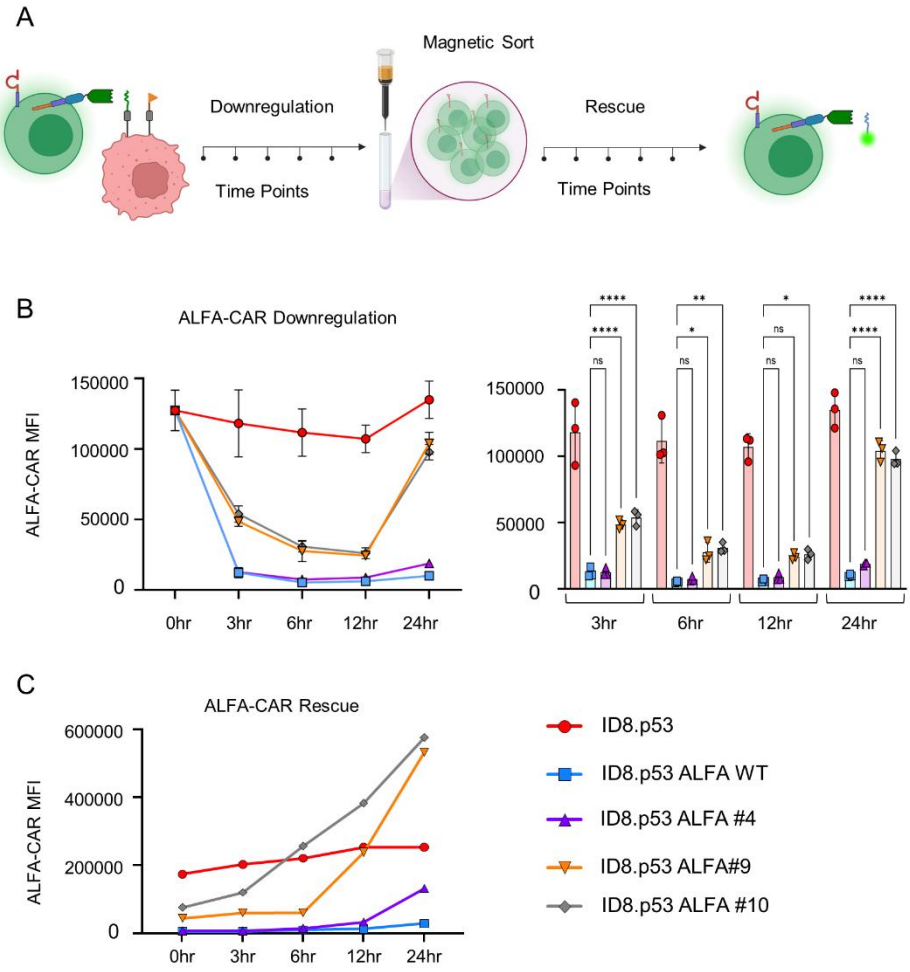

Figure 3.19: Affinity modulation of ALFA-CAR expression on T cells
(A) Graphical representation of the workflow to measure the CAR expression on T cells at different time points after co-culture with ID8.p53 affinity variants at 1:1 ET. Figure created with BioRender.com. (B) Data shown as the mean fluorescence intensity (MFI) (n=3; mean ± s.d.) of CAR expression (left) during a 24-hour co-culture, measured by flow cytometry. MFI comparison within time points (right). Statistics: ns=not significant, *p < 0.05, **p < 0.01, ****p < 0.001, Tukey’s multiple comparisons test. (C) CAR expression on magnetically sorted CAR-T cells after 24 hours of co-culture with ID8.p53 affinity variants and subsequently measured at different time points by flow cytometry (n=1). Experiments performed together with Benjamin McEnroe.

Together, higher-affinity interactions induced faster and more pronounced CAR loss, without the ability to recover even after 24 hours. Although lower-affinity interactions also demonstrated CAR loss, this effect was milder. Notably, the ALFA-CAR best recovery rate was sustained against the lowest-affinity variant. Correspondingly, the second-lowest-affinity variant also exhibited recovery but at a slower pace. Finally, no significant recovery was observed with high-affinity variants, suggesting a direct influence of CAR-T cell functionality provoked by affinity modulation.

As expected, ALFA-CAR expression remained low at baseline in cells stimulated with all affinity variants compared to cells stimulated with ID8.p53 negative control (Figure 3.19C). ALFA-CARs stimulated with “lower-affinity” variants (#9, #10) resulted in steady recovery of CAR surface expression. In contrast, ALFA-CAR loss induced by “higher-affinity” variants persisted at baseline levels up to 24 hours.

4 Discussion

Ovarian cancer is a highly aggressive malignancy that accounts for over 200,000 deaths annually (Sung et al., 2021). Among its histological subtypes, high-grade serous ovarian carcinoma (HGSOC) remains the most significant due to its high incidence and metastatic potential. HGSOC typically responds well to platinum-based chemotherapy, but relapse rates remain a major clinical challenge. Advances in our understanding of the disease have led to the development of novel therapeutic approaches. However, many of these efforts have not significantly impacted patient outcomes (Konstantinopoulos & Matulonis, 2023).

Among the most promising treatment strategies, immunotherapy has demonstrated remarkable potential across various tumor types. In particular, ovarian cancer is being currently studied due to its immunogenic nature, which makes it a target for cellular-based interventions. Specifically, in the last decade CAR T cell therapy has emerged as a major immunotherapy mainly because of the durable responses observed against hematological malignancies (Boardman & Salles, 2023).

Unfortunately, similar results have not been translated for solid tumors. Clinical studies have reported suboptimal results in CAR-T cell therapy compared to the standard of care. Several immune factors such as T cell transcriptomic profile and metabolic fitness are known to be important predictors of therapeutic success (Fraietta et al., 2018) Nevertheless, tumor-intrinsic factors such as antigen modulation, play a more prominent role in determining CAR-T cell therapy outcomes (Upadhyay et al., 2021). Additionally, most antigens on solid tumors are frequently found in healthy tissue, complicating the selection of potential targets (Guzman et al., 2023).

One of the most prominent challenges in CAR-T cell therapy is antigens loss, a resistance mechanism observed in both solid tumors and hematological malignancies (Brown et al., 2016; Maude et al., 2014; Maude et al., 2018). Traditionally, antigen selection is based on surface expression levels on tumor cells and their absence in healthy tissue. However, this method limits eligibility for CAR-T cell targets, as most cancer driver are intracellular (Tsherniak et al., 2017). This limitation has prompted the development of new screening tools

aimed at expanding the repertoire of CAR-T cell targets to include intracellular oncoproteins (Yarmarkovich et al., 2023). Alternative screening approaches have focused on selecting targets based on CAR-T cell functionality. For instance, CAR libraries engineered with IL-2 reporter systems have been used to measure T cell activation against various targets (Di Roberto et al., 2020).

These screening strategies are promising tools to increase the selectivity of potential targets for CAR-T cells. However, there is still a lack of screening platforms that allow for direct and controlled comparisons of CAR-T cell functionality across different antigens. In order to improve antigen selection, we developed a highly innovative nanobody-based CAR-T cell platform that enables straightforward screening of potential tumor antigens and thus may help identify the most promising targets. This platform also allows for the fine-tuning of key factors, such as antigen-binding affinity and epitope localization, offering a versatile tool for the personalized development of CAR-T cell therapies.

4.1 Endogenously tagged proteins as a model for tumor antigen selection in ovarian cancer

Thanks to advances in CRISPR-Cas9-based genome-editing technologies, proteins of interest can be precisely manipulated to interrogate different aspects of biology. In the context of immunotherapy, tumor antigen tagging is a powerful tool to study antigen-mediated tumor resistance mechanisms without disturbing their endogenous regulation (Dong et al., 2022).

Here, we developed a CRISPR-Cas9-based strategy that is versatile and efficient at incorporating an epitope tag at any desired genomic location within a tumor antigen gene. This is achieved by leveraging the NHEJ-based repair directed to replace a targeted genomic region with a synthetic homologous sequence containing the desired epitope tag. The system uses a dual-sgRNA vector to target the non-coding regions flanking the exon to be replaced, while a repair plasmid provides the synthetic sequence with the incorporated tag. Ultimately, successfully modified cells can be monitored via epitope tag detection using various techniques, such as flow cytometry and microscopy, among others.

Importantly, Cas9-induced double-strand breaks (DSBs) were directed exclusively at intronic regions to minimize undesired insertions or deletions, circumventing the disadvantages of NHEJ. Similar approaches for endogenous knock-ins have been demonstrated in previous studies, reinforcing the use of HDR-independent strategies as efficient genome-editing tools (Suzuki & Izpisua Belmonte, 2018; Suzuki et al., 2016; Zhong et al., 2021). Additionally, we optimized this method for tagging surface proteins at specific extracellular locations, allowing for straight-forward enrichment of modified cells via cell sorting, regardless of the initial knockin efficiency.

At a translational level, modification of endogenous proteins with synthetic sequences could disrupt their correct folding, localization, or function (Stadler et al., 2013). Larger fusion cassettes, such as fluorescent proteins, are particularly prone to inducing conformational changes (Hoffmann et al., 2005). To address this, we incorporated the 13 amino acid ALFA-tag as the inserted epitope. This hydrophilic epitope tag has a high disposition to form a resilient α-helix, minimizing the possibility of interference while ensuring high detectability (Götzke et al., 2019).

Using this technology, we tagged two potential tumor antigens expressed in HGSOC: mesothelin and nectin-2. Mesothelin is highly expressed in ovarian tumors and it has been associated with an aggressive phenotype, contributing to tumor proliferation and metastasis (Coelho et al., 2020). Although mesothelin is considered an ideal CAR-T cell therapy target, ongoing clinical trials have shown limited efficacy of anti-Msln CAR-T cells. Similarly, Nectin-2 is overexpressed in ovarian tumors compared to healthy tissue (Bekes et al., 2019). Nevertheless, there is limited data on its potential as a CAR-T target.

We successfully incorporated the ALFA-tag at the N-terminus region of both mesothelin and nectin-2 in a mouse ovarian cancer cell line. While the tagging strategy was effective, the overall efficiency was relatively low compared to other strategies that have shown up to 90% success rates. Mesothelin tagging efficiency was particularly low (1-2%), which may be attributed to the short introns flanking exon 10, limiting the possibility of finding sgRNAs with

high predicted editing performance. In contrast, nectin-2 tagging reached 20% efficiency, likely due to the longer introns flanking exon 2, which were suitable for optimal sgRNa design.

Despite these differences in efficiency, flow cytometry analysis using the Nb-ALFA confirmed the correct surface expression and localization of the ALFA-tag. This suggests that the tag did not interfere with protein folding or trafficking, as any structural disruption would have likely led to protein misfolding and degradation. Furthermore, this allowed for flow cytometry-based cell sorting, which enhanced the purity of ALFA-tag positive cells and allowed for the generation of single clone cultures.

These findings demonstrate that the NHEJ-based exon replacement strategy is a viable approach for endogenous tagging, enabling the insertion of heterologous DNA fragments at various genomic locations. However, further genomic validation is necessary. Next-generation sequencing analysis is required to further determine the tagging efficiency at each allele and to verify the genomic integrity at the modification sites.

4.2 A universal nanobody-based CAR-T cell experimental tool

To facilitate side-by-side comparisons in tumor antigen screening for CAR-T cell therapy, differences in CAR designs must be taken into account to reduce any bias. This can be extremely challenging as the recognition domains in CARs are inherently different. They are often based on antibody fragments engineered into scFvs that bind their antigens with different affinities. Consequently, traditional CARs exhibit distinct sensitivity limits, which are relevant for optimal activation, but are frequently overlooked during antigen screening processes (Hamieh et al., 2023). A common strategy to mitigate these discrepancies is the modulation of binding affinity within the recognition domain of CAR-T cells. While effective, this approach heavily depends on *de novo* antibody production, which is costly and time-intensive. (Vander Mause et al., 2022).

To overcome these challenges, we developed the ALFA-CAR, a nanobody-based CAR construct featuring the unique Nb-ALFA as the recognition domain. This binding moiety standardizes the origin, affinity, and epitope interaction of the recognition domain, making it an ideal platform for CAR-T cell comparisons. The limitation of the exclusive binding to the

ALFA-tag is circumvented by endogenously expressing this epitope in different tumor antigens, as previously described. To ensure reproducibility, the remaining of the construct was based on a standard second-generation CAR design, which includes a 45 amino acid long hinge, a CD28 co-stimulatory domain, and a CD3ζ signaling domain.

Furthermore, the ALFA-CAR platform enabled us to manipulate the epitope localization within tumor antigens. Epitope localization plays an important role in CAR-T cell functionality, as demonstrated by Nan Li and colleagues, who developed nanobody-based CARs targeting GPC1 with similar affinity but different epitope localizations, which resulted in contrasting CAR-T cell cytotoxicity (N. Li et al., 2023). To standardize comparisons in this study, we engineered mesothelin and nectin-2 to express a membrane-distal epitope. Additionally, the versatility of the ALFA-tag as the epitope can be exploited to change the localization and compare its effects without the need of producing new CAR molecules.

We demonstrated the specificity, and functionality of this platform by comparing the activation profile of the ALFA-CAR against endogenously-modified ovarian cancer cell lines that express the ALFA-tag within mesothelin or nectin-2. Notably, we observed antigen-dependent differences in the killing dynamics of ALFA-CAR T cells. Targeting nectin-2 resulted in more efficient killing than targeting mesothelin, despite using the same effector cells specific for the same epitope. Structurally, both antigens exhibit fundamental differences that could impact the efficacy of CAR-T cells. Mesothelin is anchored to the membrane by a weak GPI structure, and it endures a posttranslational cleavage whereas nectin-2 is a pure adhesion protein, designed to form strong heterophilic interactions with other proteins. These differences likely influence the stability and density of the tumor antigens, which can affect the strength and duration of immunological synapse formation, thereby modulating CAR-T cell behavior (Ritter et al., 2022).

Additionally, targeting GPI-anchored antigens poses disadvantages for cell-based therapies due to protein shedding. GPI-anchored proteins can be released into the extracellular space as soluble peptides through various mechanisms, reducing the surface antigen density and potentially blocking CAR-T cells (Müller, 2018). Such is the case of Glypican-3, a GPI-

anchored tumor antigen overexpressed in primary hepatocellular carcinoma, which has been investigated as a CAR-T cell target. Shedding of soluble Glypican-3 was found to block and inhibit CAR-T cells cytolytic capacity both *in vitro* and *in vivo* (Makkouk et al., 2021; Sun et al., 2021).

Regarding mesothelin, shedding occurs via various protease sites located proximal to the cell membrane (Xiufen Liu et al., 2020). This phenomenon has been implicated in the failure of antibody-based therapies, including CAR-T cells, and may contribute to the differences in killing kinetics observed when targeting mesothelin versus nectin-2 with the ALFA-CAR platform. To address this possibility, the measurement of soluble mesothelin and ALFA-tag in the supernatant of ID8.p53 ALFA-tagged cell lines should be established. One strategy to overcome this phenomenon is to target membrane-proximal mesothelin epitopes, as demonstrated by Xiufen Liu and colleagues, who designed a CAR-T cell recognizing the juxtamembrane region of mesothelin, thereby overcoming shedding-related limitations (Xiufen Liu et al., 2022). The ALFA-CAR platform could be leveraged to investigate this further by repositioning the ALFA-tag at different regions of mesothelin, allowing for a direct comparison of targeting efficiency.

Additionally, GPI-anchored proteins such as mesothelin appear to be more susceptible to trogocytosis, a phenomenon in which target antigens are transferred from tumor cells to CAR-T cells, leading to a reduction in antigen density on the tumor surface and rendering effector cells vulnerable to fratricide (Hamieh et al., 2019). Studies on the cellular prion protein (PRP^c) in a human neuroblastoma models have shown that trogocytosis can be significantly reduced by disrupting GPI anchorage (T. Liu et al., 2002). Furthermore, high-affinity CAR constructs have been shown to enhance trogocytosis, as antigen transfer is directly correlated with antigen-binding avidity and affinity (Chung et al., 2014; Olson et al., 2022). Given that the ALFA-CAR platform employs a high-affinity Nb-ALFA, it is possible that increased trogocytosis contributed to the differences observed in mesothelin-targeted killing dynamics. Investigating trogocytosis rates in mesothelin- and nectin-2-targeting CAR-T cells would provide valuable insights into the role of antigen transfer in CAR-T cell therapy.

4.3 Comparison of nanobody-based CAR-T cells targeting the native antigens

To confirm that the ALFA-CAR platform accurately represents the performance of conventional CAR-T cells, we replaced the ALFA recognition domain with nanobodies specific for the native Msln and Nec-2. In order to simplify this process, we produced a modular design of the CAR vector, which incorporates restriction sites flanking the recognition domain, enabling straightforward cloning. Furthermore, the Nanobody Core Facility in Bonn generously provided the nanobody sequences readily compatible with our vector, enabling the rapid production of antigen-specific CAR-T cells and enhancing the translational potential of our screening platform.

First, we tested the specificity of these CAR-T cells against cell lines expressing endogenous levels of mesothelin and nectin-2. The specific activation of the CAR-T cells against antigen-expressing cells, combined with the lack of pro-inflammatory markers expression against antigen-negative cell lines, is strongly suggestive of CAR-T cell specificity for both mesothelin and nectin-2. However, the establishment of *Msln* and *Cd112* knock-out cell lines is needed to confirm these findings.

We observed comparable CD25 and CD69 expression levels in both Msln-CARs and Nec2-CARs following stimulation with their respective tumor antigens. Furthermore, the killing dynamics of the Msln-CARs and Nec-2 CARs showed similarities to those observed using the ALFA-CAR platform against endogenously ALFA-tagged mesothelin and nectin-2 cells. In both systems, targeting nectin-2 resulted in faster cytotoxicity compared to mesothelin. However, the differences in killing kinetics observed when targeting native antigens were less pronounced than those observed with the ALFA-CAR platform.

This discrepancy is likely due to tumor cell-specific factors introduced by the genomic modifications performed at the mesothelin and nectin-2 loci. Since the experiments performed with the ALFA-CAR platform relied on engineered single-cell clones, these modifications could alter antigen expression, accessibility, or cell intrinsic properties that impact CAR-T cell engagement. Additionally, the clonal selection of modified cells may have introduced variability in growth behavior compared to heterogeneous, polyclonal cell

populations (Chignola et al., 2006; Tomelleri et al., 2008). This could result in altered tumor-immune interactions, potentially affecting the cytotoxic response of CAR-T cells.

To further validate these findings, a thorough characterization of the engineered cell lines is necessary, including quantification of antigen molecule expression per cell and comparison within sub-clones and with the parental polyclonal populations. Additionally, to establish the ALFA-CAR platform as a reliable antigen screening tool, its functionality must be demonstrated with more biological repeats, and ultimately, using in vivo models where tumor heterogeneity and other immune factors can be more accurately assessed.

4.4 Versatility of the ALFA-CAR platform: Affinity modulation

Affinity modulation is one of the most effective strategies to optimize CAR-T cell antigen recognition while avoiding tumor resistance. Generally, high-affinity CARs are better equipped to produce a strong anti-tumor response but are prone to exhaustion and reduced persistence due to excessive signaling (Hudecek et al., 2013; Lynn et al., 2019). Additionally, high-affinity CARs have shown higher risk of on-target, off-tumor toxicities, as they can be activated by low antigen densities expressed in healthy tissues. Nevertheless, a recent analysis by Mao and colleagues suggested that the majority of CAR-T cells tested in clinical trials rely on high-affinity recognition domains (K_D < 20 nM), from which the overwhelming majority has shown suboptimal response rates (R. Mao et al., 2022).

In contrast, lower-affinity CARs show different advantages. They have been shown to be safer while reducing CAR-T cell dysfunction by trogocytosis without significantly compromising their cytotoxic efficacy (Ghorashian et al., 2019; Olson et al., 2022). However, lower-affinity CARs may struggle to target cancer cells expressing low levels of antigen, increasing the risk of tumor escape (Xiaojun Liu et al., 2015). These findings suggest that there is no universal optimal affinity for all CAR constructs. The ideal balance between high and low affinity remains unclear, and a more personalized approach are needed.

The ALFA-CAR platform provides a unique, modular tool to systematically address the impact of affinity on CAR-T cell functionality. By leveraging the versatility of the ALFA-tag system, we introduced targeted mutations at key amino acid residues to reduce its binding affinity to

the Nb-ALFA. Using SPR, we validated these modifications and confirmed the exceptional affinity of the wild-type ALFA-tag (K_D = 0.228 nM), and we successfully engineered ALFA-tag variants with up to a 1000-fold reduction in binding affinity. To evaluate the impact of these affinity variants on CAR-T cell functionality, we express them on tumor cells and compare the activation and cytotoxicity of the ALFA-CAR.

Interestingly, flow cytometry analysis using the Nb-ALFA failed to detect tumor cells expressing ALFA-tag variants #9 and #10, despite SPR measurements confirming that these variants retained significantly high binding affinity (#9: K_D = 1.21 nM; #10: K_D = 2.96 nM). This discrepancy highlights a critical distinction between affinity (single interaction) and avidity (multiple interaction) (Erlendsson & Teilum, 2020). Flow cytometry detection relies on the soluble Nb-ALFA binding to ALFA-tag expressing cells through a single interaction, whereas the ALFA-CAR engages the expressing tumor cells through multiple interactions. As a result, even though variants #9 and #10 exhibit reduced affinity, their interaction in a cellular context with CAR-T cells may still be sufficient. Indeed, despite the loss of detection via flow cytometry, ALFA-CAR T cells were still able to recognize, activate, and kill tumor cells expressing variants #9 and #10.

Affinity plays a multifaceted role in CAR-T cell functionality, and its effects may not always be apparent when evaluating single parameters, particularly in vitro cytotoxicity assays. In this study, we observed no significant differences in ALFA-CAR-mediated killing across most affinity variants, even at different E:T, except for variant #8, in which the binding was completely disrupted. However, this does not rule out the functional impact of affinity in CAR-T cells. Prior studies have demonstrated that CAR-T cell activation, synapse formation, and exhaustion dynamics can be strongly influences by antigen-binding strength.

To explore this further, we investigated CAR expression dynamics during stimulation and after recovery. An interesting observation made by Davenport et al. was the downregulation of CAR molecules after prolonged stimulation, in contrast to stable expression of TCRs, which directly cripples CAR-T cell functionality (Davenport et al., 2015). To investigate whether this effect is influenced by antigen affinity, we used the ALFA-CAR platform against the affinity

variants. Our findings suggest that CAR downregulation can also occur in an affinity-dependent manner.

Higher-affinity ALFA-tag variants (WT: K_D = 0.0024 nM; #4: K_D = 0.228 nM) induced a more rapid and sustained loss of CAR expression, whereas lower-affinity variants also downregulated CARs but allowed for full recovery after antigen withdrawal. This suggests that stronger CAR-antigen binding drives faster loss. Previous studies have suggested that CAR immune synapse formation, which is influenced by antigen affinity, plays a critical role in cytotoxicity by rapid engagement and detachment of tumor cells, enabling sequential killing (serial killing) (Davenport et al., 2015; Xiong et al., 2018). If high-affinity CARs remain engaged for prolonged periods, they may undergo internalization and become unavailable for further antigen recognition, ultimately impairing their serial killing potential, which is crucial for CAR-T cell success.

The ability of lower affinity CARs to recover surface expression following antigen rescue suggests that weaker interaction allow for a more dynamic equilibrium between engagement, internalization, and recycling. This may protect CAR-T cells from rapid depletion of functional CAR molecules, preserving their cytotoxic potential for additional tumor cells. Importantly, due to the low amount of cell recovered after antigen stimulation, this experiment lacks the necessary experimental replicates to support a significant effect. If true, this phenomenon could help explain the growing preference for lower-affinity CARs, as they appear to enhance performance across various tumor entities. However, a more personalized approach remains essential, as different antigens and tumor types may require distinct affinity thresholds for optimal efficacy.

These findings highlight the versatility of the ALFA-CAR platform in dissecting key aspects of CAR-T cell functionality in an experimental fashion. By enabling precise modulation of CAR-specific properties, such as affinity, alongside tumor-specific parameter, like antigen selection, this system provides a valuable preclinical tool for optimizing CAR designs.

5 Abstract

Recent advances in cancer therapy, particularly immune checkpoint blockade (ICB), have significantly improved immune responses against tumors. However, many patients do not respond to ICB, and some experience disease recurrence after initial success.

Chimeric antigen receptor (CAR) T cell therapy has emerged as an alternative to ICB, but its effectiveness in solid tumors is limited by tumor heterogeneity, poor trafficking, CAR-T cell exhaustion, and antigen loss. Nanobody-based CAR-T cells offer a promising alternative to these challenges and represent an emerging therapeutic strategy.

Here, we developed a novel nanobody-based CAR-T cell platform using the previously described ALFA system. To generate ALFA-tag expressing cancer cell lines, we have used classical overexpression and cutting-edge CRISPR-based approaches. The latter approach enabled the precise integration of the ALFA epitope into the genomic sequences of two promising surface targets: Mesothelin and Nectin-2. In addition, we have successfully engineered murine CAR-T cells containing the nanobody-ALFA as the antigen recognition domain (“ALFA-CAR”), and demonstrated their specific activation and cytotoxicity when co-cultured with ALFA-tagged cancer cells in vitro.

To further explore the potential of the ALFA-CAR platform, we generated nanobody-based CAR-T cells targeting the native Mesothelin and Nectin-2 proteins. By comparing the activation profiles and cytotoxic capacity of ALFA-CAR cells with Mesothelin- and Nectin-2-specific CARs, we observed that ALFA-CARs resembles the killing dynamics of their native counterparts. Moreover, we have designed specific ALFA-tag mutant variants to study the impact of epitope-nanobody affinities for the functionality of CAR-T cells.

In conclusion, we developed a versatile nanobody-based CAR-T cell platform (ALFA-CAR) that can be used for both the identification of new tumor antigens and the refinement of existing targets. This approach allows for direct, side-by-side comparisons in a highly controlled setting, offering a promising avenue for advancing CAR-T cell therapies.

6 List of figures

7 List of tables

8 References

Adams, S. F., Levine, D. A., Cadungog, M. G., Hammond, R., Facciabene, A., Olvera, N., Rubin, S. C., Boyd, J., Gimotty, P. A., & Coukos, G. (2009). Intraepithelial T cells and tumor proliferation: Impact on the benefit from surgical cytoreduction in advanced serous ovarian cancer. *Cancer*, *115*(13), 2891–2902. https://doi.org/10.1002/cncr.24317

Auer, T. O., Duroure, K., Cian, A. de, Concordet, J.-P., & Del Bene, F. (2014). Highly efficient CRISPR/Cas9-mediated knock-in in zebrafish by homology-independent DNA repair. *Genome Research*, *24*(1), 142–153. https://doi.org/10.1101/gr.161638.113

Banerjee, S., Moore, K. N., Colombo, N [Nicoletta], Scambia, G., Kim, B.-G., Oaknin, A [Ana], Friedlander, M., Lisyanskaya, A., Floquet, A., Leary, A., Sonke, G. S [Gabe S.], Gourley, C., Oza, A., González-Martín, A [Antonio], Aghajanian, C., Bradley, W. H., Holmes, E., Lowe, E. S., & DiSilvestro, P. (2021). Maintenance olaparib for patients with newly diagnosed advanced ovarian cancer and a BRCA mutation (SOLO1/GOG 3004): 5-year follow-up of a randomised, double-blind, placebo-controlled, phase 3 trial. *The Lancet. Oncology*, *22*(12), 1721–1731. https://doi.org/10.1016/S1470-2045(21)00531-3

Bekes, I., Löb, S., Holzheu, I., Janni, W., Baumann, L., Wöckel, A., & Wulff, C. (2019). Nectin-2 in ovarian cancer: How is it expressed and what might be its functional role? *Cancer Science*, *110*(6), 1872–1882. https://doi.org/10.1111/cas.13992

Benloucif, A., Meyer, D., Balasse, L., Goubard, A., Danner, L., Bouhlel, A., Castellano, R., Guillet, B., Chames, P., & Kerfelec, B. (2023). Rapid nanobody-based imaging of mesothelin expressing malignancies compatible with blocking therapeutic antibodies. *Frontiers in Immunology*, *14*, 1200652. https://doi.org/10.3389/fimmu.2023.1200652

Bera, T. K [T. K.], & Pastan, I [I.] (2000). Mesothelin is not required for normal mouse development or reproduction. *Molecular and Cellular Biology*, *20*(8), 2902–2906. https://doi.org/10.1128/MCB.20.8.2902-2906.2000

Berdeja, J. G., Madduri, D., Usmani, S. Z., Jakubowiak, A., Agha, M., Cohen, A. D., Stewart, A. K., Hari, P., Htut, M., Lesokhin, A., Deol, A., Munshi, N. C., O'Donnell, E., Avigan, D., Singh, I., Zudaire, E., Yeh, T.-M., Allred, A. J., Olyslager, Y., . . . Jagannath, S.

(2021). Ciltacabtagene autoleucel, a B-cell maturation antigen-directed chimeric antigen receptor T-cell therapy in patients with relapsed or refractory multiple myeloma (CARTITUDE-1): A phase 1b/2 open-label study. *Lancet (London, England)*, *398*(10297), 314–324. https://doi.org/10.1016/S0140-6736(21)00933-8

Berek, J. S., Renz, M., Kehoe, S., Kumar, L., & Friedlander, M. (2021). Cancer of the ovary, fallopian tube, and peritoneum: 2021 update. *International Journal of Gynecology & Obstetrics*, *155 Suppl 1*(Suppl 1), 61–85. https://doi.org/10.1002/ijgo.13878

Boardman, A. P., & Salles, G. (2023). Car T-cell therapy in large B cell lymphoma. *Hematological Oncology*, *41 Suppl 1*(Suppl 1), 112–118. https://doi.org/10.1002/hon.3153

Bottino, C., Castriconi, R., Pende, D., Rivera, P., Nanni, M., Carnemolla, B., Cantoni, C., Grassi, J., Marcenaro, S., Reymond, N., Vitale, M., Moretta, L., Lopez, M., & Moretta, A. (2003). Identification of PVR (CD155) and Nectin-2 (CD112) as cell surface ligands for the human DNAM-1 (CD226) activating molecule. *The Journal of Experimental Medicine*, *198*(4), 557–567. https://doi.org/10.1084/jem.20030788

Brentjens, R. J., Rivière, I., Park, J. H., Davila, M. L., Wang, X [Xiuyan], Stefanski, J., Taylor, C., Yeh, R., Bartido, S., Borquez-Ojeda, O., Olszewska, M., Bernal, Y., Pegram, H., Przybylowski, M., Hollyman, D., Usachenko, Y., Pirraglia, D., Hosey, J., Santos, E., . . . Sadelain, M. (2011). Safety and persistence of adoptively transferred autologous CD19-targeted T cells in patients with relapsed or chemotherapy refractory B-cell leukemias. *Blood*, *118*(18), 4817–4828. https://doi.org/10.1182/blood-2011-04-348540

Brizzard, B. (2008). Epitope tagging. *BioTechniques*, *44*(5), 693–695. https://doi.org/10.2144/000112841

Brown, C. E., Alizadeh, D., Starr, R., Weng, L., Wagner, J. R., Naranjo, A., Ostberg, J. R., Blanchard, M. S., Kilpatrick, J., Simpson, J., Kurien, A., Priceman, S. J., Wang, X [Xiuli], Harshbarger, T. L., D'Apuzzo, M., Ressler, J. A., Jensen, M. C., Barish, M. E., Chen, M., . . . Badie, B. (2016). Regression of Glioblastoma after Chimeric Antigen Receptor T-Cell Therapy. *The New England Journal of Medicine*, *375*(26), 2561–2569. https://doi.org/10.1056/NEJMoa1610497

Cheng, W.-F., Huang, C.-Y., Chang, M.-C., Hu, Y.-H., Chiang, Y.-C., Chen, Y.-L., Hsieh, C.-Y., & Chen, C.-A. (2009). High mesothelin correlates with chemoresistance and poor survival in epithelial ovarian carcinoma. *British Journal of Cancer*, *100*(7), 1144–1153. https://doi.org/10.1038/sj.bjc.6604964

Chignola, R., Pra, P. D., Morato, L. M., & Siri, P. (2006). Proliferation and death in a binary environment: A stochastic model of cellular ecosystems. *Bulletin of Mathematical Biology*, *68*(7), 1661–1680. https://doi.org/10.1007/s11538-006-9078-8

Cho, S. W., Kim, S., Kim, J. M., & Kim, J.-S. (2013). Targeted genome engineering in human cells with the Cas9 RNA-guided endonuclease. *Nature Biotechnology*, *31*(3), 230–232. https://doi.org/10.1038/nbt.2507

Chung, B., Stuge, T. B., Murad, J. P., Beilhack, G., Andersen, E., Armstrong, B. D., Weber, J. S., & Lee, P. P. (2014). Antigen-specific inhibition of high-avidity T cell target lysis by low-avidity T cells via trogocytosis. *Cell Reports*, *8*(3), 871–882. https://doi.org/10.1016/j.celrep.2014.06.052

Coelho, R., Ricardo, S., Amaral, A. L., Huang, Y.-L., Nunes, M., Neves, J. P., Mendes, N., López, M. N., Bartosch, C., Ferreira, V., Portugal, R., Lopes, J. M., Almeida, R., Heinzelmann-Schwarz, V., Jacob, F., & David, L. (2020). Regulation of invasion and peritoneal dissemination of ovarian cancer by mesothelin manipulation. *Oncogenesis*, *9*(6), 61. https://doi.org/10.1038/s41389-020-00246-2

D'Aloia, M. M., Zizzari, I. G., Sacchetti, B., Pierelli, L., & Alimandi, M. (2018). Car-T cells: The long and winding road to solid tumors. *Cell Death & Disease*, *9*(3), 282. https://doi.org/10.1038/s41419-018-0278-6

Davenport, A. J., Jenkins, M. R., Cross, R. S., Yong, C. S., Prince, H. M., Ritchie, D. S., Trapani, J. A., Kershaw, M. H., Darcy, P. K., & Neeson, P. J. (2015). Car-T Cells Inflict Sequential Killing of Multiple Tumor Target Cells. *Cancer Immunology Research*, *3*(5), 483–494. https://doi.org/10.1158/2326-6066.CIR-15-0048

Deltcheva, E., Chylinski, K., Sharma, C. M., Gonzales, K., Chao, Y., Pirzada, Z. A., Eckert, M. R., Vogel, J., & Charpentier, E. (2011). Crispr RNA maturation by trans-encoded

small RNA and host factor RNase III. *Nature*, *471*(7340), 602–607. https://doi.org/10.1038/nature09886

Deriano, L., & Roth, D. B. (2013). Modernizing the nonhomologous end-joining repertoire: Alternative and classical NHEJ share the stage. *Annual Review of Genetics*, *47*, 433–455. https://doi.org/10.1146/annurev-genet-110711-155540

Deveau, H., Barrangou, R., Garneau, J. E., Labonté, J., Fremaux, C., Boyaval, P., Romero, D. A., Horvath, P., & Moineau, S. (2008). Phage response to CRISPR-encoded resistance in Streptococcus thermophilus. *Journal of Bacteriology*, *190*(4), 1390–1400. https://doi.org/10.1128/jb.01412-07

Di Roberto, R. B., Castellanos-Rueda, R., Frey, S [Samara], Egli, D., Vazquez-Lombardi, R., Kapetanovic, E., Kucharczyk, J., & Reddy, S. T. (2020). A Functional Screening Strategy for Engineering Chimeric Antigen Receptors with Reduced On-Target, Off-Tumor Activation. *Molecular Therapy : The Journal of the American Society of Gene Therapy*, *28*(12), 2564–2576. https://doi.org/10.1016/j.ymthe.2020.08.003

Dong, M. B., Tang, K., Zhou, X., Zhou, J. J., & Chen, S [Sidi] (2022). Tumor immunology CRISPR screening: Present, past, and future. *Trends in Cancer*, *8*(3), 210–225. https://doi.org/10.1016/j.trecan.2021.11.009

Erlendsson, S., & Teilum, K. (2020). Binding Revisited-Avidity in Cellular Function and Signaling. *Frontiers in Molecular Biosciences*, *7*, 615565. https://doi.org/10.3389/fmolb.2020.615565

Evan, G. I., Lewis, G. K., Ramsay, G., & Bishop, J. M. (1985). Isolation of monoclonal antibodies specific for human c-myc proto-oncogene product. *Molecular and Cellular Biology*, *5*(12), 3610–3616. https://doi.org/10.1128/mcb.5.12.3610-3616.1985

Field, J., Nikawa, J., Broek, D., MacDonald, B., Rodgers, L., Wilson, I. A., Lerner, R. A., & Wigler, M. (1988). Purification of a RAS-responsive adenylyl cyclase complex from Saccharomyces cerevisiae by use of an epitope addition method. *Molecular and Cellular Biology*, *8*(5), 2159–2165. https://doi.org/10.1128/mcb.8.5.2159-2165.1988

Fraietta, J. A., Lacey, S. F., Orlando, E. J., Pruteanu-Malinici, I., Gohil, M., Lundh, S., Boesteanu, A. C., Wang, Y [Yan], O'Connor, R. S., Hwang, W.-T., Pequignot, E., Ambrose, D. E., Zhang, C., Wilcox, N., Bedoya, F., Dorfmeier, C., Chen, F [Fang], Tian, L., Parakandi, H., . . . Melenhorst, J. J [J. Joseph] (2018). Determinants of response and resistance to CD19 chimeric antigen receptor (CAR) T cell therapy of chronic lymphocytic leukemia. *Nature Medicine*, *24*(5), 563–571. https://doi.org/10.1038/s41591-018-0010-1

Fujiwara, K., Masutani, M., Tachibana, M., & Okada, N. (2020). Impact of scFv structure in chimeric antigen receptor on receptor expression efficiency and antigen recognition properties. *Biochemical and Biophysical Research Communications*, *527*(2), 350–357. https://doi.org/10.1016/j.bbrc.2020.03.071

Gates, M. A., Rosner, B. A., Hecht, J. L., & Tworoger, S. S. (2010). Risk factors for epithelial ovarian cancer by histologic subtype. *American Journal of Epidemiology*, *171*(1), 45–53. https://doi.org/10.1093/aje/kwp314

Ghorashian, S., Kramer, A. M., Onuoha, S., Wright, G., Bartram, J., Richardson, R., Albon, S. J., Casanovas-Company, J., Castro, F., Popova, B., Villanueva, K., Yeung, J., Vetharoy, W., Guvenel, A., Wawrzyniecka, P. A., Mekkaoui, L., Cheung, G. W.-K., Pinner, D., Chu, J., . . . Amrolia, P. J. (2019). Enhanced CAR T cell expansion and prolonged persistence in pediatric patients with ALL treated with a low-affinity CD19 CAR. *Nature Medicine*, *25*(9), 1408–1414. https://doi.org/10.1038/s41591-019-0549-5

Götzke, H., Kilisch, M., Martínez-Carranza, M., Sograte-Idrissi, S., Rajavel, A., Schlichthaerle, T., Engels, N., Jungmann, R., Stenmark, P., Opazo, F., & Frey, S [Steffen] (2019). The ALFA-tag is a highly versatile tool for nanobody-based bioscience applications. *Nature Communications*, *10*(1), 4403. https://doi.org/10.1038/s41467-019-12301-7

Guirado, M., Aós, I. de, Orta, T., Rivas, L., Terhorst, C., Zubiaur, M., & Sancho, J. (2002). Phosphorylation of the N-terminal and C-terminal CD3-epsilon-ITAM tyrosines is differentially regulated in T cells. *Biochemical and Biophysical Research Communications*, *291*(3), 574–581. https://doi.org/10.1006/bbrc.2002.6492

Guzman, G., Reed, M. R., Bielamowicz, K., Koss, B., & Rodriguez, A. (2023). Car-T Therapies in Solid Tumors: Opportunities and Challenges. *Current Oncology Reports*, *25*(5), 479–489. https://doi.org/10.1007/s11912-023-01380-x

Haas, A. R., Golden, R. J., Litzky, L. A., Engels, B., Zhao, L., Xu, F., Taraszka, J. A., Ramones, M., Granda, B., Chang, W.-J., Jadlowsky, J., Shea, K.-M., Runkle, A., Chew, A., Dowd, E., Gonzalez, V., Chen, F [Fang], Liu, X [Xiaojun], Fang, C., . . . Tanyi, J. L. (2023). Two cases of severe pulmonary toxicity from highly active mesothelin-directed CAR T cells. *Molecular Therapy : The Journal of the American Society of Gene Therapy*, *31*(8), 2309–2325. https://doi.org/10.1016/j.ymthe.2023.06.006

Hamanishi, J., Mandai, M., Iwasaki, M., Okazaki, T., Tanaka, Y., Yamaguchi, K., Higuchi, T [Toshihiro], Yagi, H., Takakura, K., Minato, N., Honjo, T., & Fujii, S. (2007). Programmed cell death 1 ligand 1 and tumor-infiltrating CD8+ T lymphocytes are prognostic factors of human ovarian cancer. *Proceedings of the National Academy of Sciences of the United States of America*, *104*(9), 3360–3365. https://doi.org/10.1073/pnas.0611533104

Hamieh, M., Dobrin, A., Cabriolu, A., van der Stegen, S. J. C., Giavridis, T., Mansilla-Soto, J., Eyquem, J., Zhao, Z., Whitlock, B. M., Miele, M. M., Li, Z [Zhuoning], Cunanan, K. M., Huse, M., Hendrickson, R. C., Wang, X [Xiuyan], Rivière, I., & Sadelain, M. (2019). Car T cell trogocytosis and cooperative killing regulate tumour antigen escape. *Nature*, *568*(7750), 112–116. https://doi.org/10.1038/s41586-019-1054-1

Hamieh, M., Mansilla-Soto, J., Rivière, I., & Sadelain, M. (2023). Programming CAR T Cell Tumor Recognition: Tuned Antigen Sensing and Logic Gating. *Cancer Discovery*, *13*(4), 829–843. https://doi.org/10.1158/2159-8290.CD-23-0101

Higuchi, T [Tomoe], Flies, D. B., Marjon, N. A., Mantia-Smaldone, G., Ronner, L., Gimotty, P. A., & Adams, S. F. (2015). Ctla-4 Blockade Synergizes Therapeutically with PARP Inhibition in BRCA1-Deficient Ovarian Cancer. *Cancer Immunology Research*, *3*(11), 1257–1268. https://doi.org/10.1158/2326-6066.CIR-15-0044

Hochuli, E., Bannwarth, W., Döbeli, H., Gentz, R., & Stüber, D. (1988). Genetic Approach to Facilitate Purification of Recombinant Proteins with a Novel Metal Chelate Adsorbent. *Nature Biotechnology*, *6*(11), 1321–1325. https://doi.org/10.1038/nbt1188-1321

Hoffmann, C., Gaietta, G., Bünemann, M., Adams, S. R., Oberdorff-Maass, S., Behr, B., Vilardaga, J.-P., Tsien, R. Y., Ellisman, M. H., & Lohse, M. J. (2005). A FlAsH-based FRET approach to determine G protein-coupled receptor activation in living cells. *Nature Methods*, *2*(3), 171–176. https://doi.org/10.1038/nmeth742

Hryhorowicz, M., Lipiński, D., & Zeyland, J. (2023). Evolution of CRISPR/Cas Systems for Precise Genome Editing. *International Journal of Molecular Sciences*, *24*(18). https://doi.org/10.3390/ijms241814233

Hudecek, M., Lupo-Stanghellini, M.-T., Kosasih, P. L., Sommermeyer, D., Jensen, M. C., Rader, C., & Riddell, S. R. (2013). Receptor affinity and extracellular domain modifications affect tumor recognition by ROR1-specific chimeric antigen receptor T cells. *Clinical Cancer Research : An Official Journal of the American Association for Cancer Research*, *19*(12), 3153–3164. https://doi.org/10.1158/1078-0432.CCR-13-0330

Hudecek, M., Sommermeyer, D., Kosasih, P. L., Silva-Benedict, A., Liu, L [Lingfeng], Rader, C., Jensen, M. C., & Riddell, S. R. (2015). The nonsignaling extracellular spacer domain of chimeric antigen receptors is decisive for in vivo antitumor activity. *Cancer Immunology Research*, *3*(2), 125–135. https://doi.org/10.1158/2326-6066.CIR-14-0127

Ingram, J. R., Schmidt, F. I., & Ploegh, H. L. (2018). Exploiting Nanobodies' Singular Traits. *Annual Review of Immunology*, *36*, 695–715. https://doi.org/10.1146/annurev-immunol-042617-053327

Ishino, Y., Shinagawa, H., Makino, K., Amemura, M., & Nakata, A. (1987). Nucleotide sequence of the iap gene, responsible for alkaline phosphatase isozyme conversion in Escherichia coli, and identification of the gene product. *Journal of Bacteriology*, *169*(12), 5429–5433. https://doi.org/10.1128/jb.169.12.5429-5433.1987

Jinek, M., Chylinski, K., Fonfara, I., Hauer, M., Doudna, J. A., & Charpentier, E. (2012). A programmable dual-RNA-guided DNA endonuclease in adaptive bacterial immunity. *Science (New York, N.Y.)*, *337*(6096), 816–821. https://doi.org/10.1126/science.1225829

Kim, J.-S. (2016). Genome editing comes of age. *Nature Protocols*, *11*(9), 1573–1578. https://doi.org/10.1038/nprot.2016.104

Kipps, E., Tan, D. S. P., & Kaye, S. B. (2013). Meeting the challenge of ascites in ovarian cancer: New avenues for therapy and research. *Nature Reviews. Cancer*, *13*(4), 273–282. https://doi.org/10.1038/nrc3432

Knutson, K. L., Maurer, M. J., Preston, C. C., Moysich, K. B., Goergen, K., Hawthorne, K. M., Cunningham, J. M., Odunsi, K., Hartmann, L. C., Kalli, K. R., Oberg, A. L., & Goode, E. L. (2015). Regulatory T cells, inherited variation, and clinical outcome in epithelial ovarian cancer. *Cancer Immunology, Immunotherapy : CII*, *64*(12), 1495–1504. https://doi.org/10.1007/s00262-015-1753-x

Kochenderfer, J. N., Wilson, W. H., Janik, J. E., Dudley, M. E., Stetler-Stevenson, M., Feldman, S. A., Maric, I., Raffeld, M., Nathan, D.-A. N., Lanier, B. J., Morgan, R. A., & Rosenberg, S. A. (2010). Eradication of B-lineage cells and regression of lymphoma in a patient treated with autologous T cells genetically engineered to recognize CD19. *Blood*, *116*(20), 4099–4102. https://doi.org/10.1182/blood-2010-04-281931

Konstantinopoulos, P. A., & Matulonis, U. A [Ursula A.] (2023). Clinical and translational advances in ovarian cancer therapy. *Nature Cancer*, *4*(9), 1239–1257. https://doi.org/10.1038/s43018-023-00617-9

Konstantinopoulos, P. A., Norquist, B., Lacchetti, C., Armstrong, D., Grisham, R. N., Goodfellow, P. J., Kohn, E. C., Levine, D. A., Liu, J. F., Lu, K. H., Sparacio, D., & Annunziata, C. M. (2020). Germline and Somatic Tumor Testing in Epithelial Ovarian Cancer: Asco Guideline. *Journal of Clinical Oncology : Official Journal of the American Society of Clinical Oncology*, *38*(11), 1222–1245. https://doi.org/10.1200/JCO.19.02960

Kurman, R. J., Visvanathan, K., Roden, R., Wu, T. C., & Shih, I.-M. (2008). Early detection and treatment of ovarian cancer: Shifting from early stage to minimal volume of disease

based on a new model of carcinogenesis. *American Journal of Obstetrics and Gynecology*, *198*(4), 351–356. https://doi.org/10.1016/j.ajog.2008.01.005

Li, D., Wang, R., Liang, T., Ren, H., Park, C., Tai, C.-H [Chin-Hsien], Ni, W., Zhou, J., Mackay, S., Edmondson, E., Khan, J., Croix, B. S., & Ho, M [Mitchell] (2023). Camel nanobody-based B7-H3 CAR-T cells show high efficacy against large solid tumours. *Nature Communications*, *14*(1), 5920. https://doi.org/10.1038/s41467-023-41631-w

Li, J [Jun], Meng, X., Zong, Y., Chen, K., Zhang, H [Huawei], Liu, J [Jinxing], Li, J [Jiayang], & Gao, C. (2016). Gene replacements and insertions in rice by intron targeting using CRISPR-Cas9. *Nature Plants*, *2*, 16139. https://doi.org/10.1038/nplants.2016.139

Li, N [Nan], Quan, A., Li, D., Pan, J., Ren, H., Hoeltzel, G., Val, N. de, Ashworth, D., Ni, W., Zhou, J., Mackay, S., Hewitt, S. M., Cachau, R., & Ho, M [Mitchell] (2023). The IgG4 hinge with CD28 transmembrane domain improves VHH-based CAR T cells targeting a membrane-distal epitope of GPC1 in pancreatic cancer. *Nature Communications*, *14*(1), 1986. https://doi.org/10.1038/s41467-023-37616-4

Liu, T., Li, R [Ruliang], Pan, T., Liu, D [Dacai], Petersen, R. B., Wong, B.-S., Gambetti, P., & Sy, M. S. (2002). Intercellular transfer of the cellular prion protein. *The Journal of Biological Chemistry*, *277*(49), 47671–47678. https://doi.org/10.1074/jbc.M207458200

Liu, X. F., Onda, M [M.], Schlomer, J., Bassel, L., Kozlov, S., Tai, C.-H [C-H], Zhou, Q [Q.], Liu, W., Tsao, H.-E., Hassan, R [R.], Ho, M [M.], & Pastan, I [I.] (2024). Tumor resistance to anti-mesothelin CAR-T cells caused by binding to shed mesothelin is overcome by targeting a juxtamembrane epitope. *Proceedings of the National Academy of Sciences of the United States of America*, *121*(4), e2317283121. https://doi.org/10.1073/pnas.2317283121

Liu, X [Xiaojun], Jiang, S., Fang, C., Yang, S., Olalere, D., Pequignot, E. C., Cogdill, A. P., Li, N [Na], Ramones, M., Granda, B., Zhou, L., Loew, A., Young, R. M., June, C. H., & Zhao, Y. (2015). Affinity-Tuned ErbB2 or EGFR Chimeric Antigen Receptor T Cells Exhibit an Increased Therapeutic Index against Tumors in Mice. *Cancer Research*, *75*(17), 3596–3607. https://doi.org/10.1158/0008-5472.CAN-15-0159

Liu, X [Xiufen], Chan, A., Tai, C.-H [Chin-Hsien], Andresson, T., & Pastan, I [Ira] (2020). Multiple proteases are involved in mesothelin shedding by cancer cells. *Communications Biology*, *3*(1), 728. https://doi.org/10.1038/s42003-020-01464-5

Liu, X [Xiufen], Onda, M [Masanori], Watson, N., Hassan, R [Raffit], Ho, M [Mitchell], Bera, T. K [Tapan K.], Wei, J., Chakraborty, A., Beers, R., Zhou, Q [Qi], Shajahan, A., Azadi, P., Zhan, J., Di Xia, & Pastan, I [Ira] (2022). Highly active CAR T cells that bind to a juxtamembrane region of mesothelin and are not blocked by shed mesothelin. *Proceedings of the National Academy of Sciences of the United States of America*, *119*(19), e2202439119. https://doi.org/10.1073/pnas.2202439119

Lynn, R. C., Weber, E. W., Sotillo, E., Gennert, D., Xu, P., Good, Z., Anbunathan, H., Lattin, J., Jones, R., Tieu, V., Nagaraja, S., Granja, J., Bourcy, C. F. A. de, Majzner, R., Satpathy, A. T., Quake, S. R., Monje, M., Chang, H. Y., & Mackall, C. L. (2019). C-Jun overexpression in CAR T cells induces exhaustion resistance. *Nature*, *576*(7786), 293–300. https://doi.org/10.1038/s41586-019-1805-z

Majzner, R. G., & Mackall, C. L. (2018). Tumor Antigen Escape from CAR T-cell Therapy. *Cancer Discovery*, *8*(10), 1219–1226. https://doi.org/10.1158/2159-8290.CD-18-0442

Majzner, R. G., & Mackall, C. L. (2019). Clinical lessons learned from the first leg of the CAR T cell journey. *Nature Medicine*, *25*(9), 1341–1355. https://doi.org/10.1038/s41591-019-0564-6

Makkouk, A., Yang, X. C., Barca, T., Lucas, A., Turkoz, M., Wong, J. T. S., Nishimoto, K. P., Brodey, M. M., Tabrizizad, M., Gundurao, S. R. Y., Bai, L., Bhat, A., An, Z., Abbot, S., Satpayev, D., Aftab, B. T., & Herrman, M. (2021). Off-the-shelf Vδ1 gamma delta T cells engineered with glypican-3 (GPC-3)-specific chimeric antigen receptor (CAR) and soluble IL-15 display robust antitumor efficacy against hepatocellular carcinoma. *Journal for Immunotherapy of Cancer*, *9*(12). https://doi.org/10.1136/jitc-2021-003441

Mao, R., Kong, W., & He, Y. (2022). The affinity of antigen-binding domain on the antitumor efficacy of CAR T cells: Moderate is better. *Frontiers in Immunology*, *13*, 1032403. https://doi.org/10.3389/fimmu.2022.1032403

Mao, Z., Bozzella, M., Seluanov, A., & Gorbunova, V. (2008). Comparison of nonhomologous end joining and homologous recombination in human cells. *DNA Repair*, *7*(10), 1765–1771. https://doi.org/10.1016/j.dnarep.2008.06.018

Marchetti, C., Muzii, L., Romito, A., & Benedetti Panici, P. (2019). First-line treatment of women with advanced ovarian cancer: Focus on bevacizumab. *OncoTargets and Therapy*, *12*, 1095–1103. https://doi.org/10.2147/OTT.S155425

Matulonis, U. A [U. A.], Shapira-Frommer, R., Santin, A. D., Lisyanskaya, A. S., Pignata, S., Vergote, I., Raspagliesi, F., Sonke, G. S [G. S.], Birrer, M., Provencher, D. M., Sehouli, J., Colombo, N [N.], González-Martín, A [A.], Oaknin, A [A.], Ottevanger, P. B., Rudaitis, V., Katchar, K., Wu, H., Keefe, S., . . . Ledermann, J. A. (2019). Antitumor activity and safety of pembrolizumab in patients with advanced recurrent ovarian cancer: Results from the phase II KEYNOTE-100 study. *Annals of Oncology : Official Journal of the European Society for Medical Oncology*, *30*(7), 1080–1087. https://doi.org/10.1093/annonc/mdz135

Maude, S. L., Frey, N., Shaw, P. A., Aplenc, R., Barrett, D. M., Bunin, N. J., Chew, A., Gonzalez, V. E., Zheng, Z., Lacey, S. F., Mahnke, Y. D., Melenhorst, J. J [Jan J.], Rheingold, S. R., Shen, A., Teachey, D. T., Levine, B. L., June, C. H., Porter, D. L., & Grupp, S. A. (2014). Chimeric antigen receptor T cells for sustained remissions in leukemia. *The New England Journal of Medicine*, *371*(16), 1507–1517. https://doi.org/10.1056/NEJMoa1407222

Maude, S. L., Laetsch, T. W., Buechner, J., Rives, S., Boyer, M., Bittencourt, H., Bader, P., Verneris, M. R., Stefanski, H. E., Myers, G. D., Qayed, M., Moerloose, B. de, Hiramatsu, H., Schlis, K., Davis, K. L., Martin, P. L., Nemecek, E. R., Yanik, G. A., Peters, C., . . . Grupp, S. A. (2018). Tisagenlecleucel in Children and Young Adults with B-Cell Lymphoblastic Leukemia. *The New England Journal of Medicine*, *378*(5), 439–448. https://doi.org/10.1056/NEJMoa1709866

Menon, U., Gentry-Maharaj, A., Burnell, M., Singh, N., Ryan, A., Karpinskyj, C., Carlino, G., Taylor, J., Massingham, S. K., Raikou, M., Kalsi, J. K., Woolas, R., Manchanda, R., Arora, R., Casey, L., Dawnay, A., Dobbs, S., Leeson, S., Mould, T., . . . Parmar, M. (2021).

Ovarian cancer population screening and mortality after long-term follow-up in the UK Collaborative Trial of Ovarian Cancer Screening (UKCTOCS): A randomised controlled trial. *Lancet (London, England)*, *397*(10290), 2182–2193. https://doi.org/10.1016/S0140-6736(21)00731-5

Mitra, A., Barua, A., Huang, L., Ganguly, S., Feng, Q., & He, B. (2023). From bench to bedside: The history and progress of CAR T cell therapy. *Frontiers in Immunology*, *14*, 1188049. https://doi.org/10.3389/fimmu.2023.1188049

Müller, G. A. (2018). The release of glycosylphosphatidylinositol-anchored proteins from the cell surface. *Archives of Biochemistry and Biophysics*, *656*, 1–18. https://doi.org/10.1016/j.abb.2018.08.009

Naora, H., & Montell, D. J. (2005). Ovarian cancer metastasis: Integrating insights from disparate model organisms. *Nature Reviews. Cancer*, *5*(5), 355–366. https://doi.org/10.1038/nrc1611

Nguyen, M. Q., Kim, D. H., Shim, H. J., Ta, H. K. K., Vu, T. L., Nguyen, T. K. O., Lim, J. C., & Choe, H. (2023). Novel Anti-Mesothelin Nanobodies and Recombinant Immunotoxins with Pseudomonas Exotoxin Catalytic Domain for Cancer Therapeutics. *Molecules and Cells*, *46*(12), 764–777. https://doi.org/10.14348/molcells.2023.0155

O'Hara, M., Stashwick, C., Haas, A. R., & Tanyi, J. L. (2016). Mesothelin as a target for chimeric antigen receptor-modified T cells as anticancer therapy. *Immunotherapy*, *8*(4), 449–460. https://doi.org/10.2217/imt.16.4

Olson, M. L., Mause, E. R. V., Radhakrishnan, S. V., Brody, J. D., Rapoport, A. P., Welm, A. L., Atanackovic, D., & Luetkens, T. (2022). Low-affinity CAR T cells exhibit reduced trogocytosis, preventing rapid antigen loss, and increasing CAR T cell expansion. *Leukemia*, *36*(7), 1943–1946. https://doi.org/10.1038/s41375-022-01585-2

Onda, T., Satoh, T., Ogawa, G., Saito, T., Kasamatsu, T., Nakanishi, T., Mizutani, T., Takehara, K., Okamoto, A., Ushijima, K., Kobayashi, H., Kawana, K., Yokota, H., Takano, M., Kanao, H., Watanabe, Y., Yamamoto, K., Yaegashi, N., Kamura, T., & Yoshikawa, H. (2020). Comparison of survival between primary debulking surgery and

neoadjuvant chemotherapy for stage III/IV ovarian, tubal and peritoneal cancers in phase III randomised trial. *European Journal of Cancer (Oxford, England : 1990)*, *130*, 114–125. https://doi.org/10.1016/j.ejca.2020.02.020

Oshima, T., Sato, S., Kato, J., Ito, Y., Watanabe, T., Tsuji, I., Hori, A., Kurokawa, T., & Kokubo, T. (2013). Nectin-2 is a potential target for antibody therapy of breast and ovarian cancers. *Molecular Cancer*, *12*, 60. https://doi.org/10.1186/1476-4598-12-60

Philip, B., Kokalaki, E., Mekkaoui, L., Thomas, S., Straathof, K., Flutter, B., Marin, V., Marafioti, T., Chakraverty, R., Linch, D., Quezada, S. A., Peggs, K. S., & Pule, M. (2014). A highly compact epitope-based marker/suicide gene for easier and safer T-cell therapy. *Blood*, *124*(8), 1277–1287. https://doi.org/10.1182/blood-2014-01-545020

Prantner, A. M., Turini, M., Kerfelec, B., Joshi, S., Baty, D., Chames, P., & Scholler, N. (2015). Anti-Mesothelin Nanobodies for Both Conventional and Nanoparticle-Based Biomedical Applications. *Journal of Biomedical Nanotechnology*, *11*(7), 1201–1212. https://doi.org/10.1166/jbn.2015.2063

Prantner, A. M., Yin, C., Kamat, K., Sharma, K., Lowenthal, A. C., Madrid, P. B., & Scholler, N. (2018). Molecular Imaging of Mesothelin-Expressing Ovarian Cancer with a Human and Mouse Cross-Reactive Nanobody. *Molecular Pharmaceutics*, *15*(4), 1403–1411. https://doi.org/10.1021/acs.molpharmaceut.7b00789

Rafiq, S., Hackett, C. S., & Brentjens, R. J. (2020). Engineering strategies to overcome the current roadblocks in CAR T cell therapy. *Nature Reviews. Clinical Oncology*, *17*(3), 147–167. https://doi.org/10.1038/s41571-019-0297-y

Ritter, A. T., Shtengel, G., Xu, C. S., Weigel, A., Hoffman, D. P., Freeman, M., Iyer, N., Alivodej, N., Ackerman, D., Voskoboinik, I., Trapani, J., Hess, H. F., & Mellman, I. (2022). Escrt-mediated membrane repair protects tumor-derived cells against T cell attack. *Science (New York, N.Y.)*, *376*(6591), 377–382. https://doi.org/10.1126/science.abl3855

Rubinstein, R., Ramagopal, U. A., Nathenson, S. G., Almo, S. C., & Fiser, A. (2013). Functional classification of immune regulatory proteins. *Structure (London, England : 1993)*, *21*(5), 766–776. https://doi.org/10.1016/j.str.2013.02.022

Rump, A., Morikawa, Y., Tanaka, M., Minami, S., Umesaki, N., Takeuchi, M., & Miyajima, A. (2004). Binding of ovarian cancer antigen CA125/MUC16 to mesothelin mediates cell adhesion. *The Journal of Biological Chemistry*, *279*(10), 9190–9198. https://doi.org/10.1074/jbc.M312372200

Sakisaka, T., & Takai, Y. (2004). Biology and pathology of nectins and nectin-like molecules. *Current Opinion in Cell Biology*, *16*(5), 513–521. https://doi.org/10.1016/j.ceb.2004.07.007

San Filippo, J., Sung, P., & Klein, H. (2008). Mechanism of eukaryotic homologous recombination. *Annual Review of Biochemistry*, *77*, 229–257. https://doi.org/10.1146/annurev.biochem.77.061306.125255

Sarén, T., Saronio, G., Torrell, M., Zhu, X., Thelander, J., Andersson, Y., Hofström, C., Nestor, M., Dimberg, A., Persson, H., Ramachandran, M., Di Yu, & Essand, M. (2023). *Complementarity-determining region clustering may cause CAR-T cell dysfunction.* Nature Publishing Group. https://www.nature.com/articles/s41467-023-40303-z#citeas

Schatz, D. G., & Ji, Y. (2011). Recombination centres and the orchestration of V(D)J recombination. *Nature Reviews. Immunology*, *11*(4), 251–263. https://doi.org/10.1038/nri2941

Shih, I.-M., Wang, Y [Yeh], & Wang, T.-L. (2021). The Origin of Ovarian Cancer Species and Precancerous Landscape. *The American Journal of Pathology*, *191*(1), 26–39. https://doi.org/10.1016/j.ajpath.2020.09.006

Sim, Y. H., Um, Y. J., Park, J.-Y., Seo, M.-D., & Park, S. G. (2022). A Novel Antibody-Drug Conjugate Targeting Nectin-2 Suppresses Ovarian Cancer Progression in Mouse Xenograft Models. *International Journal of Molecular Sciences*, *23*(20). https://doi.org/10.3390/ijms232012358

Stadler, C., Rexhepaj, E., Singan, V. R., Murphy, R. F., Pepperkok, R., Uhlén, M., Simpson, J. C., & Lundberg, E. (2013). Immunofluorescence and fluorescent-protein tagging show high correlation for protein localization in mammalian cells. *Nature Methods*, *10*(4), 315–323. https://doi.org/10.1038/nmeth.2377

Stanietsky, N., Simic, H., Arapovic, J., Toporik, A., Levy, O., Novik, A., Levine, Z., Beiman, M., Dassa, L., Achdout, H., Stern-Ginossar, N., Tsukerman, P., Jonjic, S., & Mandelboim, O. (2009). The interaction of TIGIT with PVR and PVRL2 inhibits human NK cell cytotoxicity. *Proceedings of the National Academy of Sciences of the United States of America*, *106*(42), 17858–17863. https://doi.org/10.1073/pnas.0903474106

Stock, S., Schmitt, M., & Sellner, L. (2019). Optimizing Manufacturing Protocols of Chimeric Antigen Receptor T Cells for Improved Anticancer Immunotherapy. *International Journal of Molecular Sciences*, *20*(24). https://doi.org/10.3390/ijms20246223

Sun, L., Gao, F., Gao, Z., Ao, L., Li, N [Na], Ma, S., Jia, M., Li, N [Nan], Lu, P., Sun, B., Ho, M [Mitchell], Jia, S., Ding, T., & Gao, W. (2021). Shed antigen-induced blocking effect on CAR-T cells targeting Glypican-3 in Hepatocellular Carcinoma. *Journal for Immunotherapy of Cancer*, *9*(4). https://doi.org/10.1136/jitc-2020-001875

Sung, H., Ferlay, J., Siegel, R. L., Laversanne, M., Soerjomataram, I., Jemal, A., & Bray, F. (2021). Global Cancer Statistics 2020: Globocan Estimates of Incidence and Mortality Worldwide for 36 Cancers in 185 Countries. *CA: A Cancer Journal for Clinicians*, *71*(3), 209–249. https://doi.org/10.3322/caac.21660

Suzuki, K., & Izpisua Belmonte, J. C. (2018). In vivo genome editing via the HITI method as a tool for gene therapy. *Journal of Human Genetics*, *63*(2), 157–164. https://doi.org/10.1038/s10038-017-0352-4

Suzuki, K., Tsunekawa, Y., Hernandez-Benitez, R., Wu, J., Zhu, J., Kim, E. J., Hatanaka, F., Yamamoto, M., Araoka, T., Li, Z [Zhe], Kurita, M., Hishida, T., Li, M., Aizawa, E., Guo, S., Chen, S [Song], Goebl, A., Soligalla, R. D., Qu, J., . . . Belmonte, J. C. I. (2016). In vivo genome editing via CRISPR/Cas9 mediated homology-independent targeted integration. *Nature*, *540*(7631), 144–149. https://doi.org/10.1038/nature20565

Takai, Y., Ikeda, W., Ogita, H., & Rikitake, Y. (2008). The immunoglobulin-like cell adhesion molecule nectin and its associated protein afadin. *Annual Review of Cell and Developmental Biology*, *24*, 309–342. https://doi.org/10.1146/annurev.cellbio.24.110707.175339

Tang, Z., Qian, M., & Ho, M [Mitchell] (2013). The role of mesothelin in tumor progression and targeted therapy. *Anti-Cancer Agents in Medicinal Chemistry*, *13*(2), 276–280. https://doi.org/10.2174/1871520611313020014

Tomelleri, C., Milotti, E., Dalla Pellegrina, C., Perbellini, O., Del Fabbro, A., Scupoli, M. T., & Chignola, R. (2008). A quantitative study of growth variability of tumour cell clones in vitro. *Cell Proliferation*, *41*(1), 177–191. https://doi.org/10.1111/j.1365-2184.2007.00501.x

Tsherniak, A., Vazquez, F., Montgomery, P. G., Weir, B. A., Kryukov, G., Cowley, G. S., Gill, S., Harrington, W. F., Pantel, S., Krill-Burger, J. M., Meyers, R. M., Ali, L., Goodale, A., Lee, Y., Jiang, G., Hsiao, J., Gerath, W. F. J., Howell, S., Merkel, E., . . . Hahn, W. C. (2017). Defining a Cancer Dependency Map. *Cell*, *170*(3), 564-576.e16. https://doi.org/10.1016/j.cell.2017.06.010

Tsilidis, K. K., Allen, N. E., Key, T. J., Dossus, L., Lukanova, A., Bakken, K., Lund, E., Fournier, A., Overvad, K., Hansen, L., Tjønneland, A., Fedirko, V., Rinaldi, S., Romieu, I., Clavel-Chapelon, F., Engel, P., Kaaks, R., Schütze, M., Steffen, A., . . . Riboli, E. (2011). Oral contraceptive use and reproductive factors and risk of ovarian cancer in the European Prospective Investigation into Cancer and Nutrition. *British Journal of Cancer*, *105*(9), 1436–1442. https://doi.org/10.1038/bjc.2011.371

Upadhyay, R., Boiarsky, J. A., Pantsulaia, G., Svensson-Arvelund, J., Lin, M. J., Wroblewska, A., Bhalla, S., Scholler, N., Bot, A., Rossi, J. M., Sadek, N., Parekh, S., Lagana, A., Baccarini, A., Merad, M., Brown, B. D., & Brody, J. D. (2021). A Critical Role for Fas-Mediated Off-Target Tumor Killing in T-cell Immunotherapy. *Cancer Discovery*, *11*(3), 599–613. https://doi.org/10.1158/2159-8290.CD-20-0756

Vander Mause, E. R., Atanackovic, D., Lim, C. S., & Luetkens, T. (2022). Roadmap to affinity-tuned antibodies for enhanced chimeric antigen receptor T cell function and selectivity. *Trends in Biotechnology*, *40*(7), 875–890. https://doi.org/10.1016/j.tibtech.2021.12.009

Veneziani, A. C., Gonzalez-Ochoa, E., Alqaisi, H., Madariaga, A., Bhat, G., Rouzbahman, M., Sneha, S., & Oza, A. M. (2023). Heterogeneity and treatment landscape

of ovarian carcinoma. *Nature Reviews. Clinical Oncology*, *20*(12), 820–842. https://doi.org/10.1038/s41571-023-00819-1

Vincke, C., Loris, R., Saerens, D., Martinez-Rodriguez, S., Muyldermans, S., & Conrath, K. (2009). General strategy to humanize a camelid single-domain antibody and identification of a universal humanized nanobody scaffold. *The Journal of Biological Chemistry*, *284*(5), 3273–3284. https://doi.org/10.1074/jbc.M806889200

Webb, P. M., Green, A. C., & Jordan, S. J. (2017). Trends in hormone use and ovarian cancer incidence in US white and Australian women: Implications for the future. *Cancer Causes & Control : CCC*, *28*(5), 365–370. https://doi.org/10.1007/s10552-017-0868-0

Webb, P. M., & Jordan, S. J. (2024). Global epidemiology of epithelial ovarian cancer. *Nature Reviews. Clinical Oncology*, *21*(5), 389–400. https://doi.org/10.1038/s41571-024-00881-3

Winter, W. E., Maxwell, G. L., Tian, C., Carlson, J. W., Ozols, R. F., Rose, P. G., Markman, M., Armstrong, D. K., Muggia, F., & McGuire, W. P. (2007). Prognostic factors for stage III epithelial ovarian cancer: A Gynecologic Oncology Group Study. *Journal of Clinical Oncology : Official Journal of the American Society of Clinical Oncology*, *25*(24), 3621–3627. https://doi.org/10.1200/JCO.2006.10.2517

Xia, B., Lin, K., Wang, X [Xuemei], Chen, F [FeiLi], Zhou, M., Li, Y., Lin, Y [Yingtong], Qiao, Y., Li, R [Rong], Zhang, W., He, X., Zou, F., Li, L., Lu, L., Chen, C., Li, W [WenYu], Zhang, H [Hui], & Liu, B. (2023). Nanobody-derived bispecific CAR-T cell therapy enhances the anti-tumor efficacy of T cell lymphoma treatment. *Molecular Therapy Oncolytics*, *30*, 86–102. https://doi.org/10.1016/j.omto.2023.07.007

Xie, Y. J., Dougan, M., Ingram, J. R., Pishesha, N., Fang, T., Momin, N., & Ploegh, H. L. (2020). Improved Antitumor Efficacy of Chimeric Antigen Receptor T Cells that Secrete Single-Domain Antibody Fragments. *Cancer Immunology Research*, *8*(4), 518–529. https://doi.org/10.1158/2326-6066.CIR-19-0734

Xiong, W., Chen, Y., Kang, X., Chen, Z., Zheng, P., Hsu, Y.-H., Jang, J. H., Qin, L., Liu, H., Dotti, G., & Liu, D [Dongfang] (2018). Immunological Synapse Predicts Effectiveness of

Chimeric Antigen Receptor Cells. *Molecular Therapy : The Journal of the American Society of Gene Therapy*, *26*(4), 963–975. https://doi.org/10.1016/j.ymthe.2018.01.020

Yarmarkovich, M., Marshall, Q. F., Warrington, J. M., Premaratne, R., Farrel, A., Groff, D., Li, W [Wei], Di Marco, M., Runbeck, E., Truong, H., Toor, J. S., Tripathi, S., Nguyen, S., Shen, H., Noel, T., Church, N. L., Weiner, A., Kendsersky, N., Martinez, D., . . . Maris, J. M. (2023). Targeting of intracellular oncoproteins with peptide-centric CARs. *Nature*, *623*(7988), 820–827. https://doi.org/10.1038/s41586-023-06706-0

Zhai, X., Mao, L., Wu, M., Liu, J [Jie], & Yu, S. (2023). Challenges of Anti-Mesothelin CAR-T-Cell Therapy. *Cancers*, *15*(5). https://doi.org/10.3390/cancers15051357

Zhang, L., Conejo-Garcia, J. R., Katsaros, D., Gimotty, P. A., Massobrio, M., Regnani, G., Makrigiannakis, A., Gray, H., Schlienger, K., Liebman, M. N., Rubin, S. C., & Coukos, G. (2003). Intratumoral T cells, recurrence, and survival in epithelial ovarian cancer. *The New England Journal of Medicine*, *348*(3), 203–213. https://doi.org/10.1056/NEJMoa020177

Zhong, H., Ceballos, C. C., Massengill, C. I., Muniak, M. A., Ma, L., Qin, M., Petrie, S. K., & Mao, T. (2021). High-fidelity, efficient, and reversible labeling of endogenous proteins using CRISPR-based designer exon insertion. *ELife*, *10.* https://doi.org/10.7554/eLife.64911

9 Acknowledgements

The work I have accomplished over the last four years is the result of a joint effort by many people, to whom I am immensely grateful.

First and foremost, I want to thank my supervisors, Dr. Nicole Glodde, Prof. Dr. Tobias Bald, and Prof. Dr. Michael Hölzel, for giving me the opportunity to learn and work at the Institute of Experimental Oncology in Bonn. This has been an invaluable experience in my scientific training. Thank you for trusting me with your exciting ideas and for guiding me to bring them to completion. This opportunity has also allowed me to settle my life in Germany, which I now consider my home.

I would also like to thank Prof. Dr. Florian Schmidt, Prof. Dr. Jennifer Landsberg, and Dr. Paul-Albert König for always having an open door and for their continued scientific input over the years. Additionally, I am grateful to Prof. Dr. Dr. Roland Ullrich for agreeing to be part of my dissertation committee.

I am deeply thankful to all my colleagues from the IEO who, directly or indirectly, have helped me grow both personally and professionally. I want to extend special thanks to Benjamin McEnroe and Carolin Birr for working alongside me on this project. Your support and friendship have been fundamental to this project.

Thanks to my office friends, Saskia Vadder, Franziska Schneppenheim, Elisabeth Tan, and Eduard Below, for making every day brighter and more enjoyable.

I am also sincerely grateful to the Cluster of Excellence ImmunoSensation² for supporting me and my peers in every possible way. I have always felt encouraged and supported by your team.

Finally, I want to thank my friends and family. The completion of this thesis would not have been possible without your unwavering support. Muchas gracias, mamá, papá, Rafa, Rodri, Ale y Leonora, por su cariño y por siempre cuidarme. Gracias también a todos mis amigos que siempre han estado ahí, incluso estando tan lejos. Muchas gracias, Mar, no lo hubiera logrado sin ti. Y gracias, Galvis, por tu amistad y tus consejos.